Evaluating the Structural Integrity of High Strength Low Alloy Steels Considered for Shipbuilding Using Acoustic Emission

by

Shengrun Shi

A thesis submitted to the University of Birmingham for the degree of

Master of Research

School of Metallurgy and Materials
College of Engineering and Physical Sciences
University of Birmingham
September 2014

Synopsis

The modern maritime industry shows strong demand for steel grades with improved structural performance and better resistance to fatigue damage initiation and evolution. Improved structural performance permits the use of plates with lower thicknesses thus resulting in significant savings in fuel consumption and engine requirements. High Strength Low Alloy (HSLA) steel grades exhibit a favourable strength-to-weight ratio when compared with conventional maritime steel grades, such as the AH and DH steel grades. HSLA steels, e.g. X65, X70, etc., have been extensively used in various offshore oil and gas applications, including pipelines. Recent developments in maritime transport policies and regulations have incited a constantly growing interest in HSLA steel grades in the shipbuilding industry.

The main objectives of this project have been to assess the applicability of various HSLA steel grades in ships as a possible replacement to conventional maritime steel grades such as the AH36 and DH36 high strength steels. For this reason, the mechanical properties of three different HSLA steel grades (X65, S690 and FCA) of different plate thicknesses were assessed using metallography, fractography, hardness, tensile, fatigue and impact testing. Acoustic emission (AE) testing was carried out in parallel with tensile and fatigue testing in order to ascertain qualitatively and quantitatively the evolution of damage in the samples tested and verify the level of severity. In principle, the AE results acquired in the laboratory could be used to monitor the actual ship's structure, thus permitting the continuous assessment of the overall structural integrity of a ship. Various methods have been applied for the analysis of the AE data acquired in order to correlate them with the mechanical testing results obtained in parallel.

Analysis of the main results of this study has shown that the HSLA steels considered herewith exhibited better crack initiation resistance than conventional maritime steels. In addition, their resistance to crack growth was also found to be better overall. The tensile properties of the HSLA steels considered were comparable in terms of elongation to those of AH and DH grades with the S690 being the only exception from the HSLA grades tested. In terms of yield strength all of them were superior to AH36 and some of them superior to DH36 too. Since all HSLA grades tested exhibited higher fracture toughness, they are suitable to replace conventional maritime steel grades. However, the shipbuilding standards require that the steel grade used also exhibits a good level of ductility achieving at least 20% strain in tension. In the case of the S690 grade, this level of ductility has not been achieved. Thus under current shipbuilding standards it cannot be used for hull construction although it is suitable for the construction of other parts of the ship.

Acknowledgements

I would like to express a sincere gratitude to Dr. Mayorkinos Papaelias for the opportunity he has provided me to do the research under his supervision. It would be impossible for me to finish my work without his consistent support and invaluable guidance.

I am grateful to Prof. Claire Davis and Dr. Carl Slater for their precious suggestion and support throughout the project. I also want to thank the Steel Research Group of the School of Metallurgy and Materials for their help during the time of working on the project.

I am thankful for Mr. David Price and Dr. Tim Dole for their help with the fatigue and tensile test machines. I would like to thank Mr. Mick Cunningham and Ms. Avril Rogers for the help they offered with the Charpy and Vicker hardness tests.

I also want to show my gratitude to Tata Steel, Korinthos Pipeworks, Thyssen and Sumitomo AIMEN for providing the resources for the research.

Finally, I like to show sincere gratitude to my family who has been giving me support and encouragement since I studied in UK.

Table of Contents

List of Figures

List of Tables

1 Introduction

1.1 Background

The structural reliability of ships is of outmost importance in ensuring the safety of maritime freight and passenger transport operations. In-service fatigue cracking due to cyclic loading, impact damage and corrosion can adversely influence the structural integrity of maritime vessels. Significant degradation of critical structural components in the long term requires emergency repairs to be carried out before the ship concerned can be returned to service.

As shown in the schematics of Figure 1, passenger and merchant vessels often operate under severe weather conditions resulting in significant linear (surging, swaying and heaving) and angular (rolling, pitching and yawing) motions which can cause certain critical structural components of the ship to experience relatively high loading conditions. Hydrodynamic impacts or slamming due to the up and down motion of the hull, entry into wave crests and the consequent abrupt immersion of the ship into the water can also contribute to the gradual structural degradation of certain structural parts of the vessel [1].

All ships are subject to cyclic stresses during their operational lifetime. Cyclic stresses can gradually lead to fatigue crack initiation and subsequently propagation. Usually, fatigue crack initiation and propagation is restricted to structural components that sustain the loads arising from the various motions that the ship experiences while in service. Fatigue due to cyclic stresses can be divided into two main categories, low or high cycle fatigue, depending on the stress levels sustained. Corrosion can also contribute to structural damage causing deterioration of the structural integrity of the ship [2].

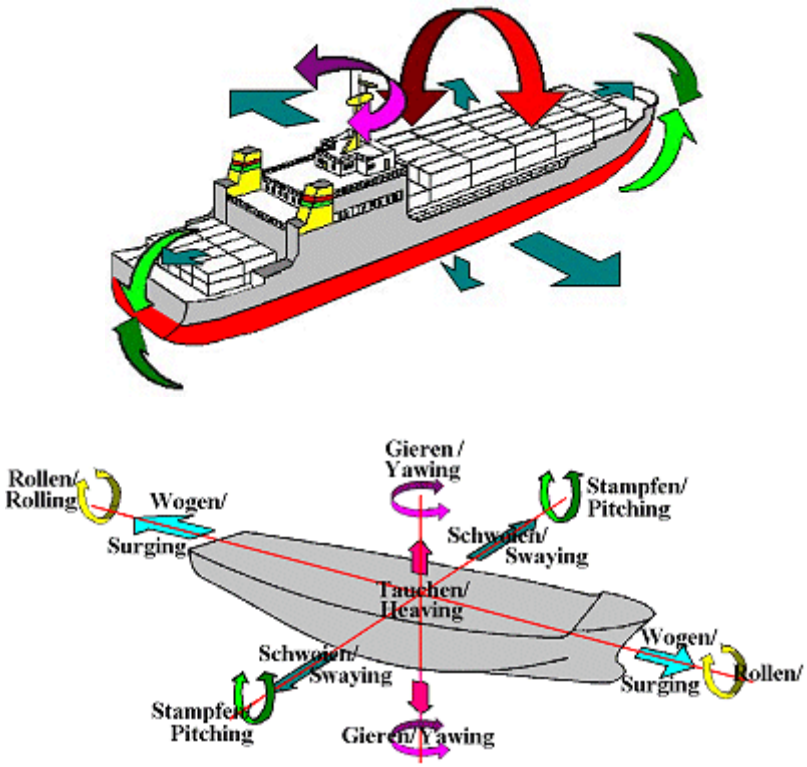

Figure 1: The schematics show the linear and rotational motions exhibited by ships [1].

Steel grades with superior mechanical properties have been of significant interest in shipbuilding applications to reduce the overall weight of the ship and minimise fuel consumption. Apart from better strength-to-weight ratio, improved resistance to crack initiation and crack propagation is desirable. Up to date, AH, DH and EH, which are three different grades for high tensile strength steels in ascending order of toughness and should have a minimum yield strength of 315 MPa, 350 MPa, or 390 MPa according to ASTM(American Society for Testing and Materials) standard A131M/A131M-08, have been widely applied in shipbuilding of every type of vessel. Conventional maritime steel grades offer a satisfactory level of structural reliability and are in compliance with the strict international standards applied in shipbuilding. However, in order to achieve the safety margin required, thicker plates need to

be used in comparison to other steel grades exhibiting better mechanical properties such as High Strength Low Alloy Steels (HSLAs).

Higher strength steel grades like the HY (High Yield Strength) steel were introduced in shipbuilding in the 1980s. However, the application of these steel grades has been largely limited to warship construction primarily due to the increased armour protection they offer against incoming ordnance. Accelerated cooling and tempering treatment is used during HY steel production to achieve the desirable microstructure and associated mechanical properties. HY steel is also used in submarines to enable the hull to sustain the immense stresses caused during deep diving while at the same time maintain the hull weight and thickness as limited as possible. The main problems associated with the application of HY steel in shipbuilding are the complexity of the manufacturing process and its weldability [3].

The greatest advantage of most HSLA steels is that they have better strength-to-weight ratio in comparison with conventional maritime steels [4].They have been extensively used in various offshore oil and gas applications, including pipelines (e.g. in Figure 2). However, whether the fatigue resistance of HSLAs is better than traditional ship steel grades remains unclear and is one of the topics researched within this study [5, 6].

Figure 2： A large-diameter pipeline [7].

Most studies considering HSLA steel for shipbuilding applications have been carried out in USA and Japan. HSLA steels are becoming more popular for the construction of warships in the US and general maritime vessels in Japan [6]. In the US HSLA-80 and HSLA-100 have been mainly used for the construction of warships rather than conventional ships [8].Compared with Japan, HSLA steels are relatively less applied in shipbuilding in Europe and research in this field should be increased [9]. In 2001, Sumitomo Metal Industries and Kawasaki Shipbuilding Corporation reported the development of the Fatigue Crack Arrester (FCA) steel. FCA is a dual HSLA steel exhibiting better fatigue initiation and crack growth resistance. FCA was one of the steels considered in this study [10, 11].

Structural reliability is crucial for the safe operation of all maritime vessels. There has been an increasing demand to ascertain the structural integrity of ships using cost-effective structural health monitoring systems [12]. Acoustic emission (AE) has been used for continuous monitoring of critical structures, such as gas pressure vessels and could be, in principle, applied for structural monitoring of critical load bearing parts of the ship.

1.2 Project aims and objectives

Disasters and accidents suffered in recent years (e.g. Costa Concordia, Sea Diamond, Prestige, Express Samina, Fedra, Braer, etc.) have highlighted some of the key weaknesses of the maritime industry leading to the implementation of a stricter regulatory framework [13-16]. The introduction of new regulations and standards on ship design, maintenance and inspection has increased the safety of maritime operations substantially. Nonetheless, the governments, the International Maritime Organisation (IMO), Classification Societies and industrial stake holders, continue to seek further improvements in vessel safety, reliability and operational efficiency [17].

The effective exploitation of vessels requires reliable and efficient operation. The recent changes in shipbuilding regulations have resulted in the use of thicker steel plates and hence heavier ships. This has led to higher fuel consumption and thus an increased cost of operation. Ship owners operate at a very small margin of profit. Therefore, any increase in operational costs is highly undesirable. As a result, the use of alternative steel grades with better structural performance particularly with respect to fatigue resistance has been high up in the agenda of the maritime industry as a whole.

The main objectives of this project were three-fold. Firstly, to identify suitable HSLA steels which could be used to replace conventional maritime grades in shipbuilding. Secondly, to carry out a quantitative comparison with reference to the mechanical properties of the various HSLA steels selected (X65 variants, FCA and S690) with conventional maritime steel grades (AH36 and DH36). Thirdly, to evaluate the applicability of acoustic emission testing for monitoring

crack growth qualitatively as well as quantitatively. The key findings of the experiments and analysis carried out are summarised and discussed in the following sections of this thesis.

2 Conventional Maritime and High Strength Low Alloy Steels

2.1 Conventional maritime steels

AH36 and DH36 are two conventional high strength steels which are commonly used in the maritime industry [18]. The maximum carbon content in these steels is 0.18% in weight. AH36 and DH36 steel plates are normalised, control rolled, and thermomechanically control processed before being supplied to shipbuilders [18]. These two steel grades have fine grain size as a result of certain alloying elements employed such as aluminium, vanadium, and niobium [18]. Shipbuilding requires relatively high yield strengths and thus the minimum yield strength tolerance for both AH36 and DH36 steel is 355MPa. Apart from high yield strength，steel grades used in shipbuilding, particularly for the construction of the hull and other critical areas, should exhibit high fatigue lifetime.

The hull is the most important structural part of the ship. It is continuously subjected to cyclic loading caused by waves, cargo loading and unloading and engine vibration. Hull fatigue is mainly attributed to high loading cycles induced by the ship's motion travelling through waves. Ship cyclic loading can reach as high as 10^8 cycles within a twenty-year service period [19].

2.2 High strength low alloy steels for maritime applications

Traditionally, mild steel has been the most widely used maritime structural material as it is fairly cheap. However, an obvious disadvantage of mild steel is that it has limited toughness and crack arresting ability[6]. The modern maritime industry shows high demand for steel grades with

high performance that permit the use of plates with lower thicknesses thus resulting in significant savings in fuel consumption and engine requirements. HSLA steel is a type of alloy steel with a more favourable ratio of strength to weight compared with conventional HY series of steels [4]. HSLA-80 and HSLA-100 were first employed by the U.S. Navy to replace HY-80 and HY-100 steels. HSLA steels are normally processed using thermomechanical control and direct quenching (DQ) as shown in Figure 3. In order to achieve high strength as well as toughness, several strengthening techniques including grain refinement, transformation strengthening, precipitation strengthening mechanisms can be employed. The addition of alloying elements like Mo, Ni, Cr and Mn in steels contributes to the improvement of the hardenability of the steel alloy. Other elements like Nb, Ti and V contribute to the refinement of the average grain size [20].

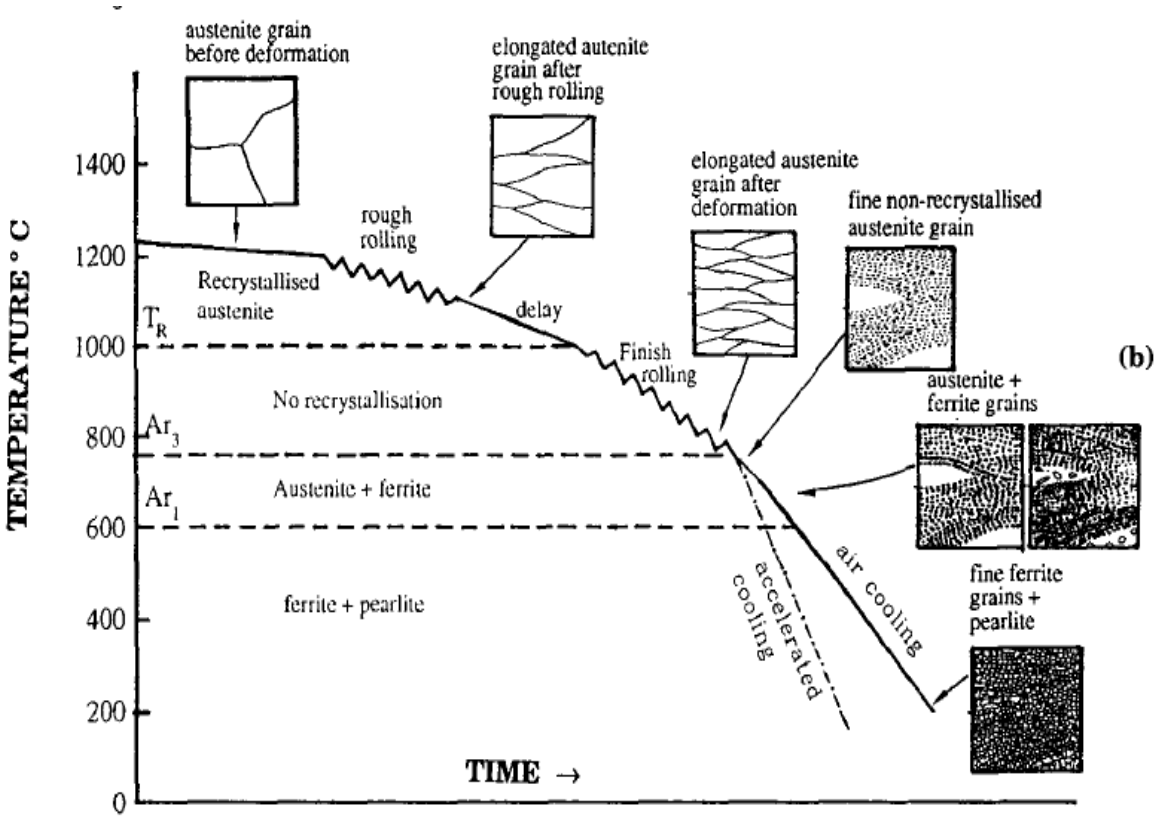

Figure 3: Schematic illustration of thermomechanical control process[7].

2.3 High strength low alloy steels considered in this study

In this study three different HSLA steel grades have been considered and compared against conventional AH36 and DH36 grades. The HSLA steel grades studied included X65 (three different variants – two procured from TATA steel and one procured from Arcelor Mittal), S690 (two different variants – procured from Thyssen and RUKKI respectively) and FCA (procured from SUMITOMO).

2.3.1 X65

The X-65 steel (Table 1) is a steel grade which is mainly used in oil and gas industry. This HSLA steel grade is already extensively used for offshore applications and thus has the corrosion resistance required in shipbuilding applications.

Table 1: Nominal composition (% by weight) of X65 steel and all values are the maximum amount allowed by the American Petroleum Institute (API) specification 5L [21] .

C_{max}	Mn	P	S	Si
0.26	1.40	0.03	0.03	_

X65 is extensively used in oil and gas industry for the construction of pipelines due to its high ratio of yield strength to ultimate strength. X65 tends to have either a ferrite-pearlite, ferrite-acicular ferrite or ferrite-bainite microstructure depending on the production method employed[22] . The strength of X65 steel is achieved through the use of appropriate hot rolling and cooling schedule and pre-straining of X65 has been seen to have a significant influence on

the measured engineering yield and tensile strength [22] .

2.3.2 S690

The S690 grade (Table 2) is an HSLA steel which has only occasionally been used by the maritime industry for constructing certain parts of the ship. The S690 grade has a higher carbon content than X-65 (approximately 0.17-0.18 in wt %).

Table 2: Nominal composition (% by weight) of S690 steel (the values are the maximum amount allowed according to EN 10025-6) [23] .

C	Si	Mn	P	S	N	Cu	Mo	Ni	Cr	V	Nb	Ti
0.2	0.8	1.7	0.02	0.01	0.015	0.5	0.7	2	1.5	0.12	0.06	0.05

Depending on the production method S690 grades may have a bainitic or martensitic microstructure. The number ”690” refers to the minimum yield strength of this steel grade. During the production of the S690 grade thermomechanical rolling together with accelerated cooling and tempering is required [24]. Fatigue tests carried by De Jesus et al. on S690 and S355，both of which are specified in the EN 10025 standard，showed that S690 has superior fatigue crack initiation resistance than S355 [24, 25] .

2.3.3 Fatigue Crack Arrester Steel

The Fatigue Crack Arrester (FCA) steel grade is an HSLA steel developed by Sumitomo for shipbuilding. FCA has been reported by Sumitomo to exhibit better fatigue initiation resistance

as well as longer crack growth resistance compared with conventional ship steels. FCA steel has a mixed microstructure which consists of ferrite and bainite. The interface between harder bainite phase and ferrite phase can detour the fatigue crack growth path eventually being arrested by the harder bainite, as shown in Figure 4. Thanks to its improved resistance to fatigue damage initiation and propagation FCA steel can be applied in ship details subjected to high cycle fatigue conditions [10].

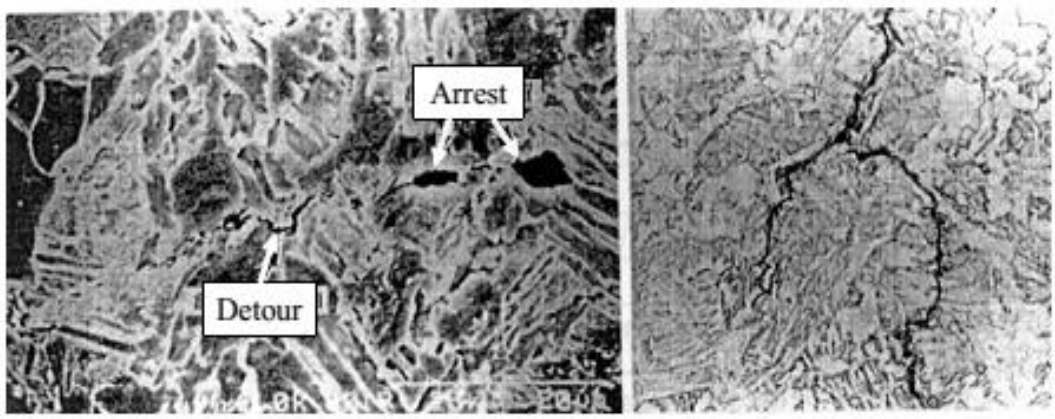

Figure 4: Fatigue crack growth behaviour in FCA steel [10].

3 Fracture

3.1 Steel strengthening mechanisms

There are several methods of strengthening steels, including transformation strengthening, grain refinement, solid solution strengthening, precipitation hardening and work hardening. Maritime and HSLA steels have more than one phases present. Transformation strengthening is achieved by controlling the dispersions of phases present other than the ferrite matrix [26].

Grain refinement can not only improve the strength but also increase the toughness of maritime and HSLA steels [27]. Alloy design and processing methods have an important influence on grain refinement as they can influence the transformation temperature. Grain refining can be achieved by lowering the transformation temperature of the steel through appropriate alloying additions. For HSLA steels, nickel, phosphorus, copper and silicon are commonly used elements for getting fine pearlite. The Hall-Petch equation below can be used to characterise the relationship between the flow stress and mean grain size for steels [28].

Equation 1

$$\sigma_o = \sigma_\tau + K_0 \times d^{-\frac{1}{2}}$$

Where σ_0 is the yield strength in MPa, σ_τ is the yield strength of a single crystal in MPa, K_0 is the experimental constant in $MPamm^{-1}$ and d is the mean grain size in mm.

Solid solution strengthening can be achieved either through interstitial or substitutional solid solution through the addition of appropriate alloying elements which diffuse in the crystal

structure of the matrix [29]. Substitutional and interstitial solid solution examples are shown in Figure 5.

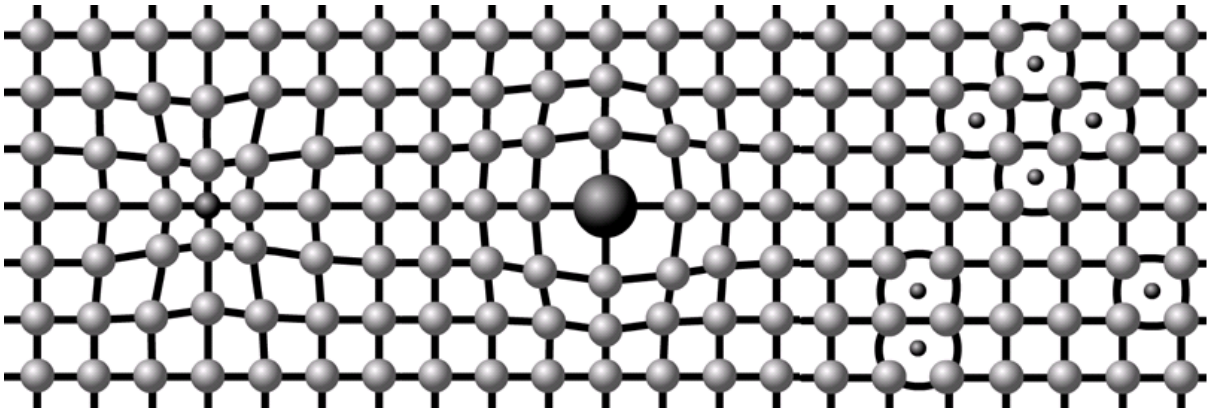

Figure 5: Illustration of interstitial and substitutional solid solution [30].

Work hardening is caused by the interactions between dislocations during the deformation process, which makes the flow stress of steel increase at a certain strain level. The flow stress is closely related to the effective free dislocation length between pinning points. The shorter the average length of the free dislocations is, the higher flow stress will be required to sustain plastic deformation. Although work hardening can increase the strength of steel, it can reduce the toughness and ductility of the steel [29].

3.2 Stress and strain

Structures in real life are normally subjected to certain loads and moments. The stress magnitude depends on the loaded area. The larger the area is, the smaller the stress will be. In most cases, the force F applied on a specific area A of a structure can be decomposed into two parts, namely a shear force and a normal force giving rise to shear and normal stresses as shown

in Figure 6.

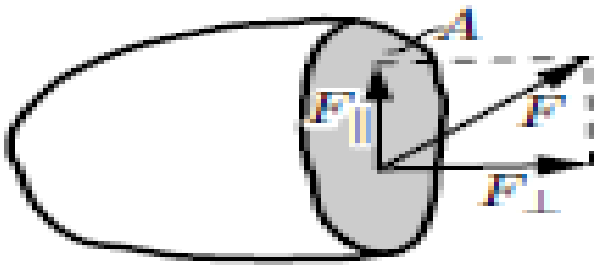

Figure 6: Mixed stress applied on a structure [31].

Structures subjected to external stress will produce linear corresponding displacements, which can be characterised by Hooke's Law. Hooke's law is only applied for small strains and describes the linear-elastic behaviour of the structure. For uniaxial loading, Hooke's law is described mathematically using the following equation.

Equation 2

$$\sigma = E\varepsilon$$

Where E represents the Young's Modulus related to the stiffness of the material in GPa and ε is the strain exhibited.

A larger Young's Modulus means a smaller elastic strain under the same load [31]. Steels for relatively low strains exhibit an elastic behaviour. This means that the overall strain can return to zero when the stress is removed. When stress continues to increase beyond a critical magnitude called elastic limit or yield stress in the stress-strain curve, permanent plastic deformation will occur [32]. The schematic in Figure 7 shows the various stages of deformation experienced by the crystal lattice of a metal as the application of external stress increases. Once

the elastic limit is exceeded plastic deformation occurring is permanent and will remain even after the stress has been removed [33].

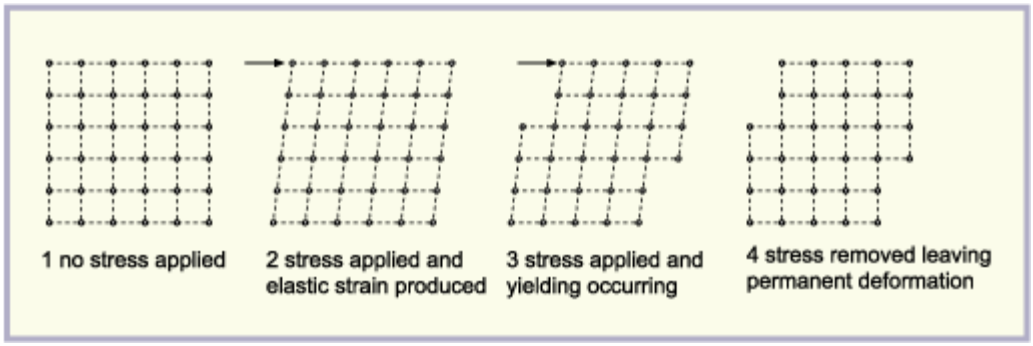

Figure 7: Schematic diagram showing the stages of deformation experienced by the crystal lattice of a metal with increasing external stress.

3.3 Typical stress-strain curve

A typical stress-strain curve for mild steel under tensile loading is shown in Figure 8. In the stress-strain curve, the section between C (upper yield point) and D (lower yield point) an increase in the strain can be seen without an obviously rising stress level.

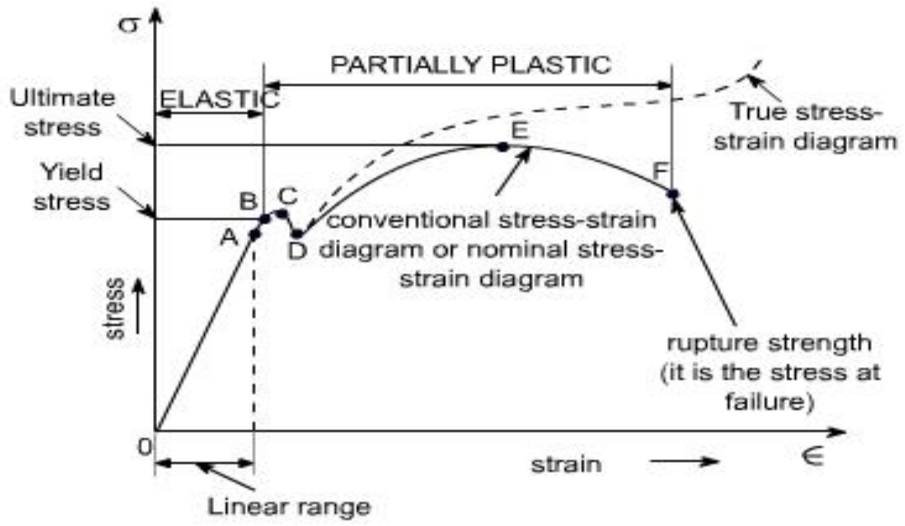

Figure 8: A typical tensile test curve for mild steel [34]

3.4 Ductility

A material's ability to bear plastic deformation is defined as ductility. It is described quantitatively by the following equation [32]:

Equation 3

$$\varepsilon\,\% = \frac{Lf}{Lo} \times 100$$

Where L_f is the final elongation and L_0 is the original elongation in mm.

Brittle materials are normally referred to those which fail before a maximum elongation of 5% is achieved. Most steel grades exhibit a significant degree of ductility at room temperature. Ductility decreases as the temperature becomes lower. The ductility of steel alloys also decreases as the amount of carbon increases due to the higher percentage of cementite forming in the microstructure. However, the higher percentage of cementite present also leads to an increase in the overall strength of the steel [32].

3.5 Toughness

Maritime steel grades can absorb energy up to a certain limit which is dependent on their toughness. Once the toughness limit is exceeded then crack initiation will occur. If the loading levels are sustained then the initiated crack will continue propagating unless it is arrested by a harder phase in the microstructure. Crack propagation will accelerate until the crack reaches a critical size at which it becomes unstable [35].

Unless a steel plate contains already a critical manufacturing defect from which cracking can initiate, then any crack initiation will take place after an appreciable number of loading cycles as long as stresses do not exceed the design parameters as shown in Figure 9. In maritime steels, after a crack initiates, it will subsequently propagate further with every loading cycle. Once critical crack size is reached, the affected component will fail abruptly in a brittle fracture mode.

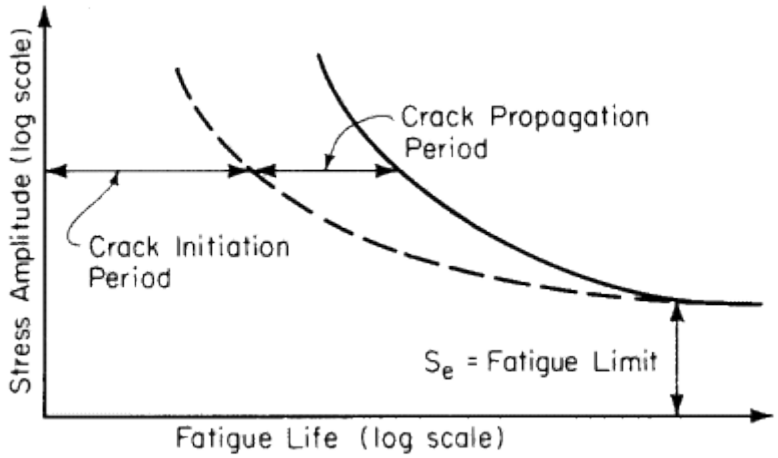

Figure 9: Crack initiation and propagation stages of fatigue lifetime [36].

3.6 Intergranular and transgranular

Crack propagation can take place either through the grains of the steel in a transgranular fashion or along the grain boundaries in an intergranular mode. In naval steel grades such as the AH36 and DH36 cracks normally grow in a transgranular mode moving through the pearlite colonies. However, in the areas where corrosion is involved then cracks can propagate in an intergranular mode. Examples of transgranular and intergranular crack propagation are shown in Figures 10 and 11.

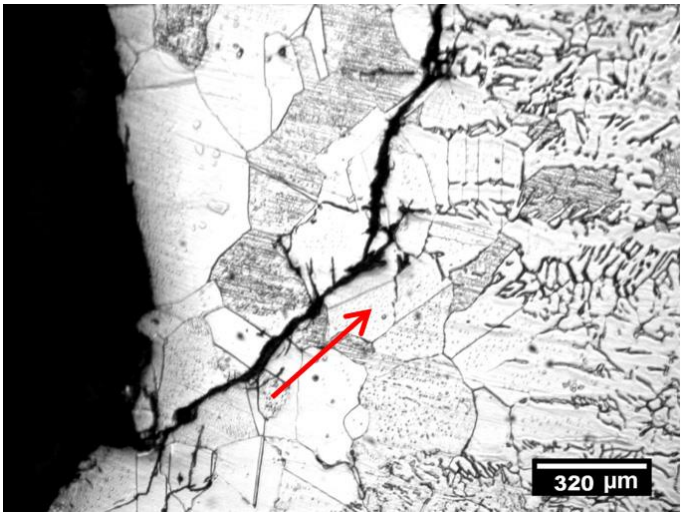

Figure 10: Optical micrograph showing transgranular crack propagation [37].

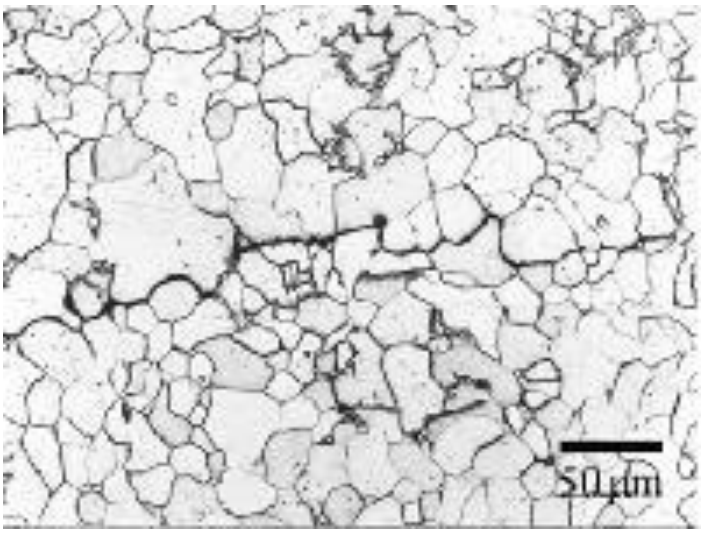

Figure 11: Optical micrograph showing intergranular crack propagation [38].

3.7 Basic fracture modes

The catastrophic fracture of the ship's hull or any other critical load bearing component while at sea may result in complete loss of the vessel. Ductile fracture and brittle fracture are the two modes of fracture exhibited by engineering materials. During ductile fracture a material absorbs

an appreciable amount of energy before it breaks. However, during brittle fracture, a material will break only after only a small amount of energy has been absorbed [35]. Figure 12 shows examples of both fracture modes macroscopically.

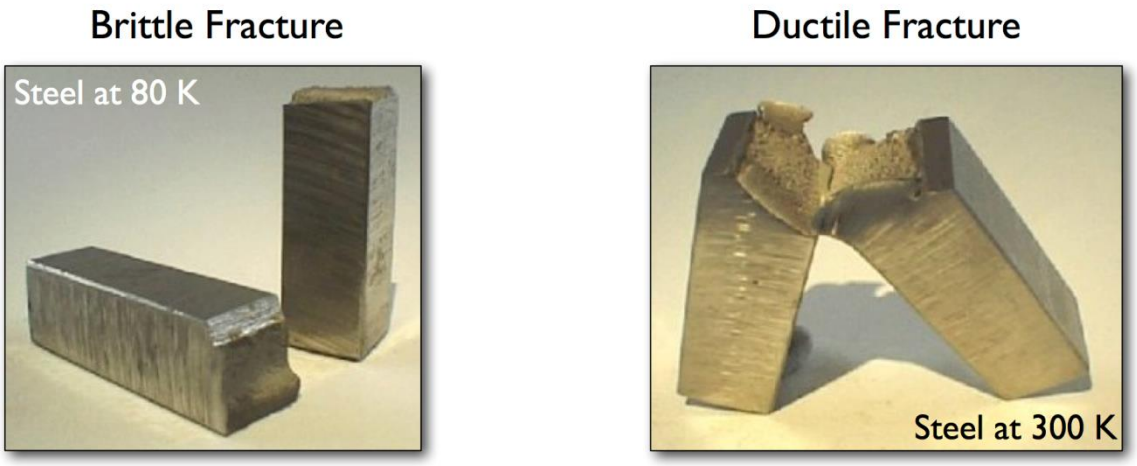

Figure 12: Brittle and ductile fracture of steel at low temperature(80K) and high temperature(300K) respectively [39].

Steel grades exhibiting ductile failure show cup-and-cone fracture surfaces. The central areas of the fractured surface have a fibrous appearance related to the plastic deformation sustained before failure occurs. The fractured surface of a ductile metal after uniaxial tensile or shear loading consists of a large amount of spherical dimples, as shown in the SEM image in Figure 13. Brittle fracture occurs through the separation caused by the breaking of the atomic bonds along a specific crystallographic plane. This is also called cleavage fracture. As cracks propagate through particular crystallographic planes, the cleavage facets are relatively flat. A shiny appearance can be observed due to the high reflectivity of a cleavage facet. Cleavage fractures are normally encountered under low temperature conditions and high strain rates and can be seen in body-centered–cubic alloys such as steel alloys [40].

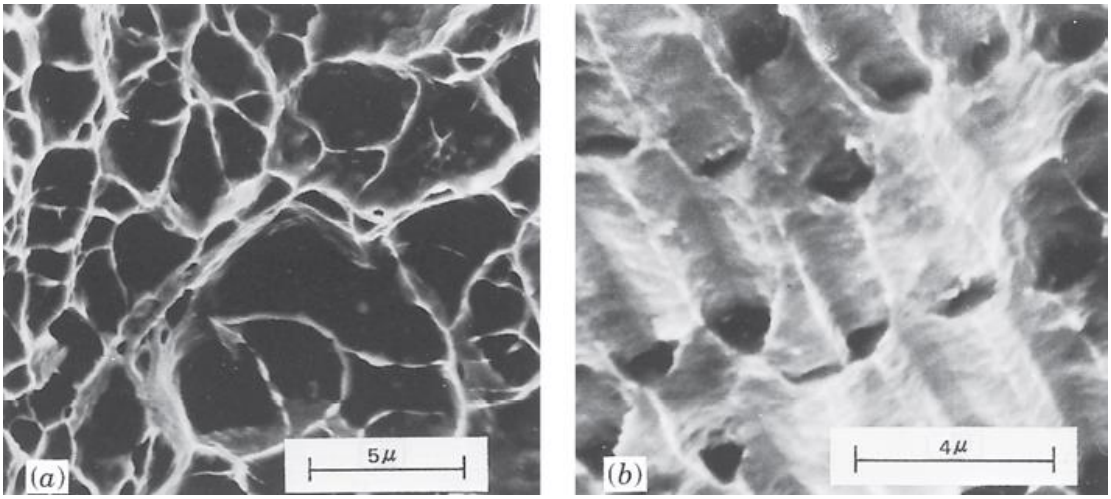

Figure 13: (a) Dimples caused by axial tensile loading, (b) dimples caused by shear loading[35].

It is important that the steel grades used in shipbuilding exhibit an acceptable level of ductility in order to avoid the occurrence of catastrophic brittle failures. Ductility should be retained throughout the operational temperature of the vessel to avoid catastrophic failures such as those experienced by Liberty ships. The steel grade used for building Liberty vessels experienced ductile-to-brittle transition at lower temperatures resulting in large cracks to initiate at stress concentration points to propagate unimpeded for large distances as shown in the photograph of Figure 14.

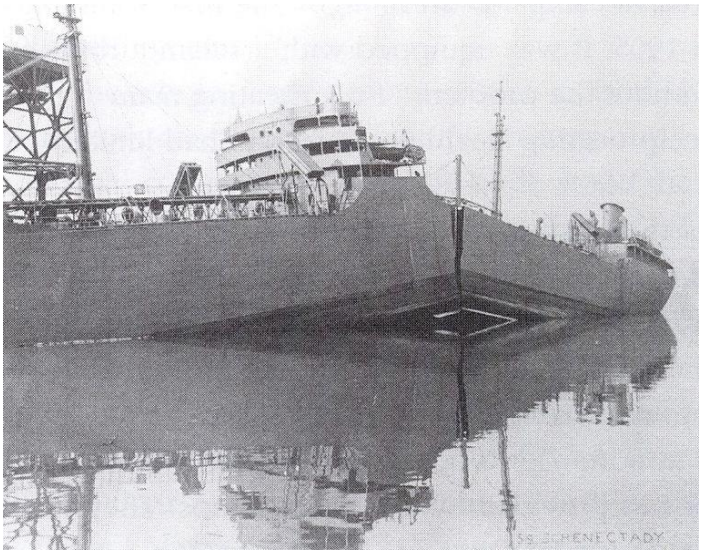

Figure 14: Photograph of the S.S. Schenectady Liberty ship after brittle failure due to ductile to brittle transition of the steel grade used [41].

Ductile-to-brittle transition of the steel used in R.M.S. Titanic has also been blamed for the extent of the impact damage caused after the ship struck on the iceberg. If modern naval steel grades had been used on R.M.S. Titanic, it is highly unlikely that the impact damage would have been such as to result in the sinking of the vessel.

The photographs in Figure 15 show the behaviour of modern naval steel grade in comparison with the steel grade used for the construction of the R.M.S[42]. Titanic. Instead of deforming after collision with the iceberg, the hull plates fractured, failing to absorb the impact energy. Figure 16 shows a photograph of the R.M.S. Titanic leaving the Irish port of Queenstown, the last port the ship visited before sinking in mid-Atlantic after the iceberg collision.

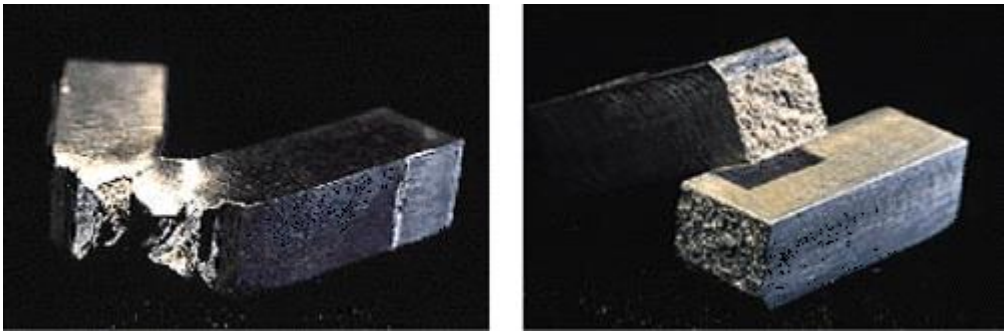

Figure 15: Photographs showing the results of Charpy testing on modern naval steel(left) and the steel grade used in R.M.S. Titanic (right) [42].

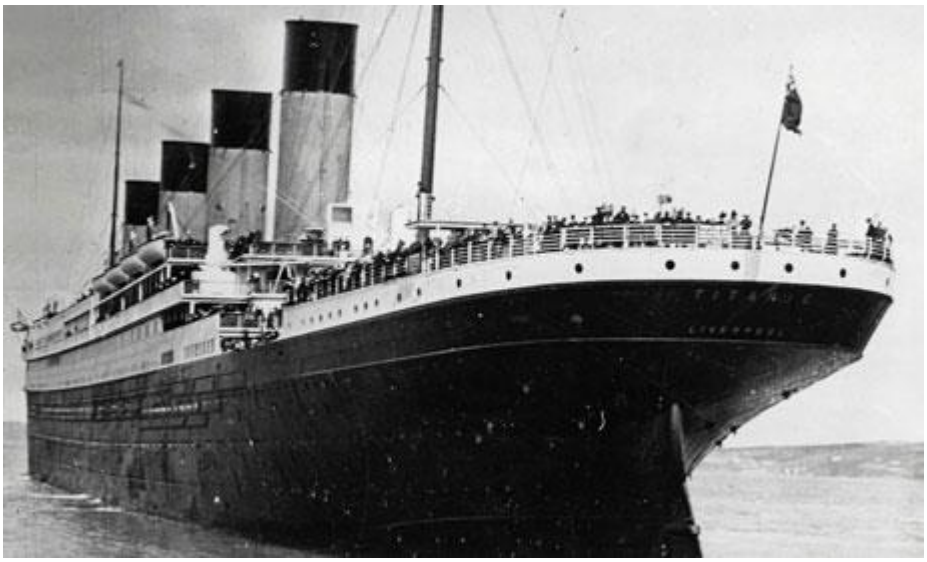

Figure 16: Photograph of the White Star Liner R.M.S. Titanic as it pulls out of Queenstown four days before it sunk (photograph is courtesy of newspaper The Guardian, 6 December 2010) [43].

Modern naval steel grades are required to exhibit ductile behaviour at temperatures as low as -60°C. For this reason the capability of naval steels in absorbing energy during impact events is assessed during Charpy tests which are carried out at a range of temperatures above and below 0°C. The graph in Figure 17 shows the absorption energy, brittle fracture surface ratio with temperature [44].

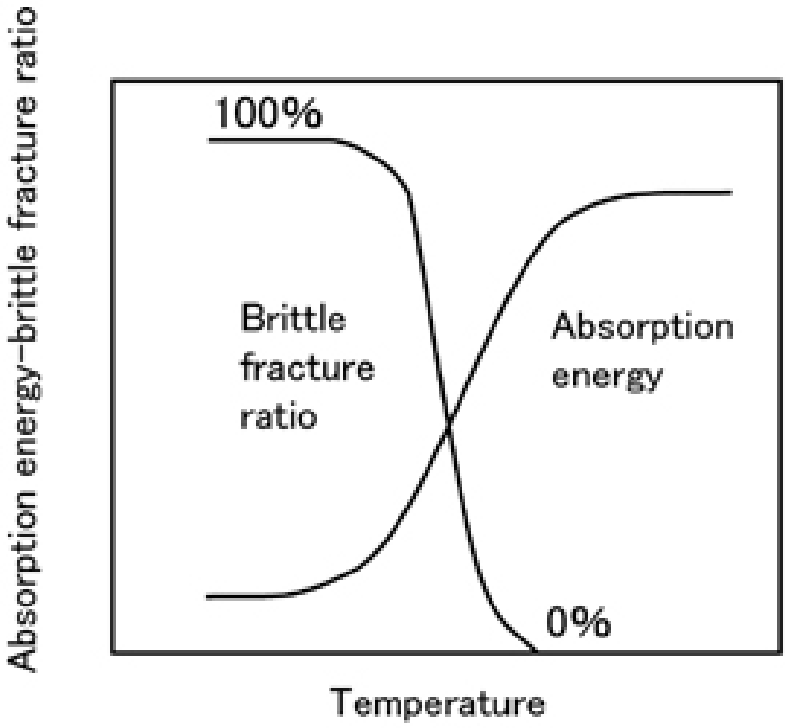

Figure 17: Absorption energy and brittle fracture surface ratio with temperature [44].

3.8 Stress intensity factor

Stress intensity factor is a critical parameter which is related to the stress level near a crack tip or stress concentrator. The stress intensity factor is described by Equation 4 below.

Equation 4

$$K_I = \sigma\sqrt{\pi\alpha}\mathrm{Y}$$

In the equation, the subscript "I" means the mode I crack displacement. "Y" is the geometry factor. Structures with different geometries have different "Y" values. σ represents the external stress applied in the structure. When the external stress σ increases, the stress intensity factor

will also increase. When K_I increases to a critical value, crack will start to propagate.

The critical stress intensity value is designated as fracture toughness [31]. Fracture toughness (K_C) is a parameter used to measure the resistance to crack growth of a material. In linear elastic fracture mechanics, the value of K_C decreases as the specimen thickness increases， as illustrated in Figure 18.

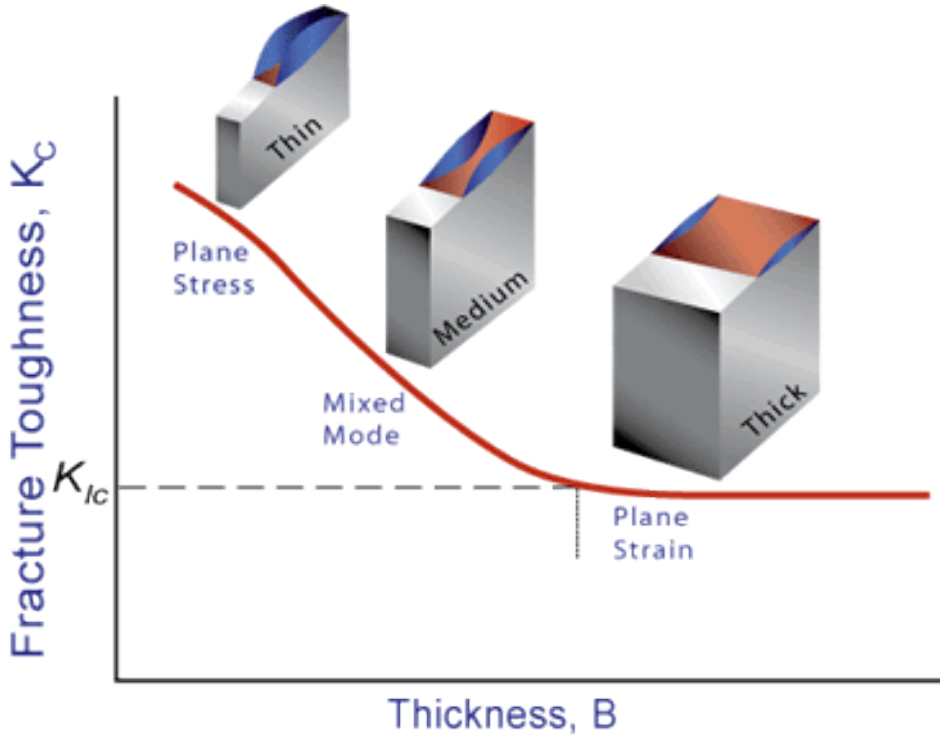

Figure 18: Effect of specimen thickness on fracture toughness [45]

Zhong et al.(2005) showed that HSLA steels with higher fracture toughness can tolerate more serious defects and exhibit lower fatigue crack growth rate compared with conventional mild steels [46].

When the thickness of a test specimen is much larger than the crack dimension, a plane strain condition occurs and in this case, fracture toughness which is independent of specimen

thickness is defined as plane strain fracture toughness (K_{IC}). K_{IC} is conservative as it represents the lower bound fracture toughness. K_{IC} can be influenced by many factors of which microstructure, temperature and strain rate are the three most influential ones. Normally a microstructure with smaller grain size exhibits higher fracture toughness. Increasing temperature and decreasing strain rate can also lead to higher fracture toughness.

The three-point bending single-notched (SEB) specimen is one of the preferred specimens used for K_{IC} testing. According to ASTM regulation E1820, in order to obtain a valid K_{IC} value, the two following requirements need to be met:

Equation 5

$$B, a \geq 2.5\left(\frac{K_Q}{\sigma_{ys}}\right)^2$$

Where B is the thickness of the specimen, and α is the crack length, and σ_{ys} is the material yield stress.

Equation 6

$$P_{max} \leq 1.1P_Q$$

Where P_{max} is the maximum load that the specimen sustained and P_Q is the force determined by the 95% offset criterion.

.

4 Fatigue in Ships

4.1 **Importance of fatigue**

Steel grades used in ship construction, especially the ship hull and other critical areas, should possess high fatigue lifetime. The ship's hull is subjected to different kinds of cyclic loadings from the ship's motion in waves, internal stress changes caused by ballast, wave impact and vibration produced by the engine or propellers.

Cyclic loading caused by waves are regarded as a major stress factor which can result in fatigue initiation and propagation in the hull structure as well as other load bearing components of the vessel. Figure 19 shows the complete hull failure of the New Carissa resulted from wave cyclic loading in 1999.Wave cyclic loading reaches a fairly high number of load cycles during the normal operational lifetime of a vessel [19].

Figure 19: Hull failure of the New Carissa subjected to excessive wave cyclic loading [47]

4.2 Cyclic stress mode

Fatigue failure occurs when structures are subjected to cyclic stress or strain and there is little plastic deformation related to the failure. In general, there are three possible cyclic stress modes; the reversed stress cycle, repeated stress cycle and random stress cycle [35]. The schematic in Figure 20 shows the three different cyclic stress cycles.

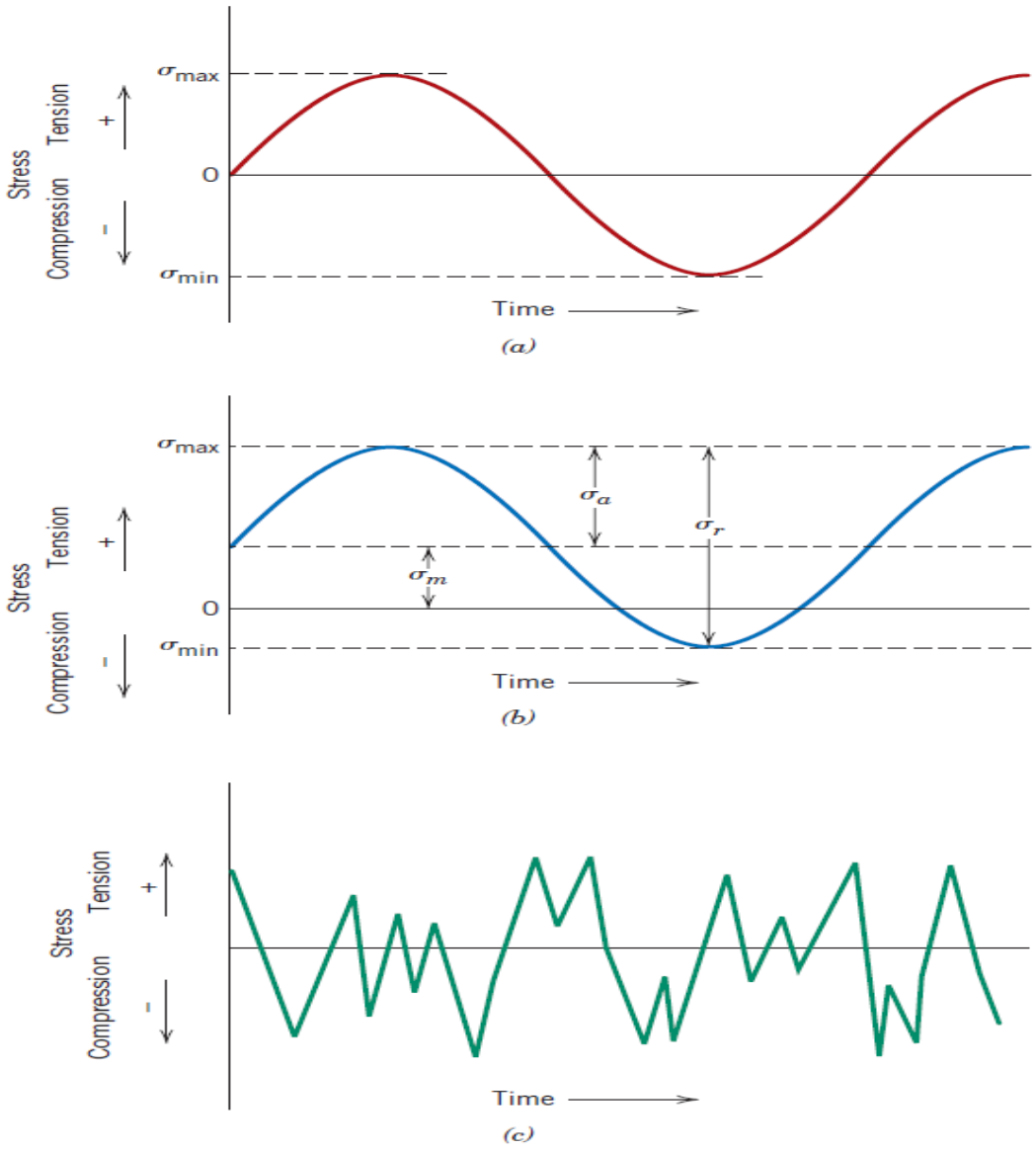

Figure 20: Three different cyclic stress modes.(a)reversed stress cycle (b) repeated stress cycle(c)random stress cycle [35].

4.3 Factors influencing fatigue life

The factors that influence the fatigue lifetime of a steel structure can be divided into four major types; a) the mechanical properties of the steel, b) structural characteristics, c) loading modes and d) environmental conditions [48].

4.3.1 Material properties

Different materials exhibit different fatigue resistance. Materials of the same type can also have different fatigue strength, because they may undergo different heat treatment process which may result in distinct microstructural features that influence the materials' fatigue resistance. Figure 21 shows fatigue crack growth behaviour at the heat-affected zone for specimens (AISI 4140 steel welded using the shielded metal arc process) normalised at 1200 °C for 5 and 10 hours and as-received condition.

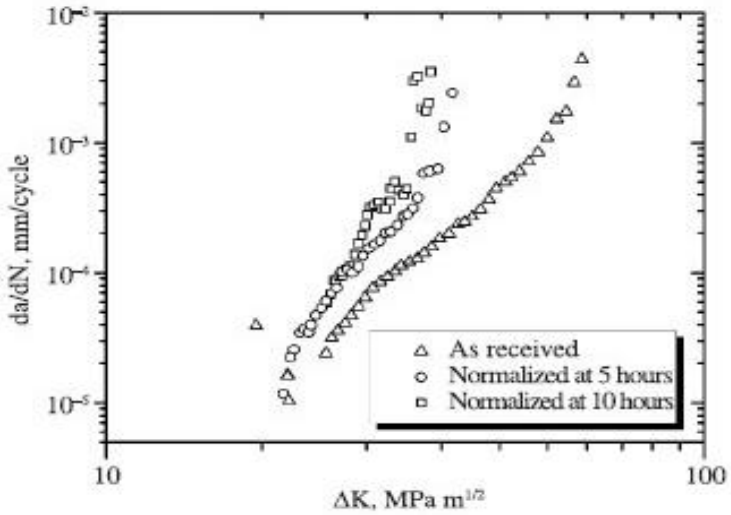

Figure 21: Fatigue crack growth property for the heat-affected zone normalized at 1200 ℃ for different time periods [49].

An example of the effect of the microstructure in the fatigue properties is the FCA steel where the presence of the harder bainite makes crack arrest become possible[10].

4.3.2 Structural characteristics

The stress intensity factor is determined by the structural characteristics and geometry of the component, thus influencing its total fatigue life. For example, different pre-cracking lengths will correspond to different shape factor values for specimens with the same geometry and hence the fatigue crack growth rate in Paris-Erdogan Regime will be different. It is inevitable that occasionally a defect will be induced during the manufacturing process of a material or component. Such manufacturing defects have a detrimental impact on fatigue lifetime and account for the wide scatter in fatigue results.

Welds have a significant influence on the fatigue strength of structures. In weld joints, some residual stress still exist, which can influence the fatigue life of welded structures. The residual stress can be changed by stress peaks and have a relaxation during the fatigue loading process [48].

4.3.3 Loading modes

Zero mean stress during fatigue test leads to longer lives compared with tensile mean stress. Figure 22 show the relationship between mean stress and stress amplitude for a given number of cycles to failure.

Many methods have been used to characterise the influence of mean stress on fatigue lives of steel structures. Kujawski and Ellyin (1995) put forward a unified method to describe the effect of mean stress on fatigue threshold [50]. In addition, fatigue crack growth rates are different for the same cycles under variable amplitude and constant amplitude loadings, which are caused by the load interaction effects. Load interaction effects are determined by a combination of various factors like microstructure, material properties and specimen geometry [51].

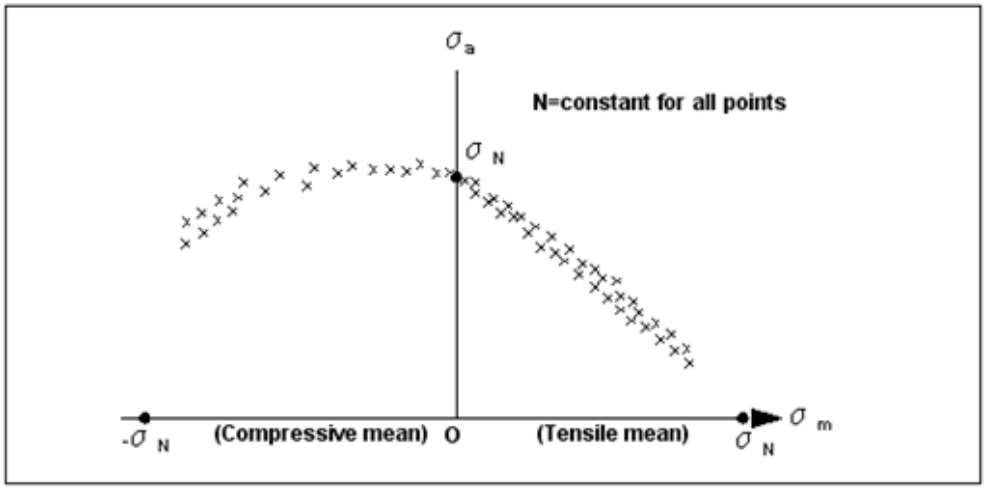

Figure 22: The Influence of mean stress on fatigue data for a given number of cycles to failure [52].

4.3.4 Environment

Temperature and corrosive substances are two major factors which can influence the fatigue lives of steel structures. At high temperature, the influence of mean stress on the fatigue behaviour of steel structures is quite complicated, which is caused by the combined effects of

fatigue, creep and environment. The linear elastic stress intensity theory does not apply any more, as a considerable amount of plasticity is induced. As the temperature increases, the critical crack size will increase due to the fact that fracture toughness increases with rising temperature. Chemical pitting tends to take place at inclusion sites in the initial stage of corrosion fatigue for steel structures. There are three stages in total during corrosion fatigue process, namely pit formation, short crack development and long crack development [53]. Figure 23 shows the influence of corrosion environment on fatigue behaviour.

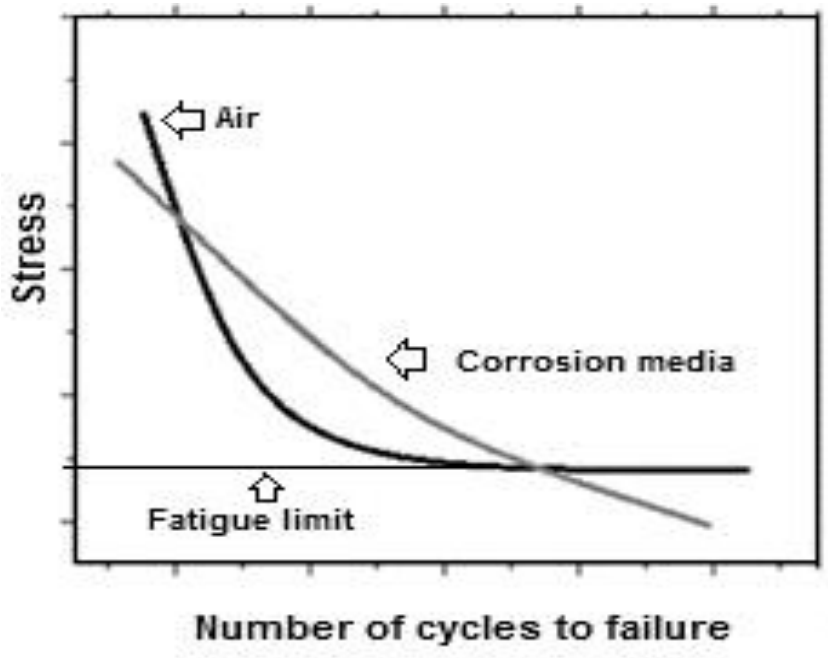

Figure 23: S-N curves in air and corrosive environment [54].

In maritime applications the effect of salt water and fouling are the most important environmental parameters.

4.4 S-N curve

The S-N curve is often used to describe the relationship between the stress amplitude and the fatigue lifetime of material. Materials subjected to the reversed cyclic stress condition have the shortest fatigue lifetime. Ferrous materials are generally assumed to have an infinite lifetime when the cyclic stress range is below a certain value on the S-N curve, which is designated as the fatigue limit of the materials [55] . For carbon and low alloy steel, the S-N curve, which is plotted as linear stress versus logarithmic time, shows a straight sloping part at low cycles. At high cycles the curve sharply changes to a straight horizontal line [56] . Examples of S-N curves are shown in Figure 24.

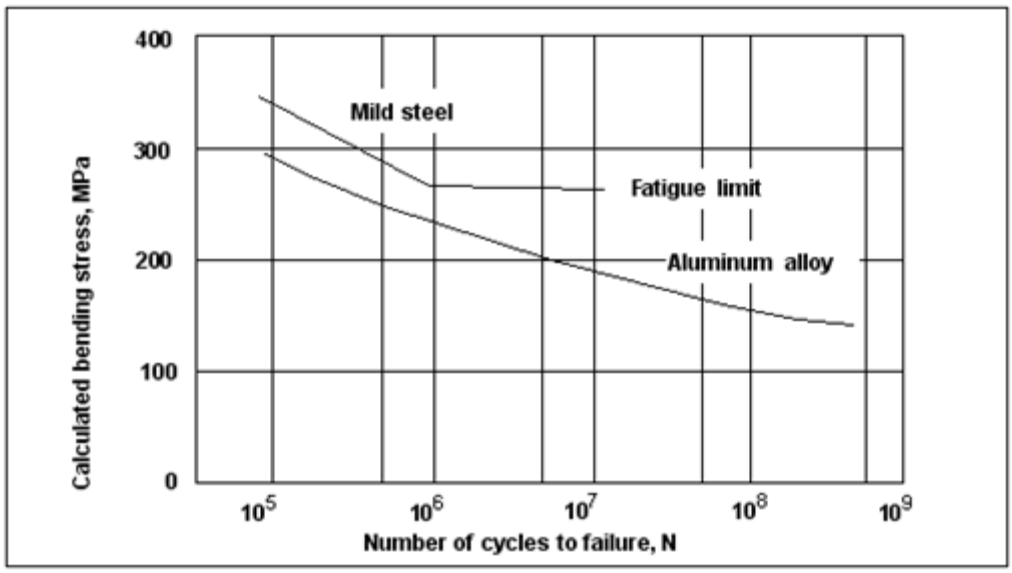

Figure 24:Typical S-N curves for Ferrous and Nonferrous Metals [52] .

Fatigue failure won't happen as long as the cyclic stress range is below the fatigue limit, regardless of the number of loading cycles. In contrast, failure will take place if the cyclic stress range is above the fatigue limit and the entire fatigue life can be predicted based on the S-N curve. The extent to which the cyclic stress range surpasses the fatigue limit in each loading cycle determines the number of cycles the material can survive. Fatigue crack will grow at an

increasing rate after its initiation until the critical crack length is reached at which unstable fracture will happen. The resistance of a structure to crack growth mainly depends on the cyclic stress range and R-ratio. Thus, without considering the influence of other unknown cracks, the number of loading cycles that the structure can withstand also depends on the two factors. The maximum stress that a structure can sustain is determined by the crack length. When the crack length exceeds a certain value, final fracture will happen immediately as shown in Figure 25 [57] .

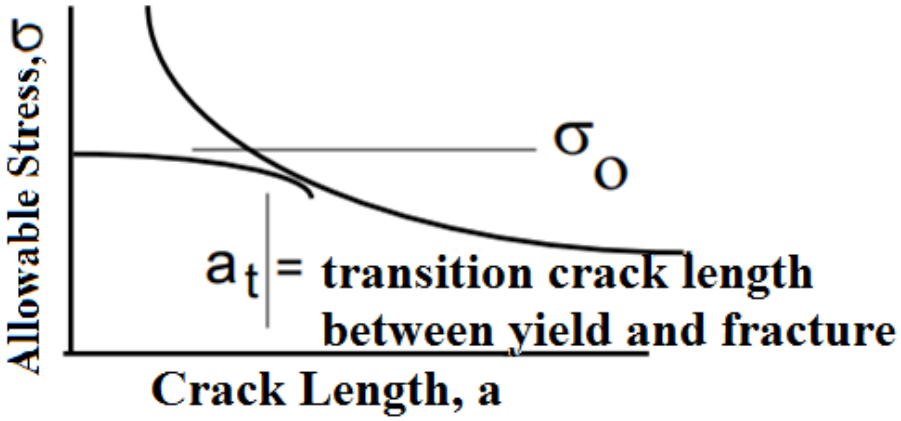

Figure 25: The allowable stress versus crack length [57].

4.5 Fatigue crack growth rate

Fatigue crack growth rate is an important parameter which is used to characterise the fatigue resistance property of a material [58]. There are three different distinct stages in fatigue crack growth. In the first stage, the crack starts to grow when ΔK reaches a certain value called threshold $\Delta K_{Threshold}$ and then the crack grows fairly slowly with a rapid changing rate. $\Delta K_{Threshold}$ refers to ΔK which corresponds to a crack growth rate of 10^{-7}mm/cycle, according to ASTM regulation E647.In the second stage， the fatigue crack growth rate satisfies the Paris-

Erdogan Law. In this regime, the crack growth rate can be of the order of 10^{-6}-10^{-3} mm/cycle. Finally, at the third stage the crack becomes unstable and crack growth progresses in an extremely high speed before brittle fracture eventually takes place. The crack growth rate can be above 10^{-3} mm/cycle [59, 60]. Figure 26 shows the effect of fracture toughness on the governing failure mechanism[61]

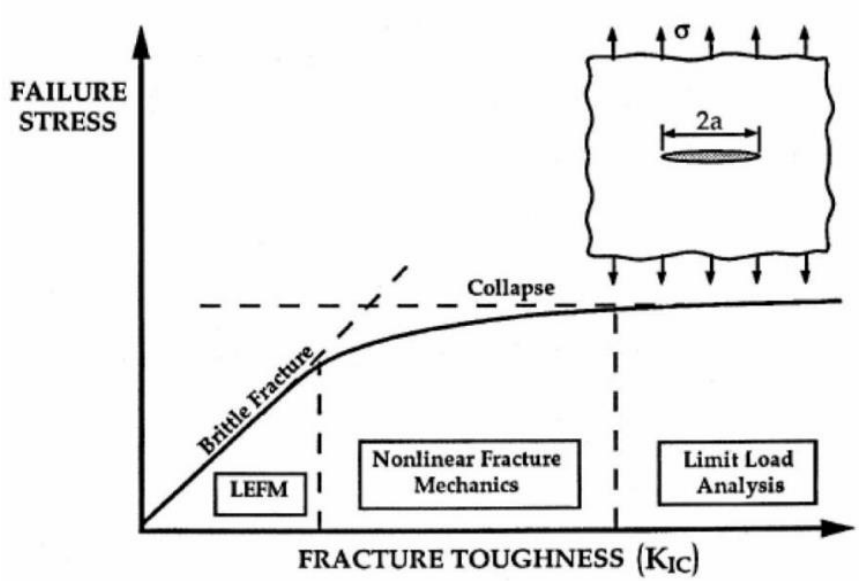

Figure 26: Effect of fracture toughness on the governing failure mechanism[61]

The three and four-point bending specimens are traditionally used specimens for crack growth rate measurements. During three and four-point bending tests the crack growth needs to be monitored with respect to the number of the loading cycles applied. At the same time the stress intensity factor ΔK also needs to be calculated.

4.6 Paris-Erdogan Equation

The Paris-Erdogan Law, describes the relationship between crack growth rate (da/dN) and the stress intensity factor range (ΔK). The Paris-Erdogan Law is described mathematically by the

following equation:

Equation 7

$$\frac{d\alpha}{dN} = C\Delta K^m$$

C and m are material constants. The equation does not apply to very low ΔK values near the value of $\Delta K_{Threshold}$, where crack initiation occurs, and near final failure when the crack has become unstable and ΔK approaches the fracture toughness. A typical curve of da/dN versus ΔK, shown in Figure 27, can be obtained by taking the logarithm of both sides in the equation.

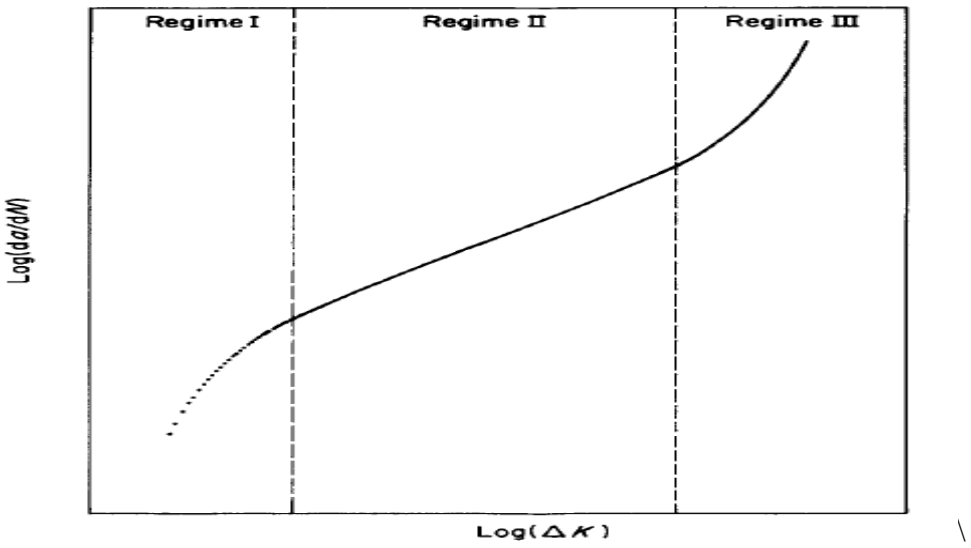

Figure 27: A typical fatigue crack propagation plot showing the three different regimes of crack growth propagation during cyclic loading [59].

4.7 Influence of R-ratio on fatigue behaviour

R-ratio, which is defined as the ratio of the minimum stress to the maximum stress during cyclic loading process as shown in Equation 8, has a significant influence on fatigue crack growth rate [62].

Equation 8

$$R = {\text{Kmin}}/{\text{Kmax}} = {\sigma\text{min}}/{\sigma\text{max}}$$

The influence of R-ratio on the fatigue life of a component structure can be significant. Pereira et al. (2008) obtained the S-N curves under constant stress amplitude with three different stress ratios of 0, 0.15 and 0.3 respectively, as displayed in Figure 28. It shows that under a constant maximum stress, the fatigue life increases with R-ratio, whereas under the same stress amplitude, an increase in R-ratio leads to a decrease in the fatigue life[63]. Thus, fatigue life can be improved by changing the R-ratio under certain circumstances.

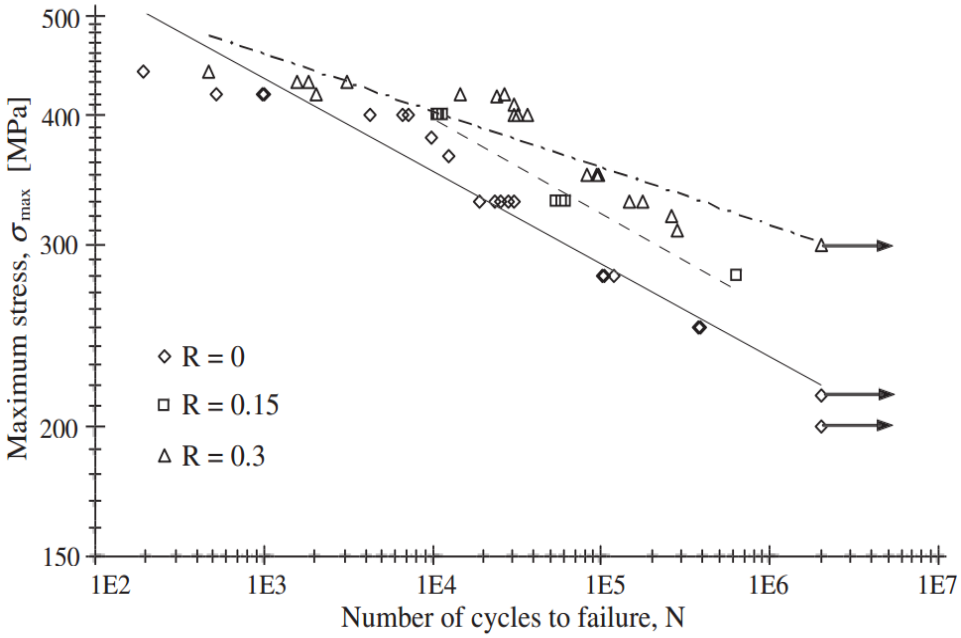

Figure 28: S-N curves for the component with three different R-ratios employed[63]

El-shabasy and Lewandowski (2004) studied the effect of R-ratio on the fatigue crack growth behaviour of a fully eutectoid pearlitic steel. They found that increasing R-ratio can reduce the threshold value as well as increase the Paris Law slope in the fatigue test at a particular temperature. In their study, they employed three-point bending tension-tension test to obtain the whole fatigue curves for the specimens. The load mode was sinusoidal and the cyclic frequency was set at 20 Hz. They observed the fracture surfaces examples of which are shown in Figure 29 over the range of ΔK using SEM and found that as ΔK increases, the percentage of cleavage fracture on the fracture surface also increases [64].

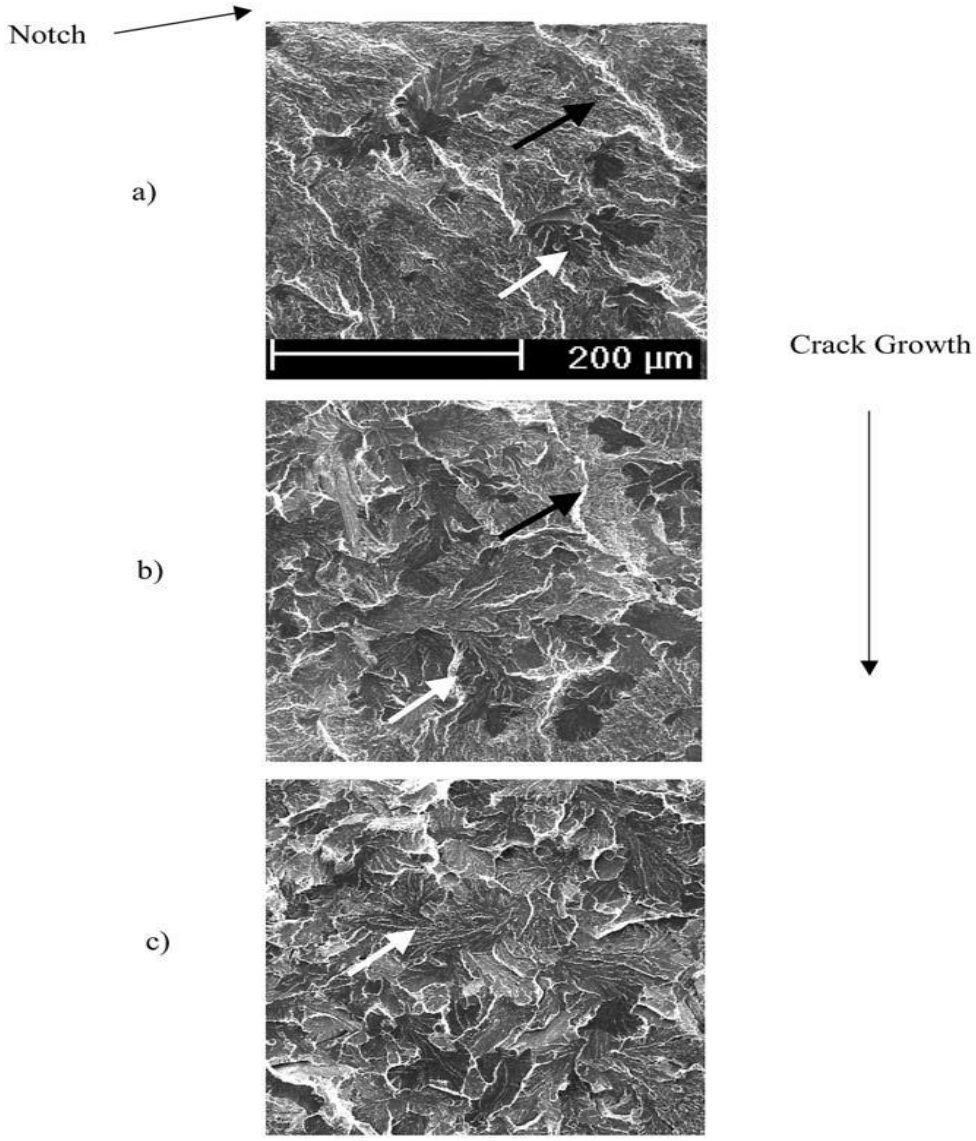

Figure 29: Typical SEM images of fracture surfaces of pearlitic steel at three different fatigue regimes: a) Near threshold regime, (b) Paris equation regime (c) Critical regime, R-ratio=0.4 and T=-125℃.White arrows represent cleavage zone, whereas black arrows denote fatigue fracture [64].

4.8 Fatigue of ship steel

There are several fatigue crack growth mechanisms in steel like striation formation, void coalescence, intergranular failure and micro-cleavage dependent on different strength

conditions. According to the loading conditions and microstructures of steels, the above growth mechanisms can sometimes be combined in a steel specimen [65, 66]. In general, striation growth can mainly be found in low and medium strength steels. Micro-cleavage and intergranular separation happen in steel grades with lower toughness, especially when K_{max} in a cycle is comparable to K_C, which is the stress intensity factor corresponding to fracture during the fatigue test [67].

The hull is the most important part of a ship structure which is continuously subjected to cyclic loading. Igi et al [19] studied the fatigue properties of two conventional ship steels, DH32 and DH36. The fatigue crack growth rates obtained exhibited a relatively wide distribution range as shown in the plot in Figure 30.

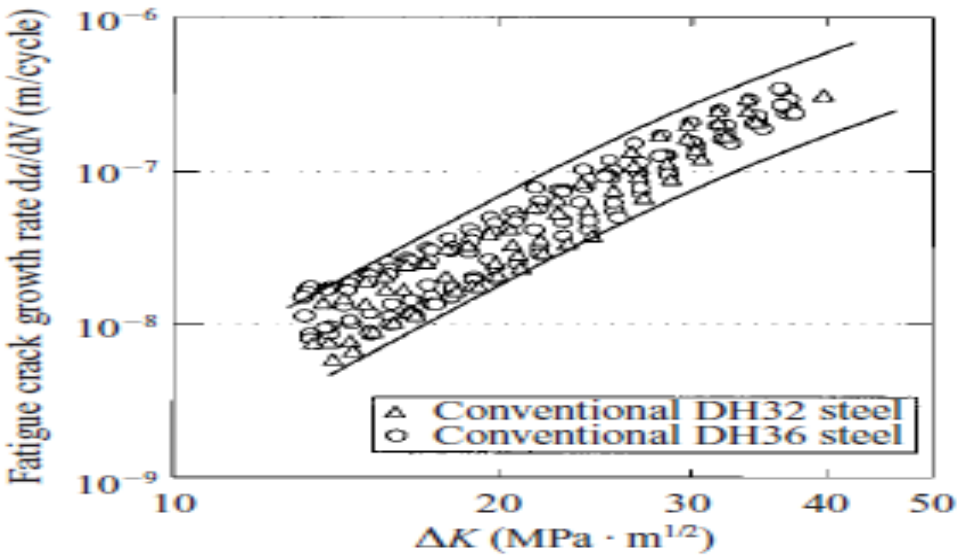

Figure 30: Fatigue properties of DH32 and DH36[19].

Fatigue behavior of another conventional ship steel grade EH36 was investigated by Y.W.Cheng. Standard compact specimens and modified compact specimens of EH36 steel were used to measure the fatigue crack growth rate. The test results showed that fatigue crack growth rate

from 2×10^{-5} mm/cycle to 10^{-3}mm/cycle was independent of stress ratio for constant amplitude stress range. However, the stress ratio may influence fatigue crack growth rate in lower and higher crack growth rate zones [58].

5 Acoustic Emission Technique

5.1 Principles of AE testing

Acoustic Emission (AE) testing is a dynamic non-destructive testing technique which is extensively used for structural integrity condition monitoring and evaluation. The principle of AE as shown in Figure 31 is based on the detection of transient elastic waves emitted when the component under evaluation is loaded up to a sufficient level to cause damage growth AE signals have very small intensity and are high frequency events which are detectable using extremely sensitive AE sensors incorporating piezoelectric crystals. The piezoelectric crystals convert the displacements in the surface of the sample to electric signals which are then suitably amplified using appropriate pre-amplifiers and amplifiers.

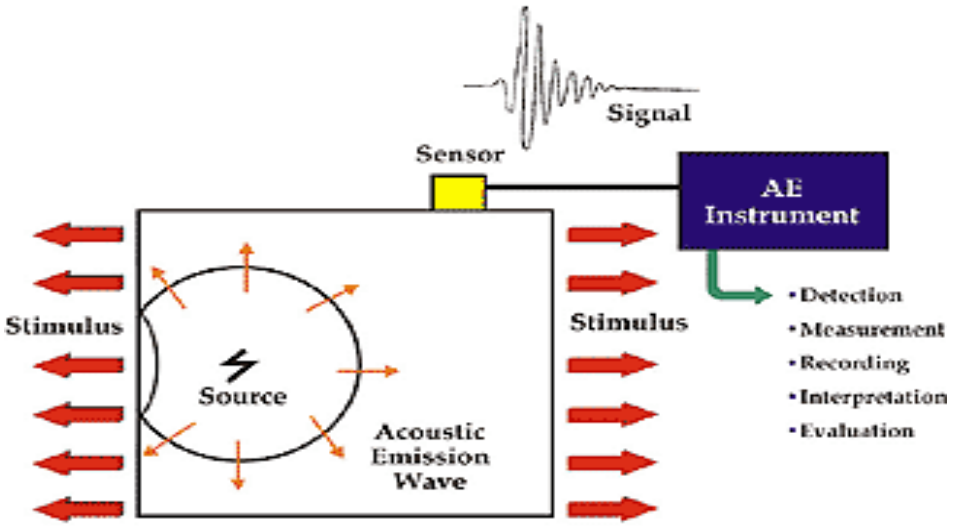

Figure 31: Principle of AE technique [68].

AE signals can be generated from various sources including dislocation movement, plastic deformation, crack growth, corrosion, erosion, impact, friction and even phase transformation.

In composite materials signals can arise from debonding, delamination, matrix cracking and fiber failures. Depending on the type of damage evolution mechanism different wave types may appear [69]. Crack growth is the most common source of AE signals with high amplitude [70]. By analyzing the different waveforms and other features of the AE signal it is possible to recognise the feature in the material that is giving rise to specific aspects of the recorded AE activity. In some cases depending on the extent of AE activity being recorded it is possible to assess the severity of defects present [71]. Since the deformation of materials is not reversible, it is necessary to know the stress history of the materials when the AE monitoring technique is employed [72].

Care must be given to filter unwanted noise when setting out the data acquisition parameters. A proper threshold setting is a fairly useful tool to eliminate background noise interference. Any signals of which amplitudes are below the threshold value will not be logged as AE hits [73]. The quality of the AE measurement is affected by the way the Peak Definition Time (PDT), Hit Definition Time (HDT) and Hit Lock-out Time (HLT) have been set since these three parameters fundamentally influence the way AE hits captured as shown in Figure 32. PDT is used to make a reliable identification of AE peak by determining the rise time and measure the peak amplitude correctly. HDT is used to prevent several AE events from merging into a single hit. HLT enables higher or lower data acquisition speeds depending on the requirements of the measurement by keeping the system locked away from recording superfluous signals during the decay process of a detected AE event [74].

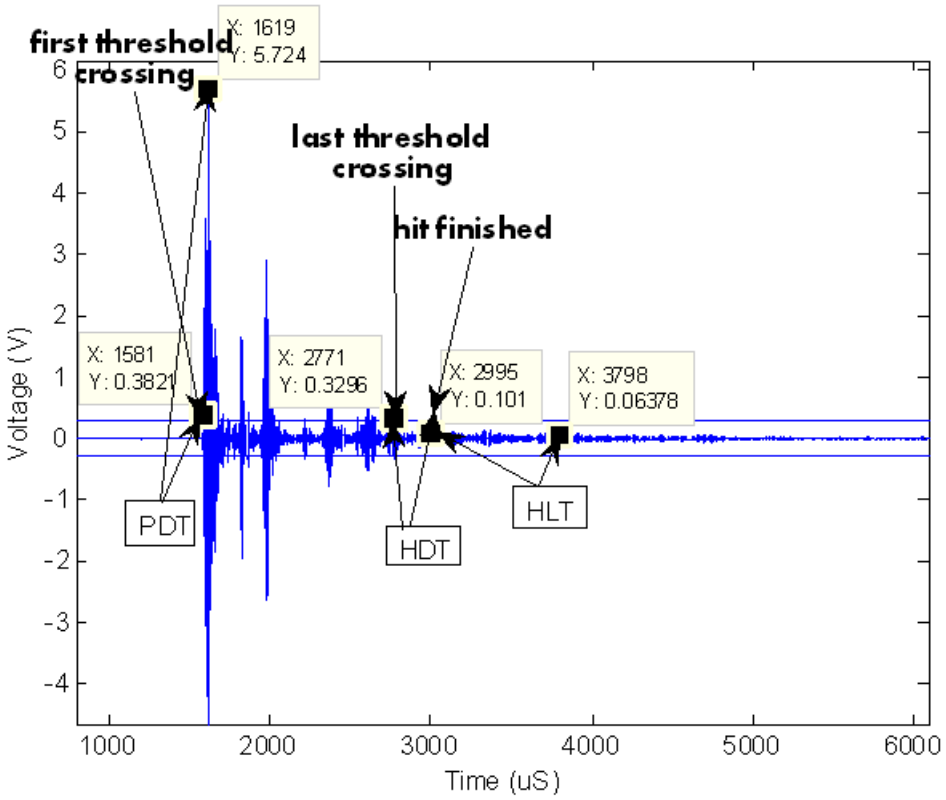

Figure 32: Illustration of the determination of AE hit based on PDT, HDT and HLT [75].

Normally, AE activity can be represented by two main types of waveforms; burst and continuous as shown in Figure 33 [72, 76]. Continuous waveforms are mainly attributed to deformation processes like cross-slip and dislocation pinning or noise and the amplitude of the signal is normally very small with relatively low duration and energy. Moreover, it is rather difficult to discriminate discrete signals from the others in a continuous waveform. Burst waveforms are often associated with events which emit higher energy such as crack initiation and propagation. In this study the useful signals are burst type and are related to crack growth or fracture. However, some burst signals are unwanted, such as echoes and need to be removed. Most of continuous waveforms captured are associated with mechanical noise or friction [76].

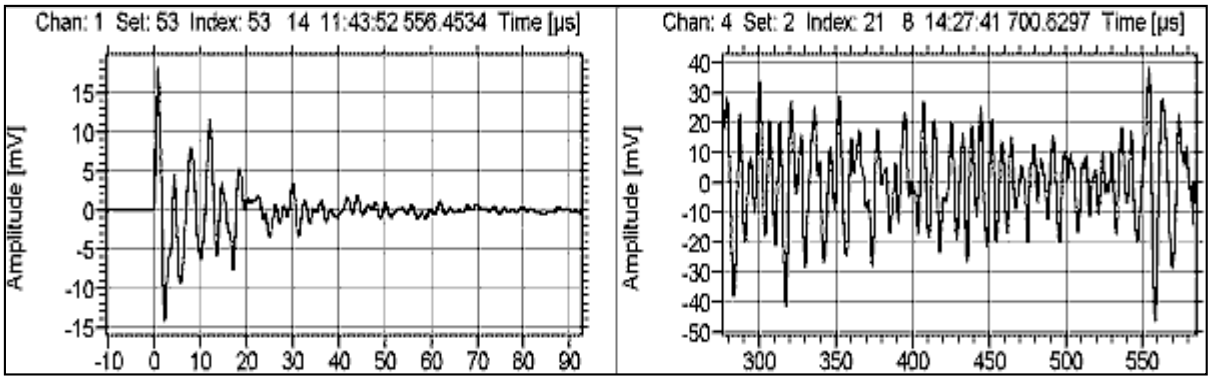

Figure 33: Burst(left) and continuous (right) AE signals [76].

There are several different waves which can be recorded by the transducers, such as shear, compression, Rayleigh (surface) and Lamb (plate) waves as shown in Figure 34. The detected waves are followed by a series of echoes and reverberations, which can complicate analysis of results [77]. For large structures the number of AE sensors that can be used to cover the entire structure is limited. Thus, AE sensors are likely to be located at some distance away from the source. In this case Lamb waves and Rayleigh waves are particularly useful in AE since they attenuate very slowly as they propagate over long distances.

Rayleigh waves account for a large part of the waveform when the distance between the sensor and source event is higher. For fairly thin plate specimens, Lamb waves are more likely to dominate the waveform [78]. An unavoidable problem is that the characterisation of the source event become difficult， as it is almost impossible to infer the initial wave form from the source event with energy converted into Rayleigh and Lamb waves[77].

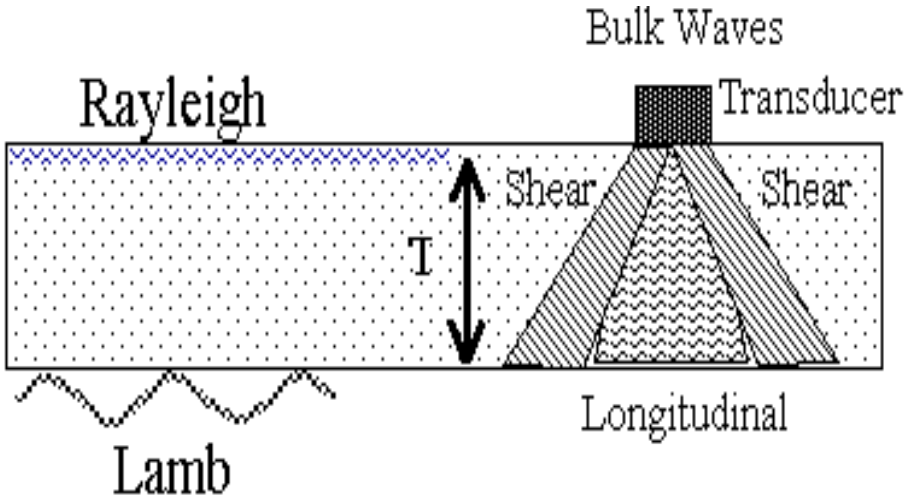

Figure 34: Different waves recorded by a transducer [79].

5.2 Common AE parameters

There are five main parameters which are most commonly measured during an AE test including threshold-crossing counts, amplitude, duration, rise time, and energy envelope. , as shown in Figure 35 [72].

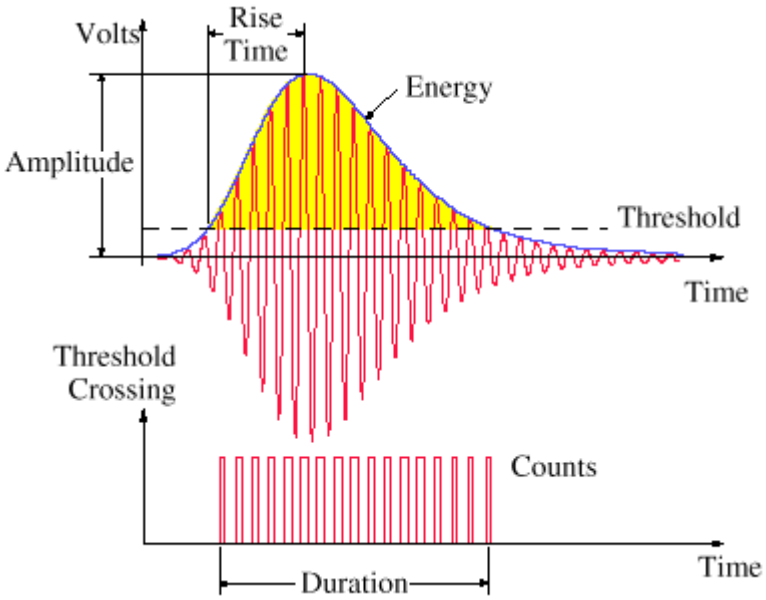

Figure 35: A typical burst AE signal and its commonly used parameter [80].

Threshold-crossing counts are defined as the number of pulses which are beyond the threshold set manually and are emitted by the measurement circuit. Amplitude of the signal represents the largest voltage in the recorded waveform and it is measured in decibels (dB), which is a logarithmic scale in which 100mv is defined as 40dB. Duration represents the time between the first threshold crossing and the last threshold crossing and it is determined by the signal source and is a useful tool to distinguish genuine signal from noise. Rise time refers to the time between the first threshold crossing and the peak signal and it can be easily influenced by the propagation in the material structure. The area between the threshold and the energy envelope is defined as MARSE. As MARSE is more easily influenced by the amplitude and duration than the threshold and operating frequency, it is a vital tool in determining the deformation degree in the source [72].

5.3 Kaiser effect

The Kaiser effect was established during studies on AE carried out by Joseph Kaiser [81] . The graph in Figure 36 shows the loading and unloading cycles of a metallic sample. Each time the sample is unloaded, in the following loading cycle the maximum load amplitude is higher than before. In the graph the AE activity is represented by the black-coloured solid lines. The light-coloured solid lines represent the load amplitude. The dashed lines indicate at each loading cycle the load amplitude at which significant acoustic emission activity resumes. Until the previous maximum load is exceeded there is no appreciable amount of AE activity recorded. However, once the previous maximum load is exceeded, the AE activity recorded becomes appreciable again. This behaviour of the AE response related to loading and unloading events is known as the Kaiser effect and needs to be taken into consideration when carrying out AE

measurements[81]. The Kaiser effect is fairly obvious in simple loading modes. For example, in uniaxial cyclic compression test, AE hits do not appear until the stress reaches the previous largest value. When stress attains the maximum value, AE signals are generated immediately. However, in some cases, AE events still take place even though the stress is below the previous maximum stress, which is probably caused by the friction in the existent cracks. In this case, the Kaiser effect causes a change in the slope of the plot of total AE hits versus stress, which is shown in Figure 37 [82].

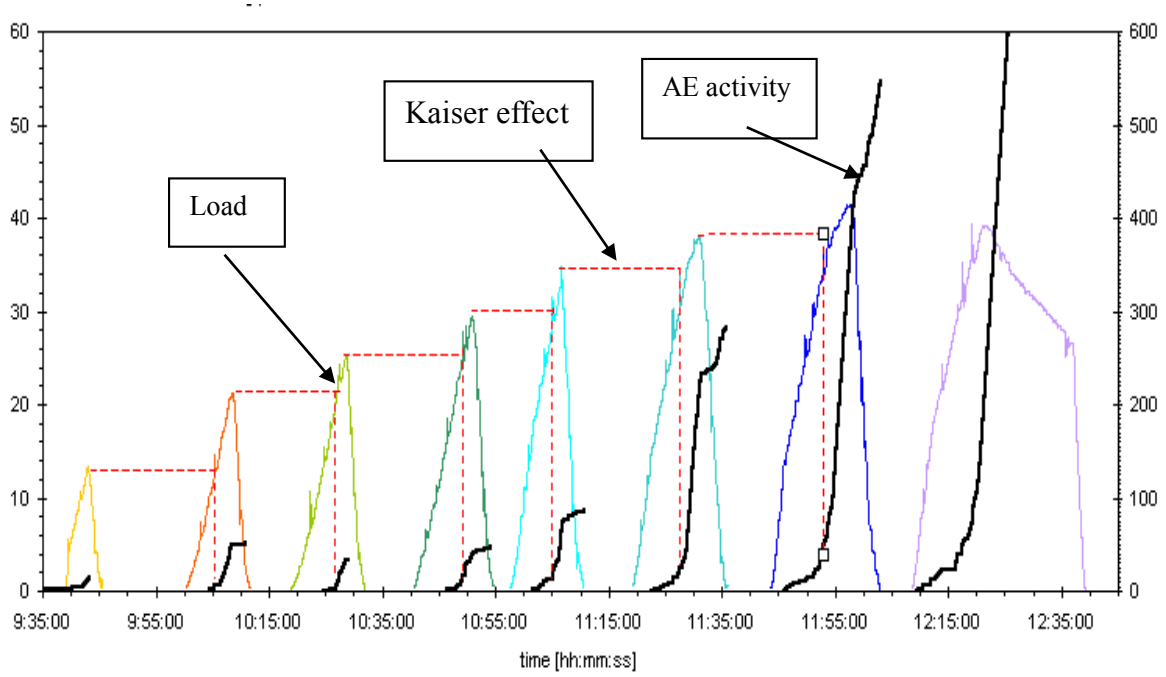

Figure 36 : Kaiser effect in a cyclically loaded concrete specimen [81].

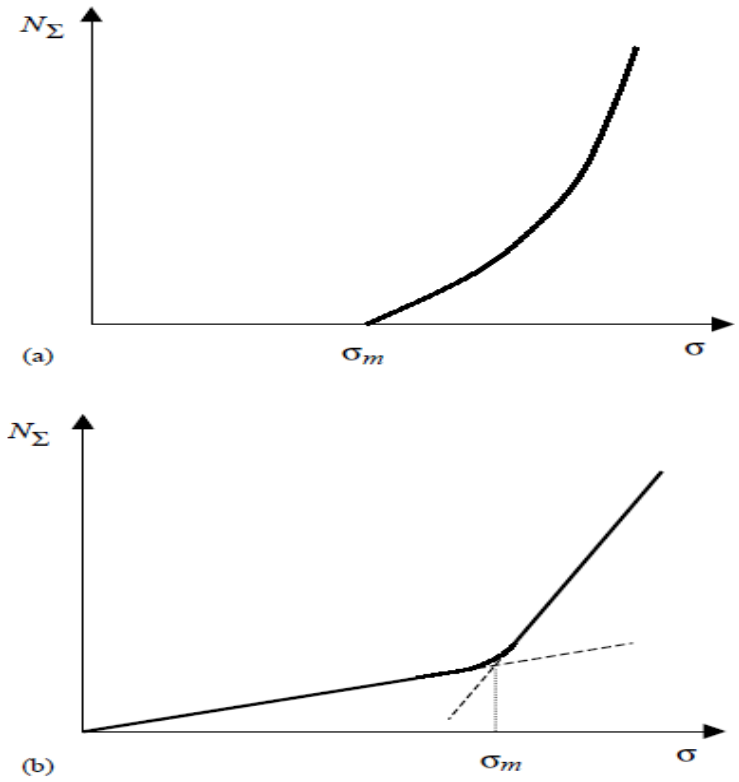

Figure 37: Plot of cumulative AE hits versus stress in the second cycle of uniaxial compression loading. The maximum stress in the first cycle is σ_m. In the second cycle, AE activity may be (a)zero or (b)non-zero when the stress is lower than σ_m [82].

5.4 AE application in fatigue and tensile tests

During fatigue tests, different mechanisms associated with cyclic softening, crack initiation, crack closure and final failure can result in AE signals being generated. If AE signals caused by crack closure and opening are removed in a fatigue test specimen, then the AE hits captured during testing will be associated with dislocation movement, cyclic hardening and softening, crack incubation and crack growth [80]. Before analysing the waveform characteristics of signals generated during fatigue tests, an important task is to filter the unwanted noise. Yu et al. employed AE technique to predict the remaining life of in-service steel bridges [83]. In their

research, they adopted several measures to eliminate noise arising from different sources. To filter the noise generated during the friction process caused by crack closure, AE signals captured below 80% of peak load were discarded. Certification tests were carried out to check the feature of noise generated by fretting. To achieve this, the maximum load was reduced so as crack growth rate approached zero. Hence, in this case AE signals generated by the crack growth process were not detected [83]. Figure 38 shows a 3D plot that summarises the changes in AE activity with stress changes and cycle numbers for the 3 different stages of failure for a smooth-plate sample.

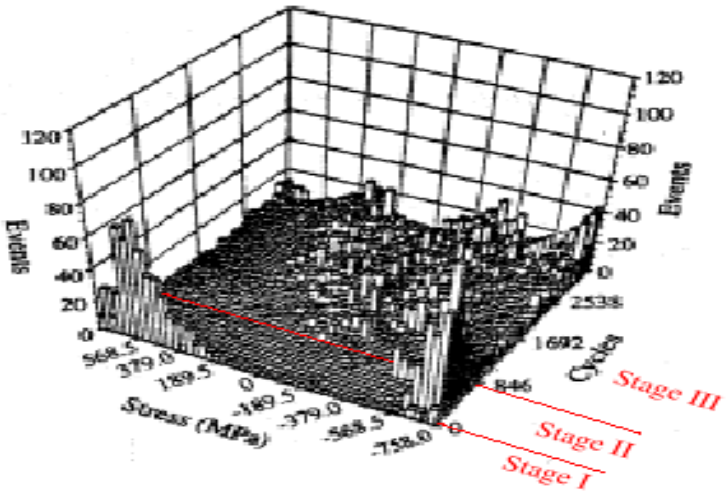

Figure 38: 3D illustration of variation of AE activity with stress and cycle during the fatigue test on a smooth-plate sample [84].

Khan, S.A., et al. [85] investigated the deformation mechanism of Fe-Si steels during tensile testing using AE testing and fractographic analysis. Continuous wavelet transform rather than Fourier transformation was employed to to process the AE signals capture . Low and high frequency signals were found to be present. The differences in the frequency content of the two types of signals recorded were determined to be associated with two different source

mechanisms; inclusion debonding/breaking (low frequency signals) and cleavage fracture (high frequency signals) [85].

Han Z, et al. [86] studied the influence of strain rate on AE during tensile tests carried out on notched and unnotched Q345 steel samples. Two different types of AE waveforms were detected during tests. The first type of signals was burst waveforms originating from micro-yielding and work hardening. The second type was continuous waveforms observed during the discontinuous yielding stage. Compared with burst-type signals, the strain rate had a greater influence on continuous-type signals. The energy of continuous-type signals increased as the strain rate became higher [86].

5.5 AE signal analysis method

AE signal analysis can be based either on parameter-driven or signal-driven analysis. In parameter-based analysis higher data storage speeds are possible. Moreover , there is no need to have a dead time for storing the waveforms recorded by sensors like in signal-based analysis, avoiding in this way loss of information [87]. In addition, statistical values of AE parameters have been studied intensively to infer the degree of damage for a given material or structure. The b-value, i.e., the log-linear slope of amplitude-frequency distribution of acoustic emission, has been investigated as a means of analyzing AE data during local monitoring of a concrete reinforced beam. This technique is capable of showing the relative contribution made by high or low energy to the total acoustic emission results, with high b-value corresponding to a low-energy predominant signal and low b-value corresponding to a high-energy predominant signal. Precipitation fracture, crack nucleation and propagation in a precipitation hardening alloy

system is accompanied by a high energy release thus corresponding to a low b-value, while the higher b value is mainly due to the contribution from events like dislocation glide, particle-matrix decohesion, etc. [88, 89]. Colombo et al. [88] compared the trend of b-value with the damage process of a concrete beam subjected to cyclic load and found that the trend of b-value has a good relationship with micro and macro-crack evolution measured during the loading process of the beam. More specifically, it was found that the maximum b-value trend is related to micro-crack growth while the minimum b-value trend means a macro-crack has formed, as shown in Figure 39.

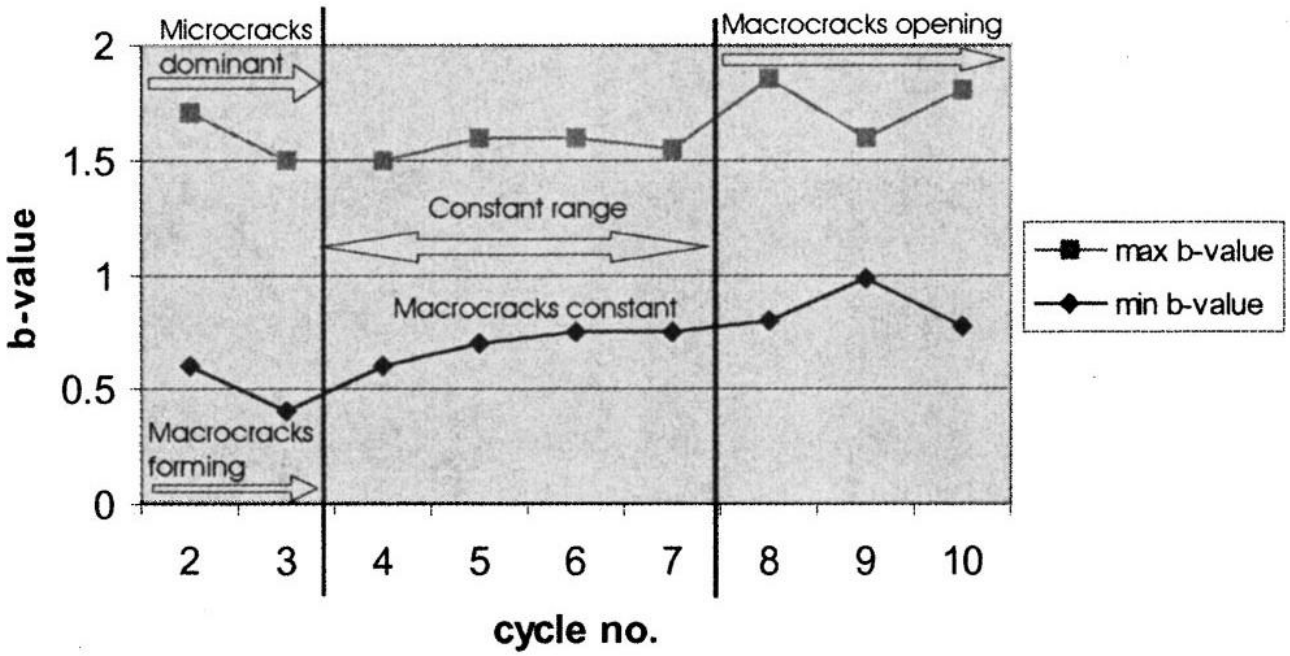

Figure 39: Variation of b-value with cycle number during the test [88] .

Other AE parameters like energy, RA value which is defined as the ratio of rise time to peak amplitude and average frequency have been reported to be closely related to the fracture mode [90]. Spectral analysis techniques such as Fast Fourier Transform (FFT) have also been investigated for the analysis of AE signals. In FFT the peak frequency is a useful parameter to

discriminate the different AE sources producing the corresponding signals. FFT-based spectral analysis has been used to identify the different fatigue crack growth mechanisms within the threshold and Paris regimes for aged 9Cr-1Mo steel [91]. It has been seen that the peak frequencies in both cases are similar, suggesting that the crack growth mechanisms are more or less the same in the two regimes, i.e. a mixture of quasi-static cleavage and plastic deformation along boundaries.

Chang, H., et al. [92] used FFT to identify different corrosion fatigue crack growth mechanisms for two different aluminum alloys, which is difficult to achieve using conventional amplitude distribution technique alone. The different peak frequencies represent different corrosion fatigue crack growth mechanism. Moreover, they used Frequency Centroid Ratio (FCR) to discriminate different AE sources. FCR can not only take into account the magnitude of the signal but also the frequency distributions [92].

Compared with FFT, wavelet analysis offers better time and frequency localisation capability. Serrano and Fabio [93] employed wavelet transform to analyze AE signals. Time-frequency analysis on some physical parameters, such as amplitude, counts, ringdown counts can be used to tackle the AE signal analysis problem [93]. Wavelet packet analysis has also been reported to be used to investigate the influence of martensite volume on AE activity generated during tensile testing of a dual steel [94]. Different micro-mechanisms corresponded to different frequency ranges and energy concentration. Three different components of the AE signals with the frequency ranges of 0-125kHz,125-250kHz and 500-625kHz were found to be associated with three corresponding AE sources namely, ferrite/martensite interface failure, ferrite deformation and martensite fracture ,respectively [94]. Qi et al. [95] studied fracture

characteristics of fiber-reinforced composites also using wavelet-based analysis. The tensile specimens they employed during testing had drilled central holes. They obtained the exponential values through the relationship between stress and wavelet energy and compared these values with those acquired using conventional AE techniques.

5.6 AE during crack growth process

Crack growth is an important source of AE activity [83, 84, 96-101]. AE signals produced in the plastic zone of the crack-tip and crack-front movement have different characteristics. AE generated by plastic zone growth has lower amplitude than those generated by crack growth. Moreover, AE signals can also be influenced by the microstructure of the test specimens. Many AE signals generated from yielding are caused by pearlite cracking in the ferrite/pearlite microstructure. Spheroidisation of pearlite can reduce the total amount of AE activity[102].

Sinclair et al. [98] carried out AE data analysis during fatigue crack growth in three different steels. They used the ACEMAN system to analyze and locate AE sources. During fatigue tests carried out by Sinclair et al., the total number of AE events, N, generated over a certain number of cycles were proportional to the fatigue crack area, A, produced in the same period as shown in Equation 9[98].

Equation 9

$$N = \gamma A$$

Hamel et al. [103] investigated the influence of R-ratio on the AE count rate. It was found that the AE count rate increases with decreasing R-ratio (from R=0.4 to R=0.2). This increase in AE count rate was deemed to arise due to a combination of two different modes, new plastic

yielding and crack tip fracture processes [103].

Berkovits and Fang [84] used AE to investigate the characteristics of fatigue crack initiation and crack closure in specimens of nickel-based Incoloy 901 superalloy. A burst peak in the plot of cumulative AE counts versus cycles was observed during fatigue crack initiation. The crack closure stress with AE result and compared the stress obtained by AE signature with those calculated from several formulae, some of which are shown in Equations 10 to 12. They found that the Schijve 1 equation show a high similarity with the obtained data from AE measurement [84].

Schijve 1[104] : Equation 10

$$\gamma = 0.45 + 0.2R + 0.25R^2 + 0.1R^3$$

Kumar and Garg [105]: Equation 11

$$\gamma = 1 - (1 - R) \cdot (0.5R + (\sigma_y/42))$$

Maddox[106] : Equation 12

$$\gamma = 0.25 + 0.5R + 0.25R^2$$

Where R is stress ratio, γ is crack-opening stress ratio defined as crack opening stress divided by maximum stress during one cycle and σ_y is yield strength.

Pinar et al.[107] found that the amplitude of noise from a Dartec 50 KN Servo-Hydraulic Universal Test Machine which is also used for the fatigue test in this thesis during a four-point bending test on rail steel samples with AE monitoring the whole process was restricted to 40dB [107]. It was concluded that almost all the hits with amplitude higher than 40dB in the test were related to crack growth events. Most high amplitude events were recorded in the final stage of

the test, as the final failure of the samples was near. The hits recorded after the critical crack length had been reached had the highest duration, signifying that duration can be used as a tool to remove unwanted noise [107].

Kostryzhev, et al. [108] employed AE technique to monitor the fatigue crack growth process and then analyzed the results using different signal parameters. They have found that AE signal characteristics depend on fracture mechanisms.AE signals with high duration and low frequency are generated by ductile fracture, whereas those with low duration and high frequency correspond to brittle fracture as shown in Figure 40 [108].

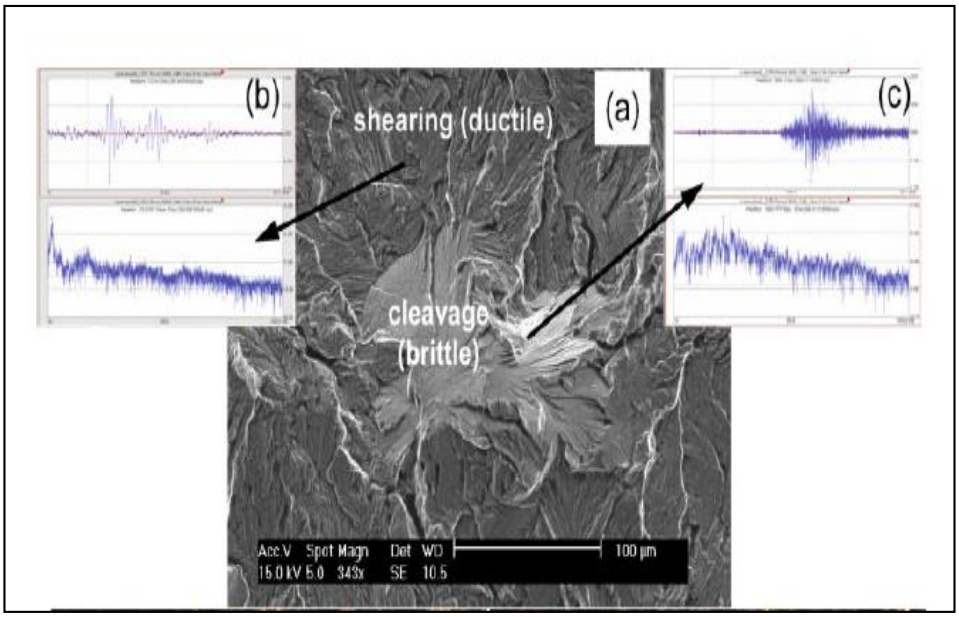

Figure 40: (a)a typical SEM image of fracture surface after fatigue with the corresponding AE waveforms and power spectral for (b) ductile fracture and (c)brittle fracture [108]

6 Experimental Methodology

6.1 Steel grades studied

Four different steel grades have been supplied in the form of steel plates of various thicknesses. These include two conventional X65 plates with thickness of 13 (X65-1) and 18mm (X65-3) respectively, one modified X65 plate with thickness of 50mm (X65-2), two S690 steel plates with thicknesses of 12 and 20mm respectively and Fatigue Crack Arrestor (FCA) steel plate with thickness of 12mm. The data regarding the steel thickness considered in this study are summarized in Table 1. The compositions (% by weight) of the steel grades studied are given in Table 2. The thicknesses were chosen based on the different structural components found on ships such as the hull.

Table 3: Steel thickness considered in this study

Steel grade	**Thickness in mm**
X65-1	13
X65-2	50
X65-3	18
S690-1	12
S690-2	20
FCA	12

.

Table 4: Steel compositions (% by weight) for each steel studied.

Composition of conventional X-65 steel (1) and (3)

C	Si	Mn	P	N	Al	Cu	Mo	Ni	Cr	V	Nb	Ti
0.075	0.38	1.47	0.01	0.006	0.047	0.01	0.005	0.01	0.01	0.074	0.036	0.002

Composition of modified X-65 steel (2)

C	Si	Mn	P	N	Al	Cu	Mo	Ni	Cr	V	Nb	Ti
0.053	0.18	1.59	0.013	0.006	0.037	0.23	0.002	0.17	0.26	0.001	0.097	0.016

Composition of S690 steel

C	Si	Mn	P	N	Al	Cu	Mo	Ni	Cr	V	Nb	Ti
≤0.2	≤0.80	≤1.70	≤0.20	-	-	-	-	≤2.0	≤1.5	-	-	-

Composition of FCA steel

C	Si	Mn	P	S	N	Al	Cu	Mo	Ni	Cr	Nb	Ti
0.04	0.42	1.5	0.009	0.002	-	-	-	-	-	-	-	-

The results for the HSLA steels were compared to those of the AH36 and DH36 traditional naval grades also tested by other researchers at AIMEN, Spain also involved in the project.

6.2 Microstructural characterization

Microscopy samples 10mmx10mm were cut from the plates studied in order to examine the

microstructure of the different steel grades. The samples were mounted on bakelite and then ground using abrasion paper to 1200 grade. The samples were then fine polished down to 1μm. The polished samples were etched using 2% Nital to reveal the microstructure. The etched samples were examined using a Karl Zeiss optical microscope.

Vicker's hardness tests were also carried out on all steel samples. The hardness values measured are summarised in Table 5.

Table 5: Hardness results for HSLA steels

HSLA Steel	**Hardness (HV20)**			
	1	2	3	Average*
X65 – 1	179.2	176.4	178.5	178 (1.46)
X65 – 2	151.1	153.6	151	152 (1.47)
X65 – 3	194.8	194.9	192.3	194 (1.47)
S690	288	283.4	285.9	286 (2.3)
FCA	188	189.2	187.5	188(0.87)

*Value in brackets is the standard deviation

The microstructure for each steel grades tested is shown in the optical micrographs included in Figure 41. The optical micrograph of FCA shows a mixed ferritic-bainitic microstructure whilst for the S690 a tempered martensite structure is evident. Both X65-1 and X65-2 steel grades show a ferrite pearlite microstructure. The X65-3 on the other hand shows an acicular ferrite structure. The nature of the microstructure, i.e. the phases present and grain size influence the

hardness and ductility of the samples. This has an effect in the level of acoustic emission energy emitted during crack growth. The microstructure also influences the rate at which the crack growth will grow and if any arrest events will occur due to the presence of a harder phase in the path of the crack tip as it propagates. If the crack is arrested or propagates slower, no or little acoustic emission activity is expected to be recorded. However, in the case of rapid crack growth the acoustic emission activity recorded increases dramatically.

a) 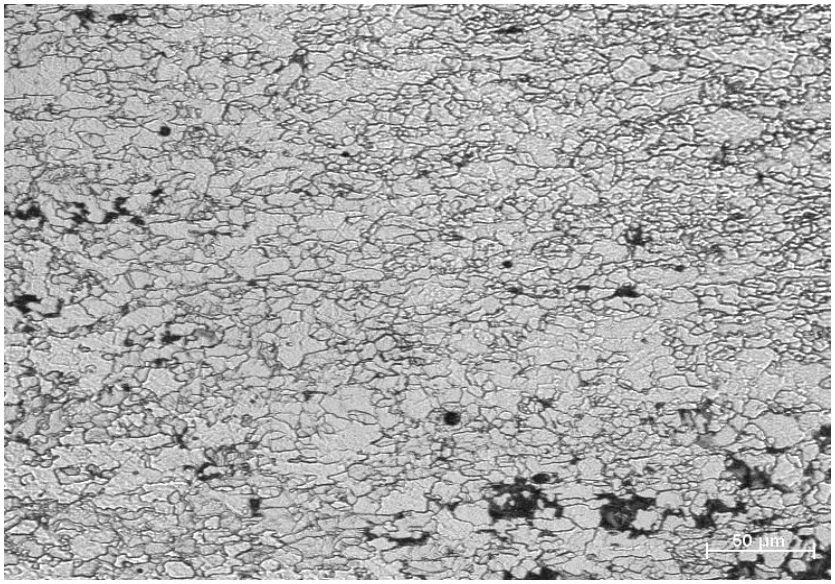

b) 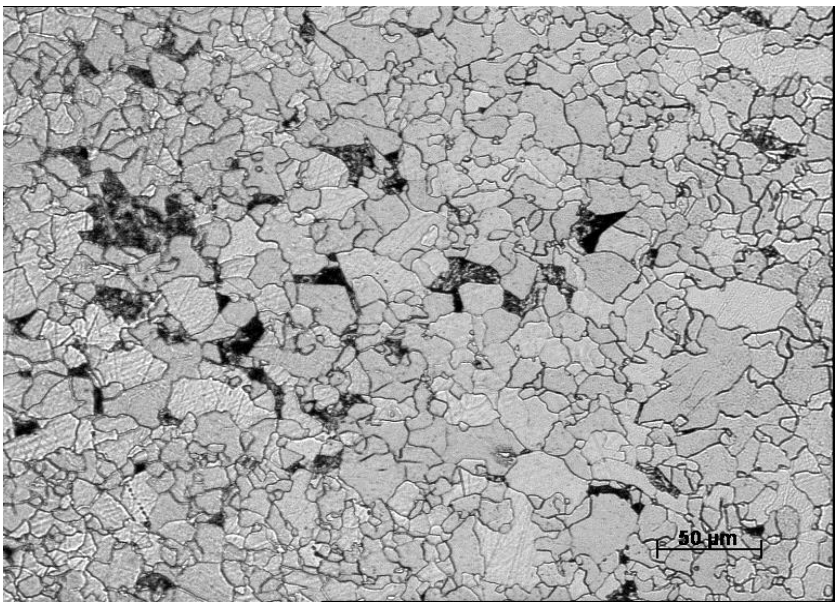

c) 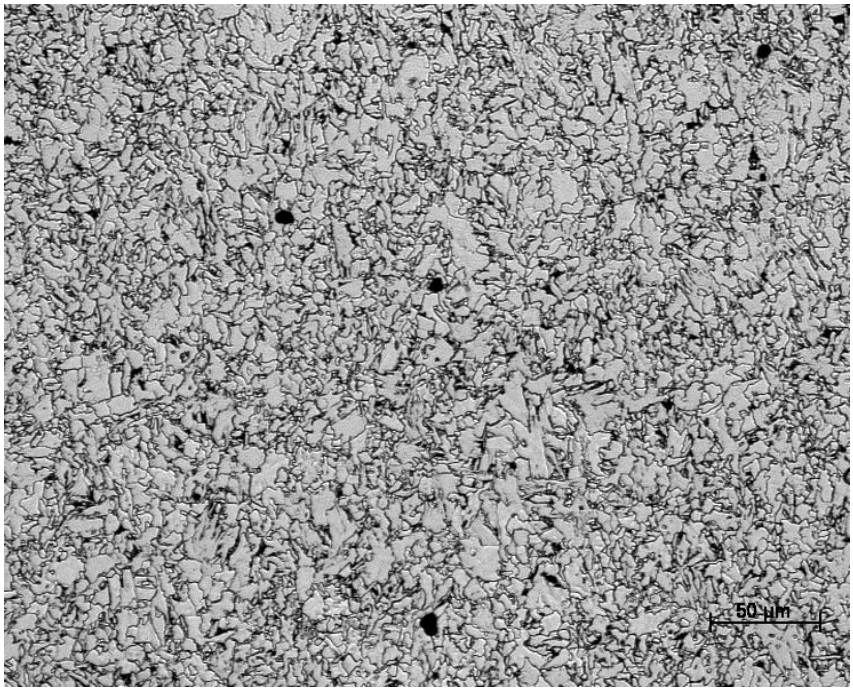

d) 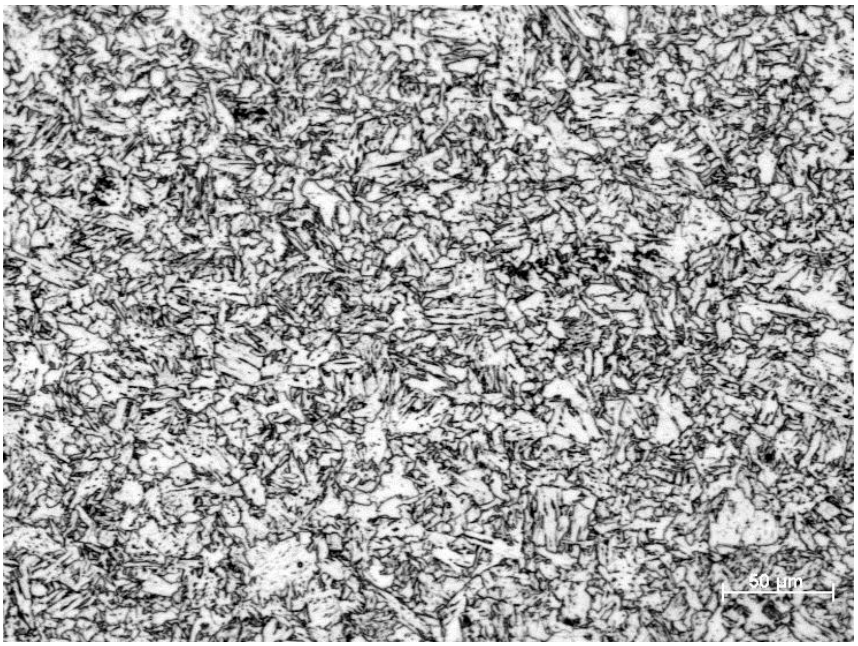

e) 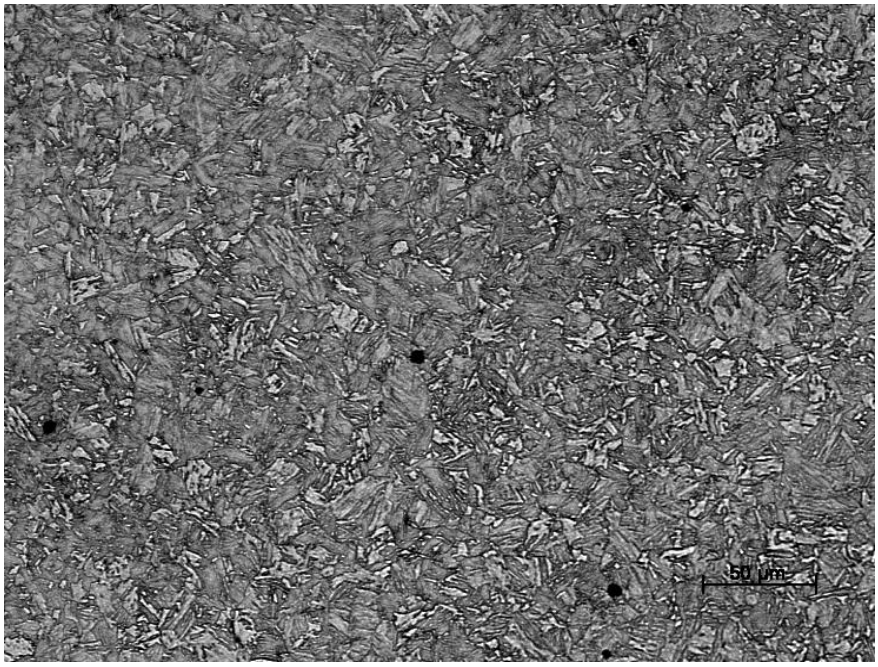

Figure 41: Microstructure of a) conventional X65-1 steel (18mm steel plate) and b) modified X65 -2 steel (50mm thick steel plate), c) X65-3 steel, d) S690 steel and e) FCA steel

It should be noted that the optical micrographs for the five HSLA steel grades considered have been taken in the rolling direction only.

6.3 Impact tests

Charpy tests were carried out on four steel grades at -20□ in both longitudinal and transverse direction. The results are summarized in Table 6 and confirm that steel grades meet the requirement prescribed in the Lloyd's Regulation for construction of naval vessels [109].

Table 6: Results of Charpy tests for all the four steel grades.

Steel	Direction	Impact Energy / J			
		Test 1	Test 2	Test 3	Average
X65 - 1	L	298	298	298	298
	T	233	259	237	243
X65 - 2	L	260	285	294	280
	T	240	234	240	238
X65 - 3	L	298	298	298	298
	T	298	298	298	298
S690	L	286	298	298	294
	T	298	298	298	298
FCA	L	252	290	298	280
	T	201	171	169	180

6.4 Tensile tests

Dog-bone-shaped tensile specimens were obtained according to the specifications set in the ASTM A131/A131M-08 standard [18]. Figure 42 shows the geometry of the specimen used for tensile tests.

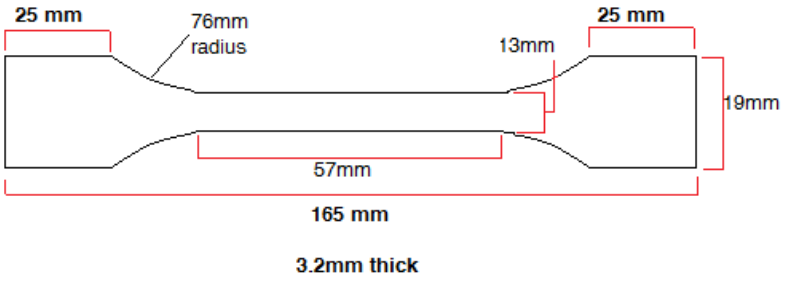

Figure 42: Test specimen dimensions employed for tensile testing.

A Zwick Roell 1484 testing machine was used to perform the tensile tests. Figure 43 shows the experimental configuration. An extensometer was used to measure strain during testing. AE measurements were carried out using a four-channel system manufactured by Physical Acoustics Corporation. Two differential wideband AE sensors with operational frequencies of 0.1-1MHz were employed during testing. Wideband sensors were preferred in this case because they can detect the resulting AE signals as close as possible to their original frequency. Although their peak sensitivity is lower than that of resonant sensors, the finite size of the specimens limits losses due to attenuation satisfactorily.

Paraffin was used to couple the sensors on the surface of the tensile sample. The sensors were held in place using duct tape. The sensor signals were amplified using PAC pre-amplifiers with the gain set at 40dB. AE acquisition parameters were set as summarised in Table 7.

Table 7: AE acquisition parameters for Peak Definition Time (PDT), Hit Definition Time (HDT), Hit Lock-Out Time (HLT) and maximum hit duration.

PDT	**HDT**	**HLT**	**Max duration**
300µs	600µs	1000µs	25000 µs

Load and strain were acquired together with the AE activity that occurred during testing of tensile test samples from the four aforementioned steel plates. Tests were carried out on using displacement rate 0.2mm/min and 0.5mm/min with other specimens. The gauge length used was 50mm in the case of no AE sensors attached on the specimen.

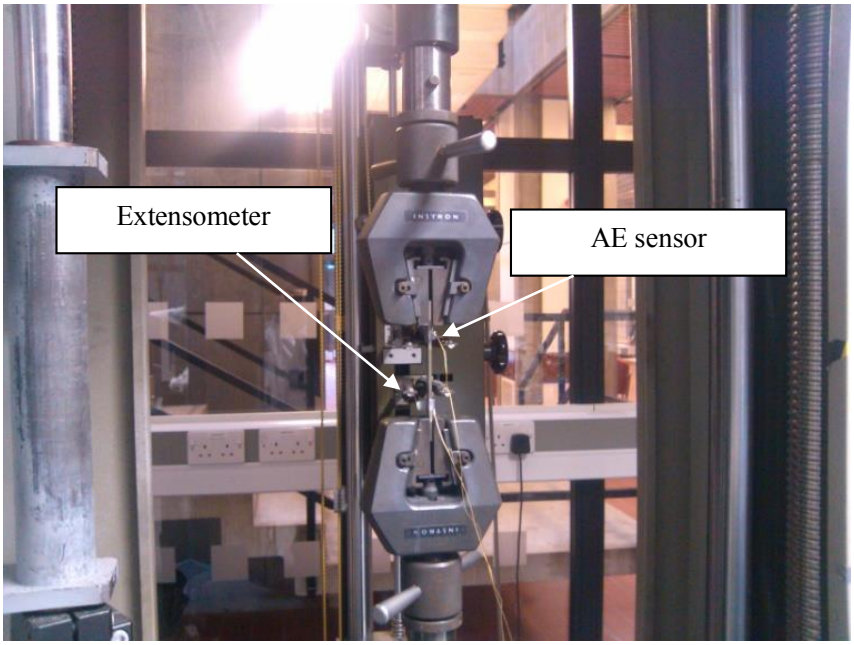

Figure 43: Tensile testing experimental configuration with AE sensors attached.

6.5 Fatigue crack growth (FCG) testing

Bending samples were produced from the four steel plates. The three-point bending samples were manufactured according to the ASTM standard and were used to assess the fracture toughness as well as to assess the crack growth propagation during fatigue testing. For fatigue testing a sinusoidal loading mode was employed. AE activity was also monitored during tests using the aforementioned PAC system. The three-point bending samples were pre-notched. The notch acted as a crack initiation point during the pre-cracking process using a Vibrophore

machine. The schematic in Figure 44 shows the shape and dimensions of the samples in the flexural and three-point bending fatigue tests.

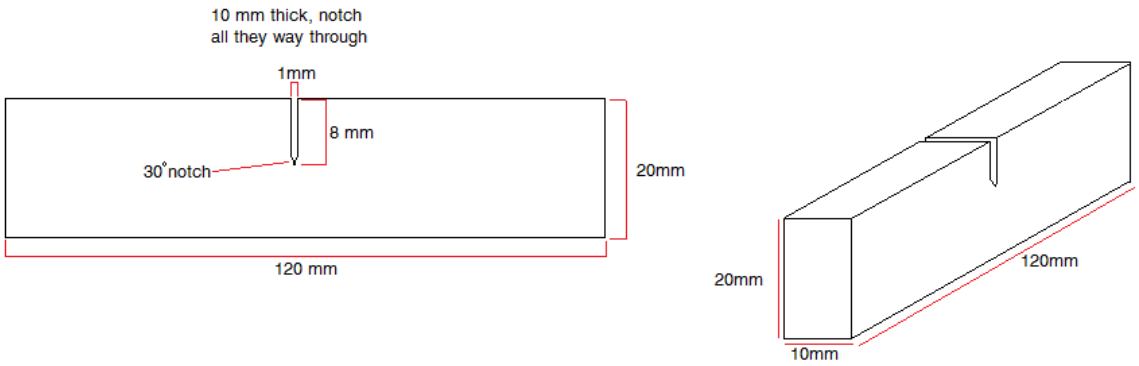

Figure 44: Dimensions of the three-point bending test specimens employed for this study.

The three point bending specimens for fatigue test were pre-cracked first using Vibrophore machine. Before pre-cracking the samples, fracture toughness tests were carried out using one sample for each steel grade to decide the load to be used for the pre-cracking and fatigue test. However, as too much plasticity was induced in front of the crack for all the four different steel grades samples, the K_Q value rather than K_{IC} was obtained using the existing samples at room temperature.

An Amsler 20KN Vibrophore electro-mechanical high frequency fatigue machine was employed to pre-crack the three point bending specimens. The loading mode during the pre-cracking process was sinusoidal with an approximate frequency of 76HZ.The maximum load of the high frequency pre-cracking process was 3.3KN based on the previous fracture toughness test and the R-ratio was kept at 0.1. In order to make sure the crack length in a certain range, microscopy replicas were used to monitor the pre-cracking process.

After the pre-cracking process， the samples were removed from the Vibrophore machine and placed in a Dartec 50KN Servo-Hydraulic Universal Test Machine shown in Figure 45. Before the three-point bending test, the maximum and minimum load during the cyclic loading process were determined. The determination of the load was based on the previous pre-cracking length and the configuration of the samples.

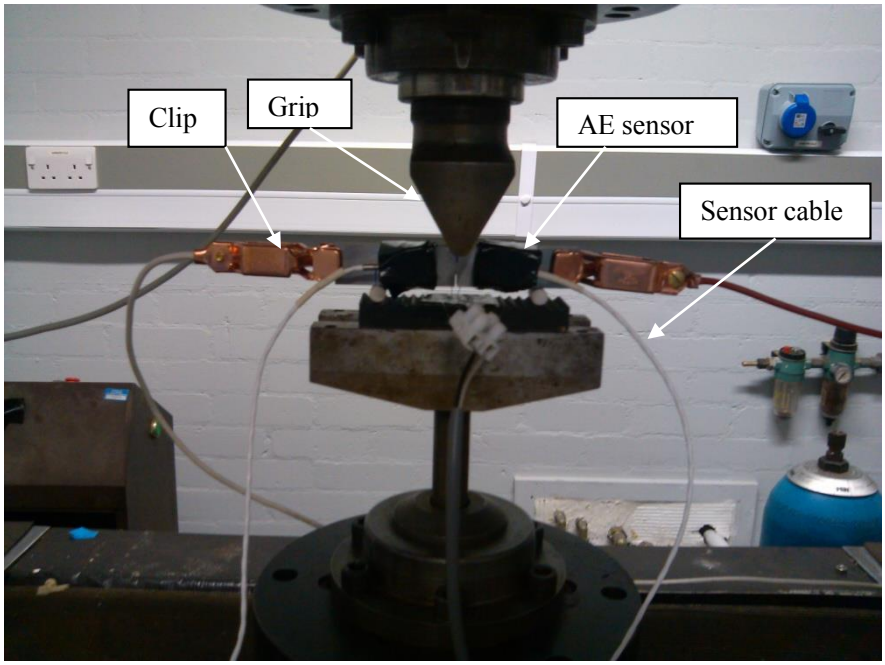

Figure 45: Experiment configuration for the three-point bending test.

During three-point bending test, a sinusoidal loading mode, as shown in Figure 46 was employed and the total time of a loading cycle was 4s, which meant that the loading was in a low frequency situation. The loading ratio was 0.1 and kept constant throughout the whole test. Table 8 shows the cyclic loading range for different steel grade specimens.

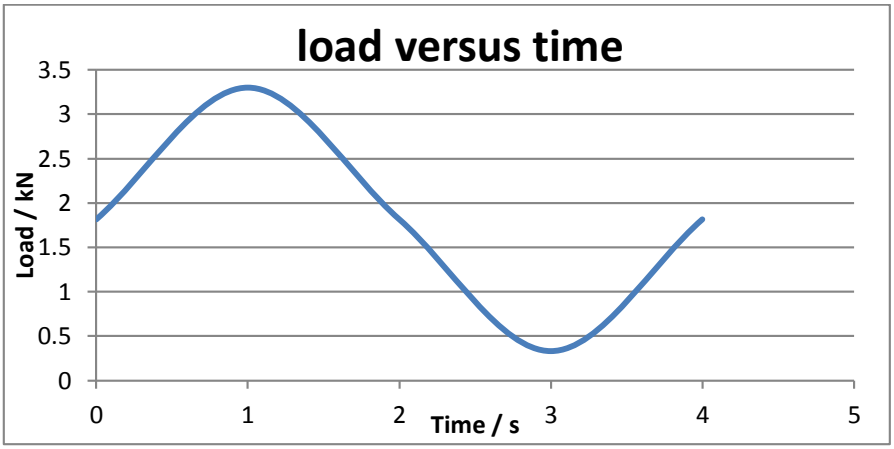

Figure 46: Sinusoidal loading cycle for three point bending test.

Table 8: Load ranges for fatigue tests. R=0.1 in all cases.

Steel grade	**Number**	**Maximum Load(KN)**	**Mean Load(KN)**	**Minimum Load(KN)**
X65-1	1	3.3	1.8	0.33
X65-2	1	3.3	1.8	0.33
	2	3.3	1.8	0.33
	3	3.3	1.8	0.33
X65-3	1	2.6	1.4	0.26
	2	3.3	1.8	0.33
	3	1.8	1.0	0.18
S690-1	1	3.3	1.8	0.33
	2	3.3	1.8	0.33
	3	3.5	1.9	0.35
FCA	1	3.3	1.8	0.33
	2	4.1	2.3	0.41

A chart recorder was used to record the data with the chart speed set at 2mm/min. The fatigue life of each sample was obtained measuring the chart length, which could be then translated into total time and then to fatigue cycles.

During the tests, crack length was monitored using Direct Current Potential Drop (DCPD) technique as well as the AE system. As the crack grows, the cross-section of the specimens becomes smaller and the cross-section resistance increases, resulting in an increase in the potential drop recorded by the pair of electrodes placed around the crack. The potential drop difference is proportional to the input current and is influenced by factors like the configuration of the specimens and the distance between the electrodes. The initial voltage during the discussed tests was set at 0.4 mV.

7 Results and Discussion

7.1 Analysing the suitability of HSLA steel grades to replace AH and DH grades

The shipbuilding industry has been using AH and DH steel grades for the construction of naval vessels and offshore platforms for several decades. However, recent changes in the regulations imposed by the classification societies require higher plate thicknesses to increase impact strength as well as minimise the likelihood of cracking. It is common in practically every type of commercial vessel for cracks to initiate and propagate at various load bearing locations with time.

To prevent the propagation of such cracks from reaching a level of severity that poses danger to the safety of the ship and its overall structural integrity, shipbuilders resort in the installation of additional plates in the areas of concern in order to strengthen the structure at these particular locations and increase the overall rigidity of the ships structure. The plates installed to offer additional strength to the structure have very high thicknesses which can normally exceed 30mm. Although such strengthening approaches are recognised to be reliable they tend to add considerable extra weight to the vessel. This leads to increases in fuel consumption and reduction in the overall efficiency of power to weight ratio produced by the ship's engines. Furthermore, the fact that cracks tend to develop much earlier than predicted by finite element models employed by naval architects emphasises the requirement for better steel grades which offer better resistance to crack initiation as well as crack propagation to improve maintenance and life cycle costs of ships.

It is undeniable that AH and DH grades are reliable for ship building and have been proven in the field for several decades. However, in recent years the need for improved fuel and maintenance efficiency has resulted in the emphatic requirement of more innovation in the materials used for the construction of ships, particularly alternative steel grades with improved performance over traditional ship steel grades. In this study, the mechanical properties of the HSLA steels considered have been studied using tensile, fatigue and fracture toughness tests along with impact and hardness tests reported earlier. Acoustic emission has been employed to investigate the suitability of this particular technique for structural health monitoring purposes. The mechanical properties of the HSLA steels have been compared to those of AH and DH36. The mechanical tests on the AH and DH36 grades were carried out at AIMEN, Spain and provided to the author for his thesis.

7.2 Tensile test results

Tensile tests were carried out using the experimental procedure described earlier in chapter 6. The stress-strain results for the AH and DH36 conventional steels were provided by AIMEN for comparative purposes and can be seen in Figure 47. For AH36 grade an average Yield Strength (YS) of 393.4 MPa and Ultimate Tensile Strength (UTS) of 524.4 MPa were recorded by AIMEN for the batch of the samples tested. The maximum strain, ε, recorded for the tested samples varied from 0.3-0.35. It should be noted that the minimum tensile strain tolerance for the hull of a ship is 0.22 according to the regulations of classification societies. However, for other structural components such as supporting beams, etc. lower maximum tensile strains are also acceptable.

For DH36 grade the YS was significantly higher, 464.8 MPa. The UTS was comparable to that of AH36 but slightly higher at 559.8 MPa. The DH36 grade also exhibited a higher YS to UTS ratio in comparison to AH36, 0.83 (DH36) in comparison to 0.75 (AH36).

a)

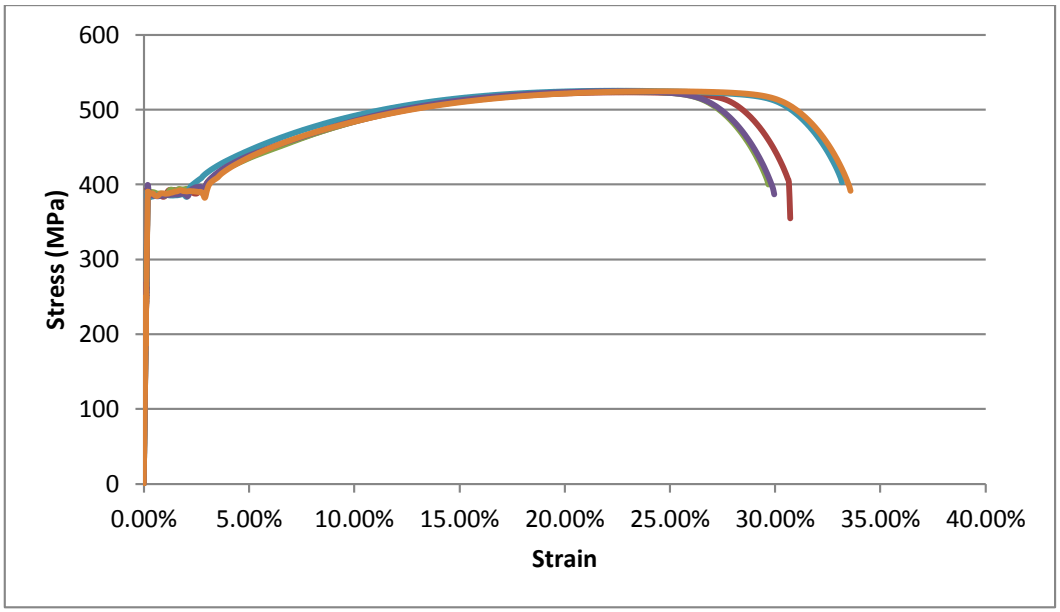

b)

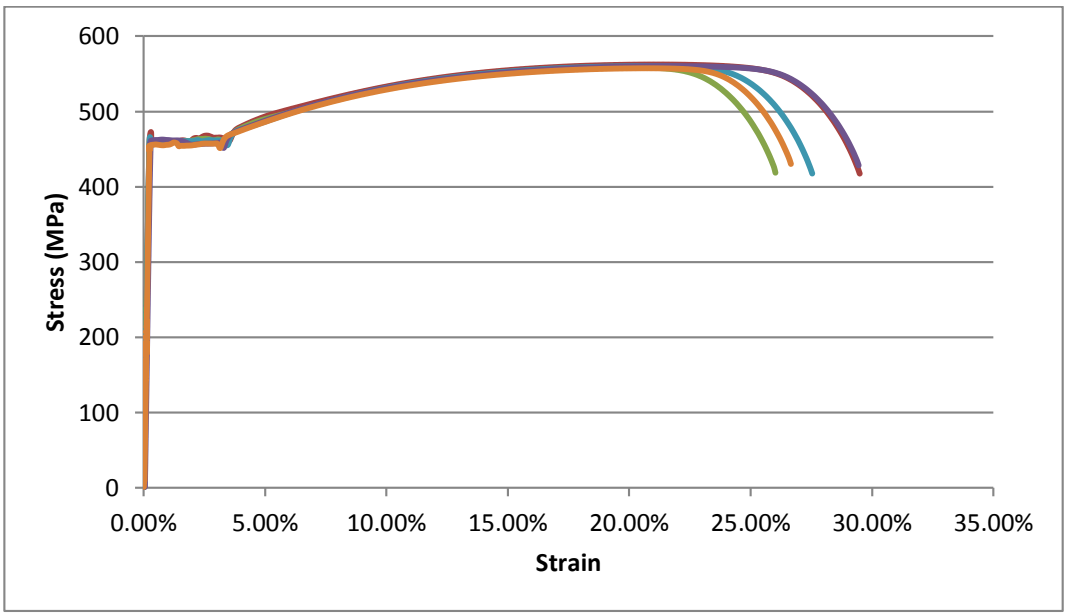

Figure 47: Stress-strain curves for both a) AH36 and b) DH36 conventional steel grades provided by AIMEN, Spain.

Stress-strain curves of all tensile tests carried out for the HSLA grades considered in this study are shown in Figure 48. It can be clearly seen that all HSLA steel grades exhibited a higher YS than the AH36 grade, however the X65 grades show similar or a reduced UTS in comparison to the AH36. Also in comparison to DH36 only the S690 exhibits higher YS. In the case of UTS both the S690 and FCA perform better than DH36 but the X65 grades exhibit lower UTS. In terms of maximum tensile strain the HSLA steel grades perform comparably to both the AH36 and DH36 grades with the exception of S690. The S690 grade exhibited a maximum tensile strain of 0.126 which means it is not suitable for the construction of the hull as it fails to fulfill the requirements of the regulations provided by the classification societies. Nonetheless, it is applicable for the construction of other structural parts of the vessel offer in much higher YS and UTS in comparison to traditional grades. Also all HSLAs exhibited better YS to UTS ratio. Table 9 summarises the results of the tensile tests for all steel grades tested.

a)

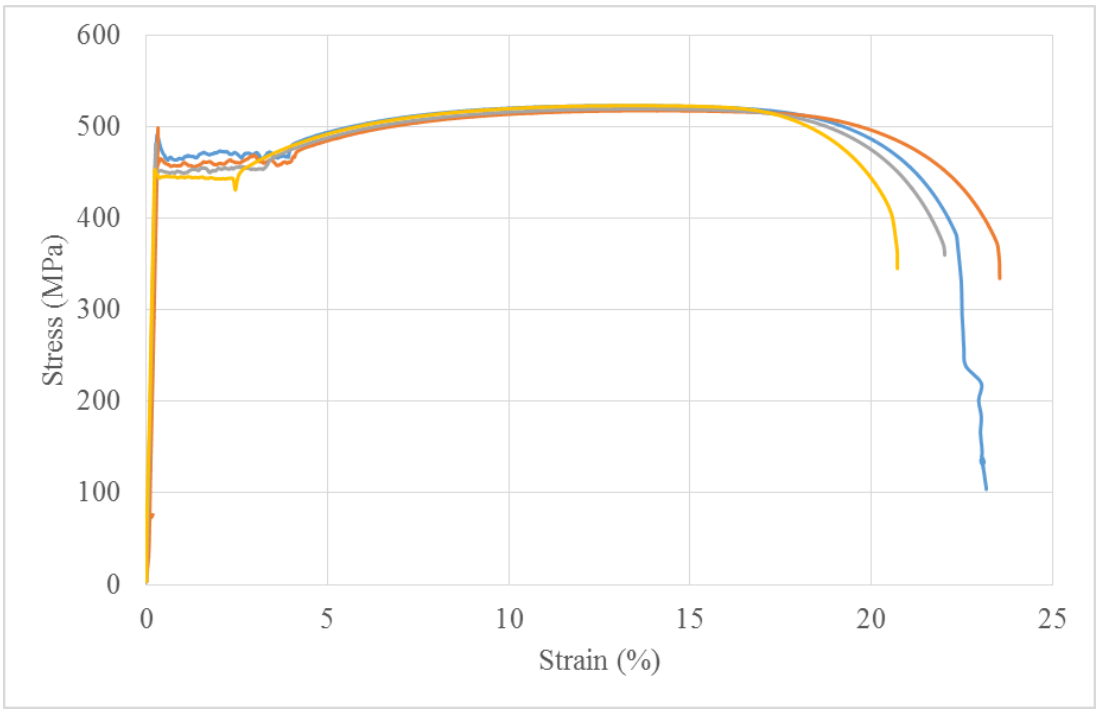

b)

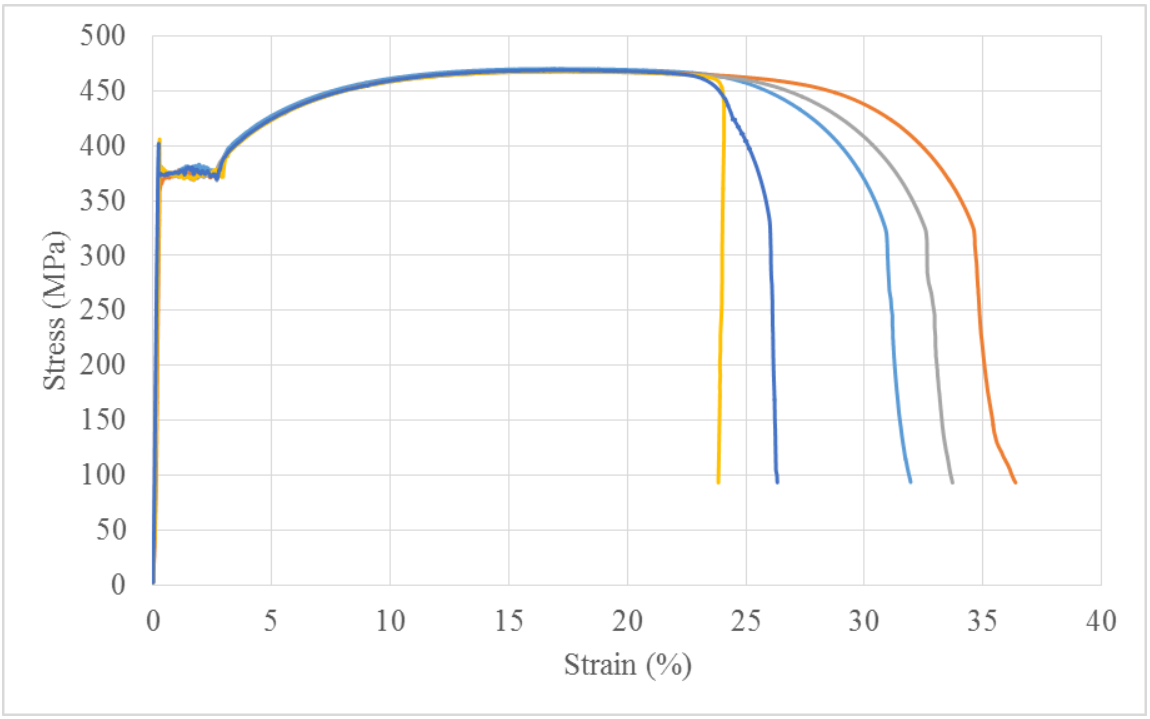
500
450
400
350
300
250
200
150
100
50
0
Stress (MPa)
0
5
10
15
20
25
30
35
40
Strain (%)

c)

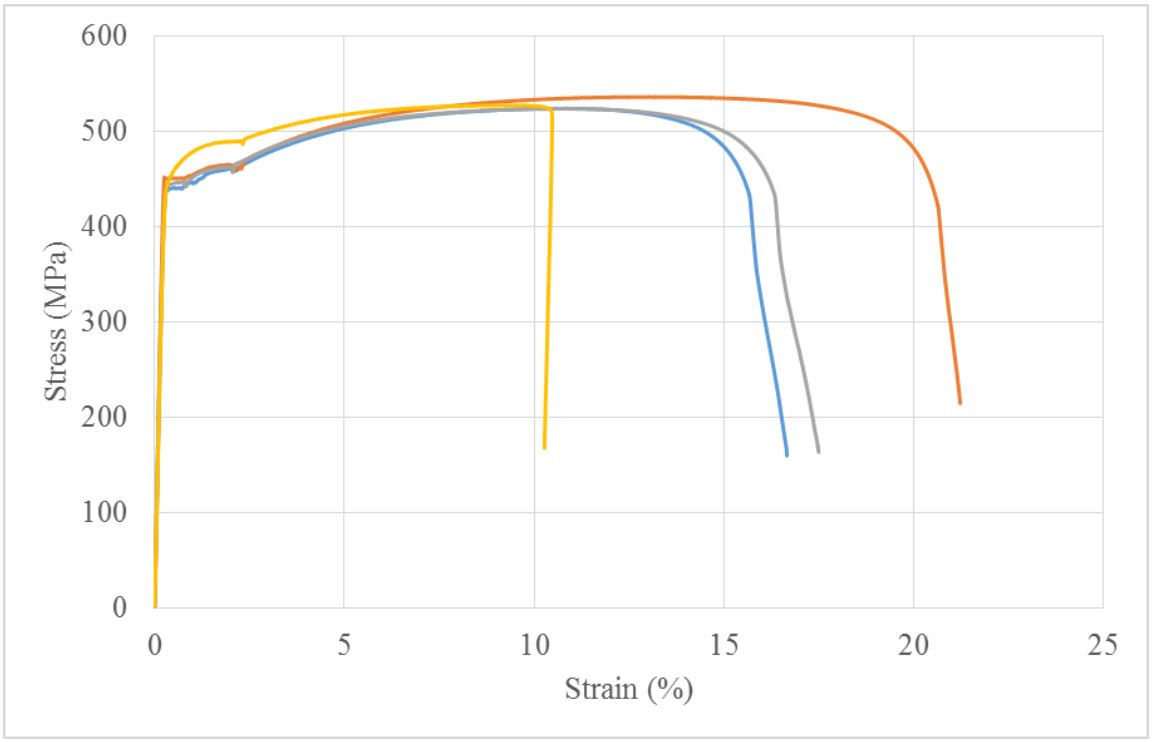
600
500
400
300
200
100
0
Stress (MPa)
0
5
10
15
20
25
Strain (%)

d)

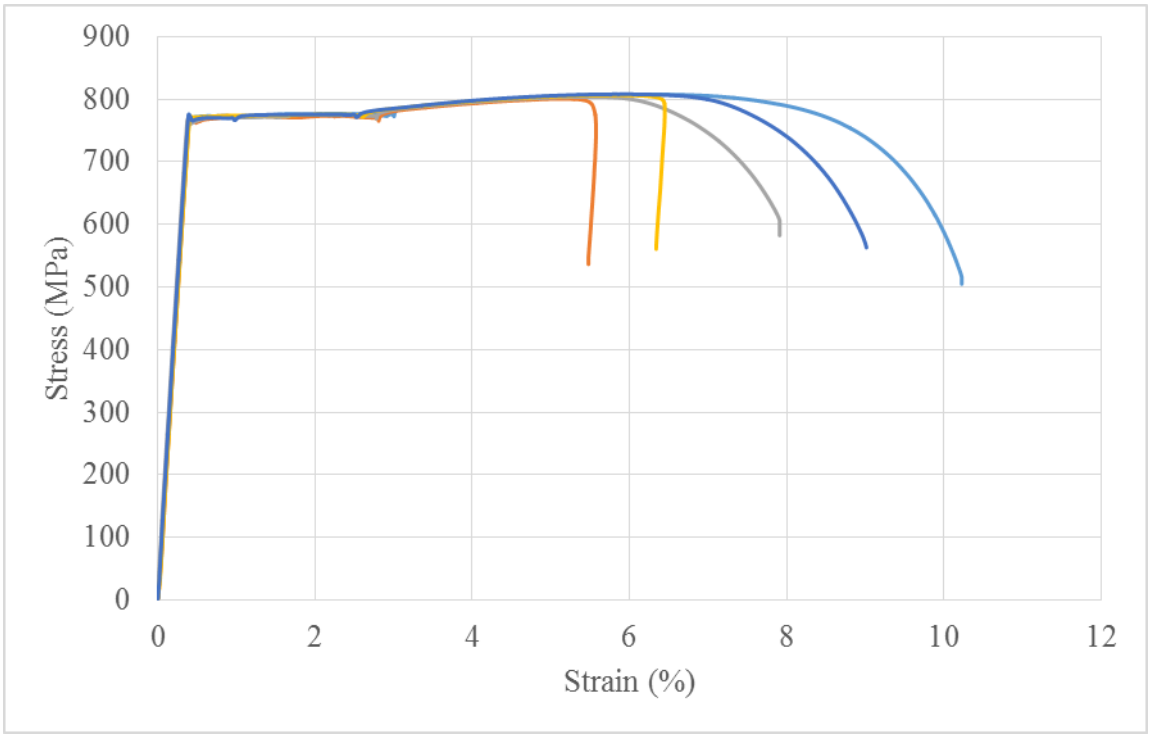
900
800
700
600
500
400
300
200
100
0
Stress (MPa)
0
2
4
6
8
10
12
Strain (%)

e)

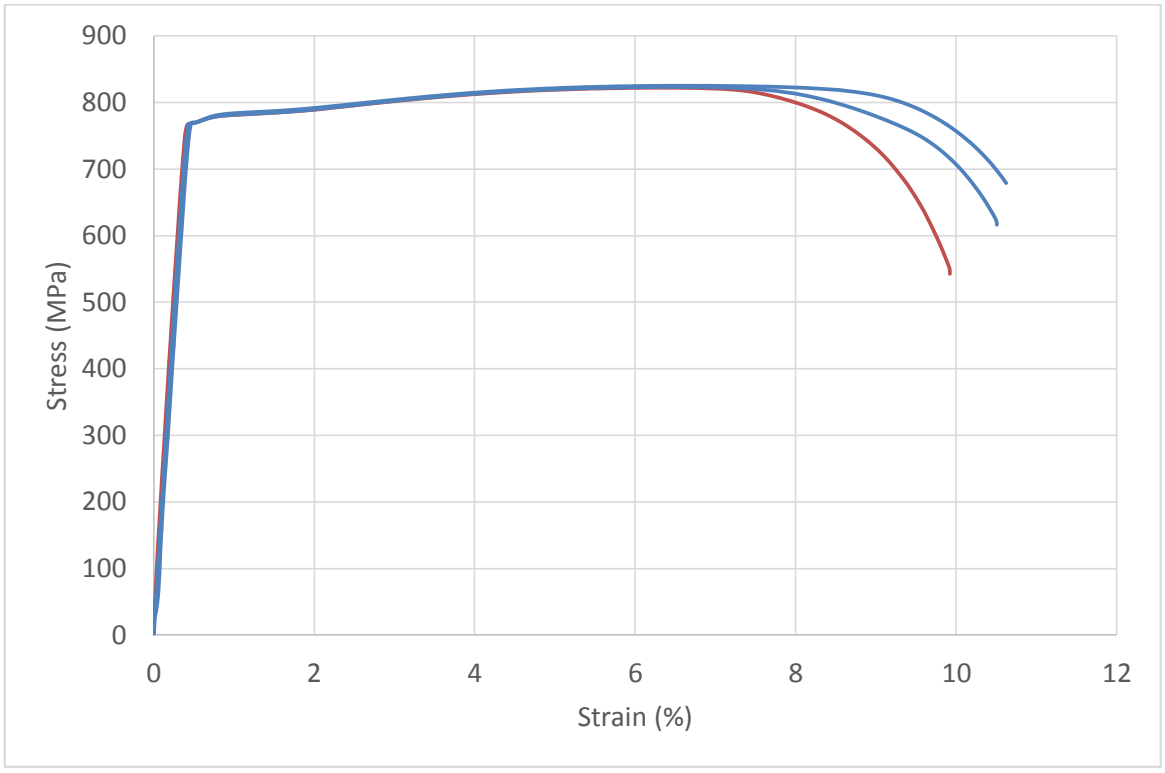
900
800
700
600
500
400
300
200
100
0
Stress (MPa)
0
2
4
6
8
10
12
Strain (%)

f)

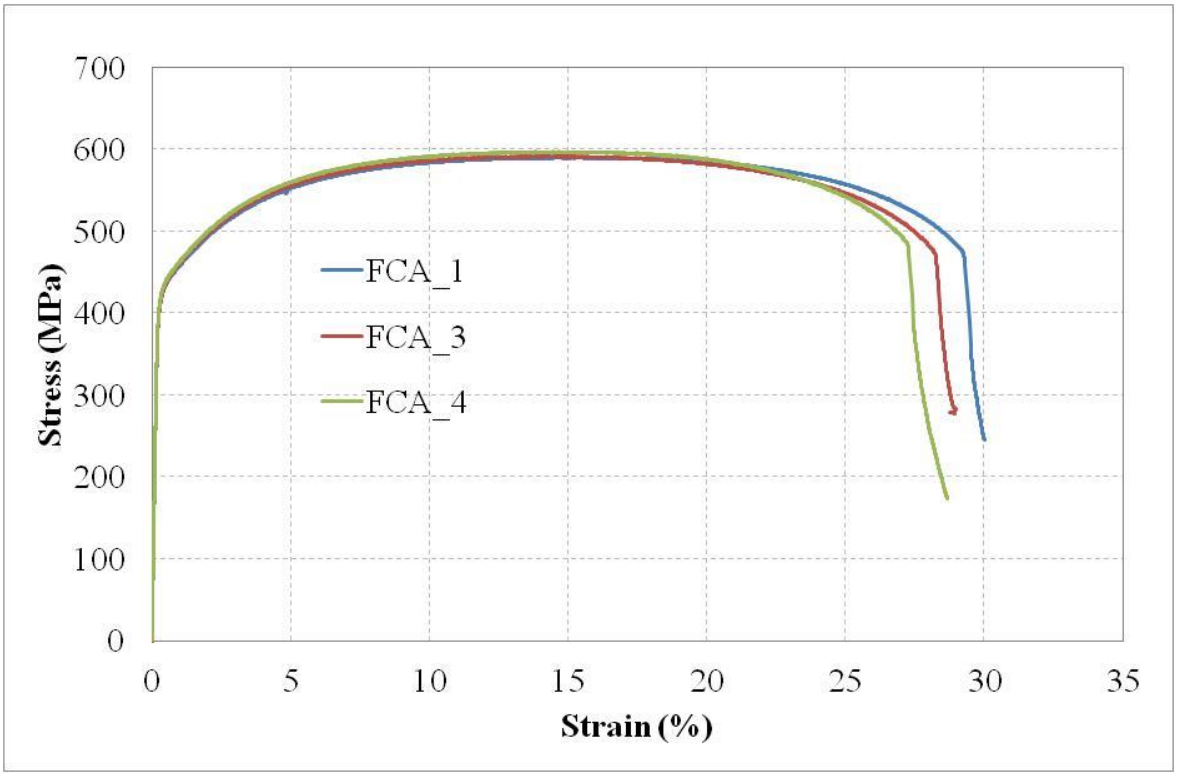

Figure 48: Stress-strain curves for a) X65 -1, b) X65-2, c) X65-3 d) S690-1, e) S690-2 and f) FCA.

Table 9: Summary of the tensile properties of the HSLA steel grades compared to AH36 and DH36 values provided by AIMEN. The value in brackets represents the data scatter from the tensile tests carried out for at least 3 samples for each steel grades.

Steel Name	Upper Yield (MPa)	UTS (MPa)	Yield/Tensile Strength Ratio	Equivalent Elongation to Failure (%)
AH36 (AIMEN)	393.4 (±3.4)	524.4 (±1.1)	0.75	32.5 (±1.3)
DH36 (AIMEN)	464.8 (±3.9)	559.8 (±1.9)	0.83	30.2 (±1.5)
X65 - 1	483.1 (± 18)	521.8 (± 3)	0.93	26.7 (± 1)
X65 - 2	392.1 (± 12)	468.3 (± 1)	0.84	36.4 (± 5)
X65 - 3	443.5 (± 5)	527.3 (± 6)	0.84	21.6 (± 5)
S690 - 1	770.6 (± 3)	805.1 (± 3)	0.96	10.3 (± 2)
S690 - 2	770 (± 2)	823 (± 2)	0.94	12.6 (± 4)
FCA	408 (± 3)	593 (± 4)	*0*.69	29 (± 1)

From the results obtained from the tensile tests, it can be seen that the HSLA steel grades fulfill practically all the requirements specified for naval construction and thus are suitable for replacement of AH36 and DH36 grades. Although the differences are marginal in comparison to DH36 grade with the exception of the S690 grade, which is considerably stronger and has a much higher yield strength, the decision on whether replacement of AH36 and DH36 with HSLAs is beneficial should be based on a comparison of the fatigue crack initiation and

propagation resistance. The fatigue tests along with the AE results will be discussed next.

7.3 Fracture toughness tests

Fracture toughness tests were carried out for all HSLA steel grades. Again the values of AH36 and DH36 grades used for comparative purposes were provided by AIMEN after tests carried out by them in Spain.

To accurately assess the fracture toughness or critical stress intensity factor (K_{1c}) value, the two following rules must be met;

- Firstly the load at which crack growth occurs, P_Q, should be within 10% of the maximum load
- Secondly the effective crack length (α), thickness (B) and the difference of the width when subtracting the effective crack length (W-α) as shown in Figure 49 must all be less than $2.5(K_Q/\sigma_{ys})^2$, where σ_{ys} is the material yield stress .

As long as both aforementioned criteria are applicable then K_Q has identical value with K_{1C}. For the HSLA steels tested herewith these criteria could not be met and thus K_{1C} could not be determined. Considering the J integral method ($J = K^2/E$ where K is the stress intensity factor and E the Young's Modulus of Elasticity) based on the peak load (J_m), then all HSLA steels exhibit higher fracture toughness values than AH36 and DH36 grades. The only exception is the X65-3 grade which exhibit slightly lower fracture toughness values than the DH36 grade but it is still better than the AH36. The results of the fracture toughness tests are summarised and compared in Table 10.

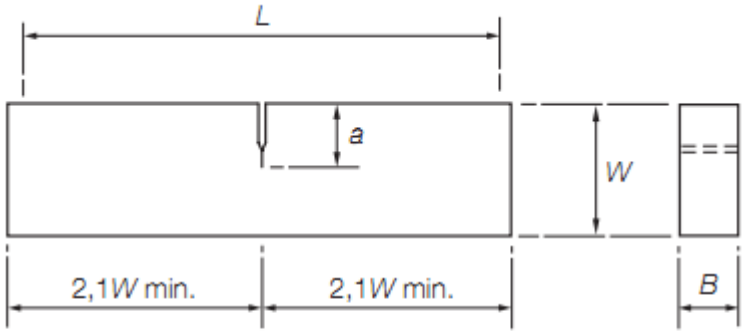

B = thickness
W = width = $2B$
a = effective crack length = $0{,}45W$ to $0{,}55W$
L = loading span = $4W$

Figure 49: Schematic of standard fracture toughness specimen.

Table 10: Summary of the fracture toughness properties of the HSLA steel grades tested. The results for AH36 and DH36 are courtesy of AIMEN.

Steel Code	**F_{max} (N)**	**F_q (N)**	**K_q (MPa $m^{1/2}$)**	**J_m (kJ/m^2)**
AH36	6139 (±665.2)	3687 (±327.1)	33.0 (±1.2)	243.1 (± 27.6)
DH36	7876 (±703.3)	4415 (±518.9)	36.0 (±2.3)	428.8 (± 26.2)
X65 – 1	10151	6306	56.0	911.9
X65 – 2	8160	6394	56.8	737.9
X65 – 3	6230	3900	34.6	349.5
S690 – 1	10800	8380	74.4	302.6
FCA	8200	5750	51.1	576.3

7.4 Fatigue crack growth testing

Fatigue crack growth testing together with the fracture toughness results are very important in determining the crack initiation threshold and crack propagation rate for the HSLA steel grades considered in this study. Higher resistance to crack initiation of an HSLA steel grade signifies its capability of sustaining a higher cyclic load before a crack can initiate and subsequently propagate. Also slower crack growth rates signify the capability of the alloy to resist crack propagation per loading cycle. In order to enable the replacement of AH36 and DH36 with HSLA steel grades then the HSLA steels should ideally be more resistant to both crack initiation and subsequently propagation.

Fatigue crack growth tests carried out using cyclic sinusoidal loading pattern revealed that the S690 performs better than the other steels throughout the range of ΔK as shown in Figure 50. The FCA performs comparably to S690 at a range of ΔK between 25-30 MPa $m^{1/2}$. X65-2 grade performs worse at lower ΔK ranges but becomes comparable to S690 above 55 MPa $m^{1/2}$. The poorest performer was the X65-1 grade but still exhibits better crack growth resistance than the AH36 and DH36 steel grades. The FCG results for the AH36 and DH36 have been provided by AIMEN for comparative purposes and are shown in Figure 51.

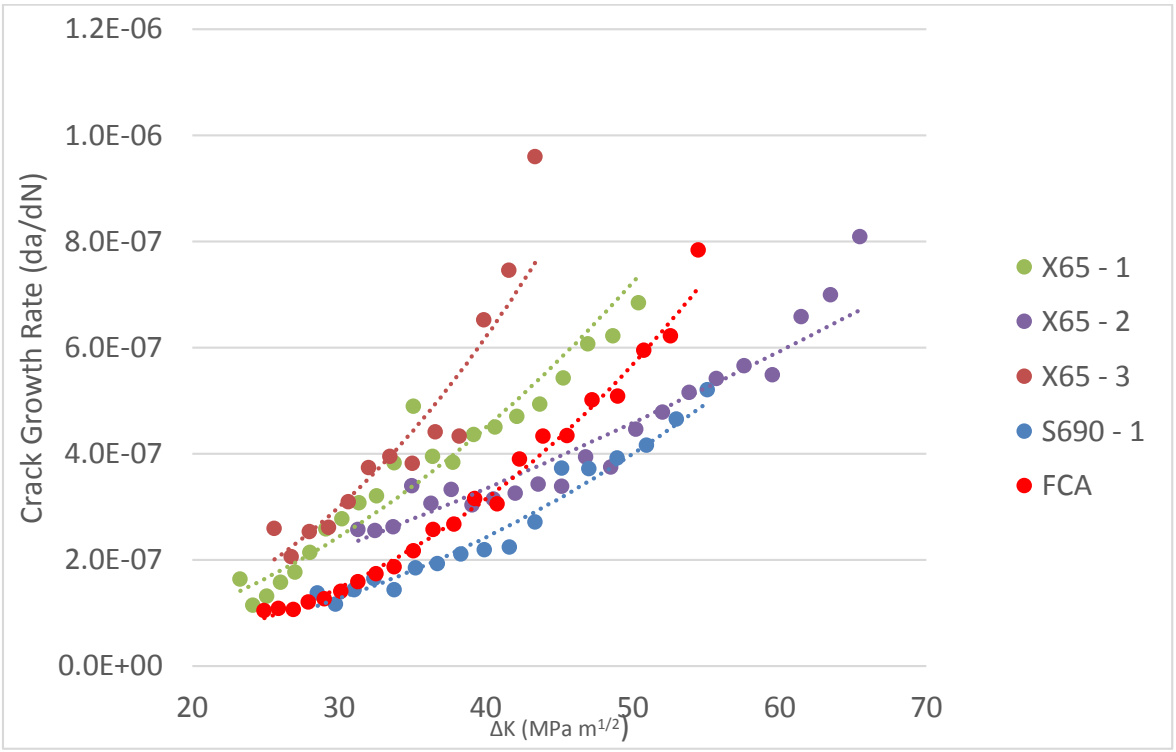

Figure 50: Fatigue crack growth rate curves for the HSLA steel grades.

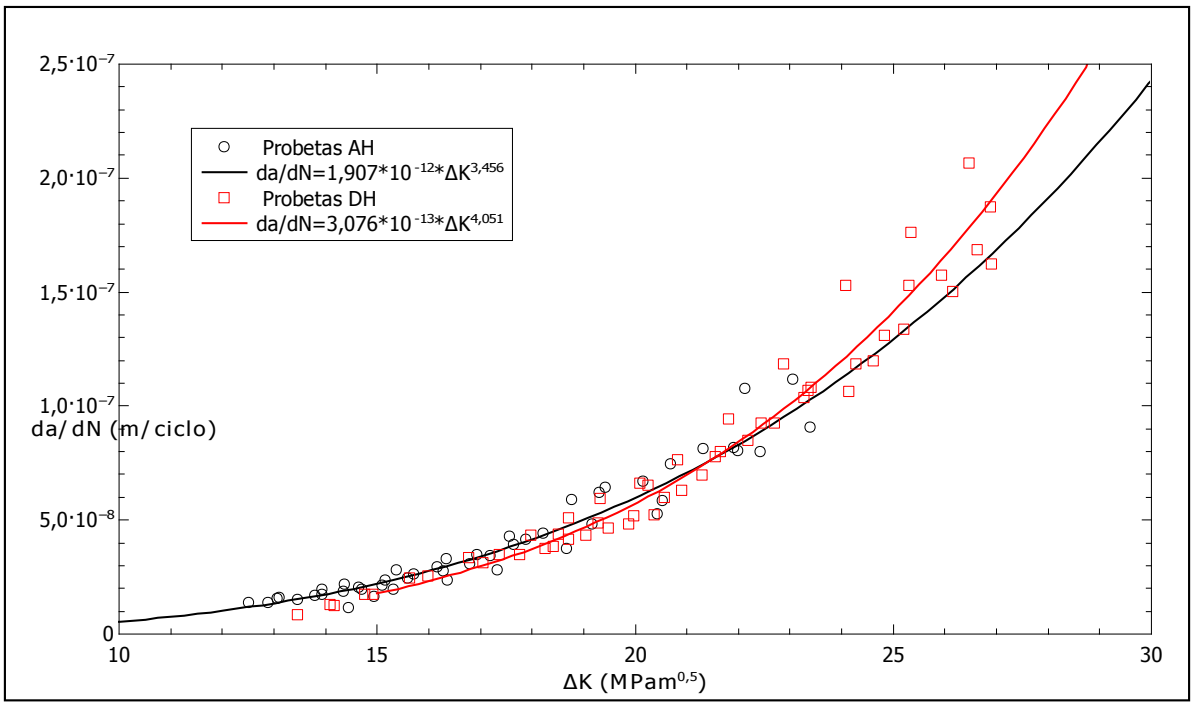

Figure 51: Fatigue crack growth rate curves for AH36 and DH36 steel grades. The results are courtesy of AIMEN.

Paris fitting parameters have also been estimated based on the aforementioned results and are presented together with the stress intensity factor value at which crack initiation can occur in the material, $\Delta K_{Threshold}$. The calculated values are summarised and compared in Table 11.

Table 11: Summary of the fatigue crack growth test results showing the Paris fitting parameters and $\Delta K_{Threshold}$.

Steel	C	m	$\Delta K_{Threshold}$ ($m^{1/2}$)
AH36	$2x10^{-12}$	3.46	12.5
DH36	$3x10^{-13}$	4.05	13.5
X65 – 1	$2x10^{-10}$	2.13	23
X65 – 2	$2x10^{-9}$	1.41	23
X65 – 3	$5x10^{-11}$	2.53	25
S690-1	$6x10^{-11}$	2.24	28
FCA	$2x10^{-11}$	2.65	24

From the results presented it is obvious that the HSLA steel grades considered in this study outperform AH36 and DH36 steel grades. It is particularly important to know the much higher resistance of the HSLA grades to crack initiation meaning thinner plates can be used instead leading to substantial weight reductions and thus lower fuel consumption.

7.5 Acoustic emission testing

During fatigue crack growth tests acoustic emission sensors were fitted on the samples in order to assess the applicability of the technique in detecting damage initiation and evolution in HSLA

steel grades. As discussed in the experimental methodology chapter, a commercial AE system procured from PAC with two wideband AE sensors coupled on the sample using paraffin was used during testing. The sensors were held in place with duct tape.

Load and strain were acquired together with the AE activity that occurred during testing of tensile test samples from the HSLA samples. In tensile testing the plots shown in Figure 52, indicate that cumulative counts increase at a relatively high rate before the specimens reach the yield stress. When plastic deformation begins, the rate at which the cumulative counts accumulate becomes smaller. When the final fracture of specimen is imminent, cumulative counts start to increase sharply until the specimens finally fail. The AE activity recorded during the elastic deformation is attributed to the movement of dislocations within the crystal lattice of the steel. All HSLA steel grades generated similar AE responses. For the S690-1, although the majority of AE activity was recorded during the elastic deformation and yielding of the sample, the pattern of the AE response was similar to the other HSLAs. However, since the S690-1 is much harder as a material, it was expected that during the elastic deformation of this steel grade a much higher activity during this stage of deformation could be observed.

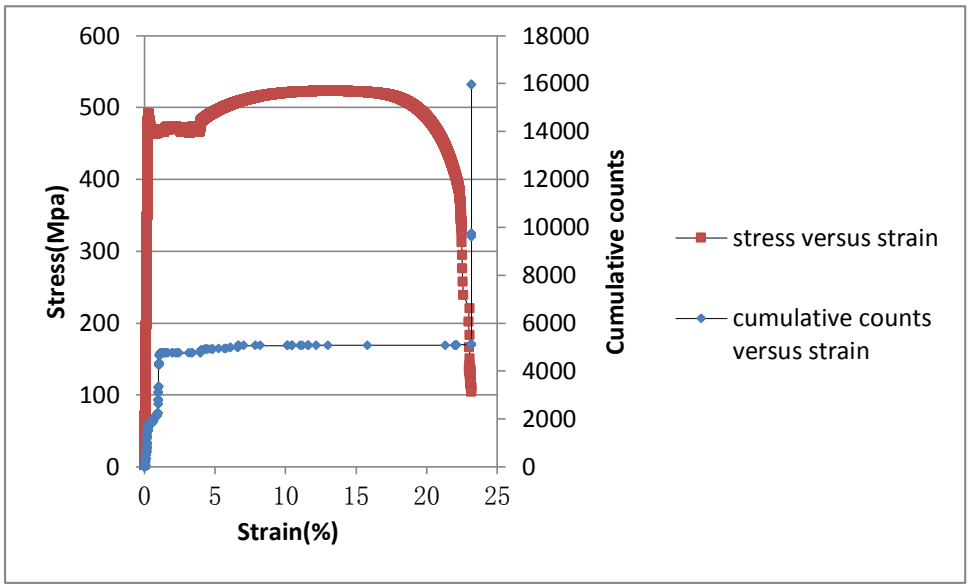

Cumulative AE hits compared with stress-strain curves for X65-1

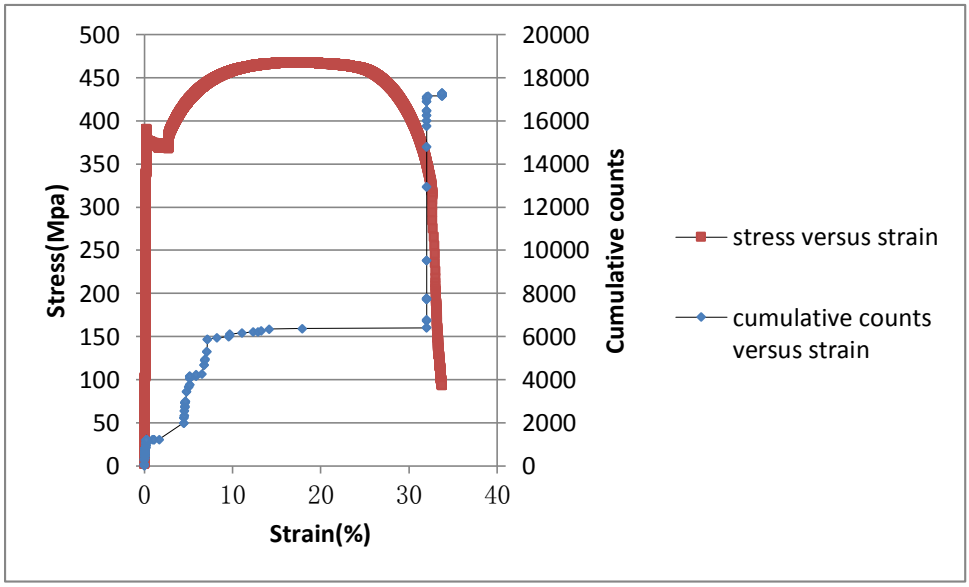

Cumulative AE hits compared with stress-strain curves for X65-2

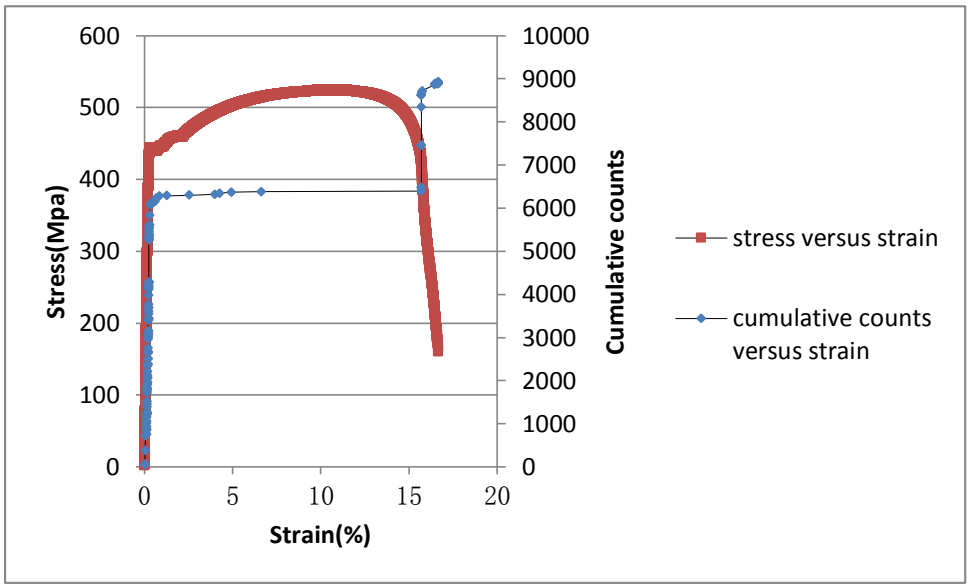

Cumulative AE hits compared with stress-strain curves for X65-3

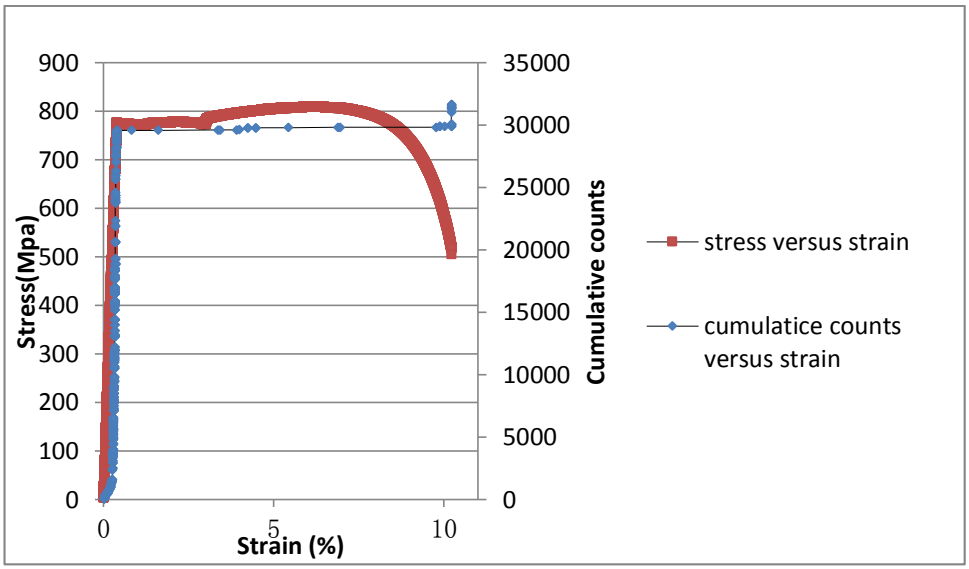

Cumulative AE hits compared with stress-strain curves for S690-1

Figure 52: Cumulative AE hits compared with stress-strain curves for HSLA steel grades. AE tests were not carried on the FCA during tensile testing.

Figure 53 shows the plots of normalised cumulative counts versus the normalised fatigue lifetime for the different HSLA steel grades tested during cycling three point bending loading.

It can be seen that the crack propagation can be successfully detected using AE for all HSLA steel grades tested. However, it is also noted that the AE activity is not identical in all cases and depends on the crack growth behaviour. For X65-1 significant AE activity is seen at the beginning of the test which is related to an initial instability in crack growth. As the crack growth rate increases more steadily, later on the AE activity largely grows linearly. However, as the failure point is approached, the AE activity increases dramatically signifying the imminent failure of the sample. This is observed for all HSLA steel grades with the exception of FCA and X65-2. FCA also shows some step changes in the AE activity at which no crack growth occurs confirming the ability of this steel grade to temporarily at least arrest cracks. X65-2 is the most ductile of the HSLAs tested and the least hard, thus AE activity does not increase as a burst before the steel fails. It appears final failure leads to very little AE activity probably due to the way the crack finally propagates through the steel sample until it finally fails.

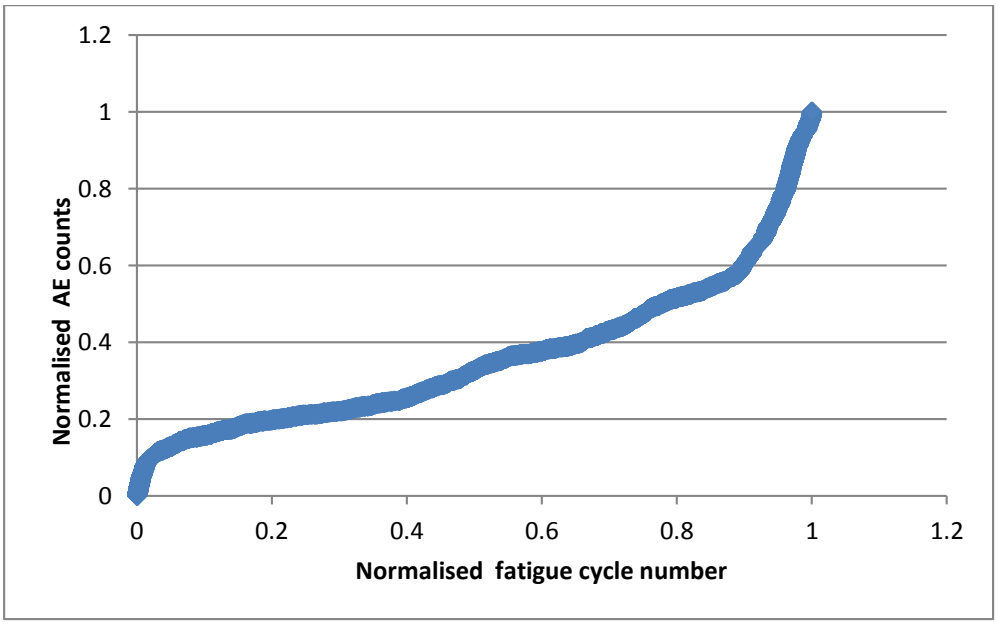

Normalised cumulative counts versus normalized fatigue life cycle of X65-1

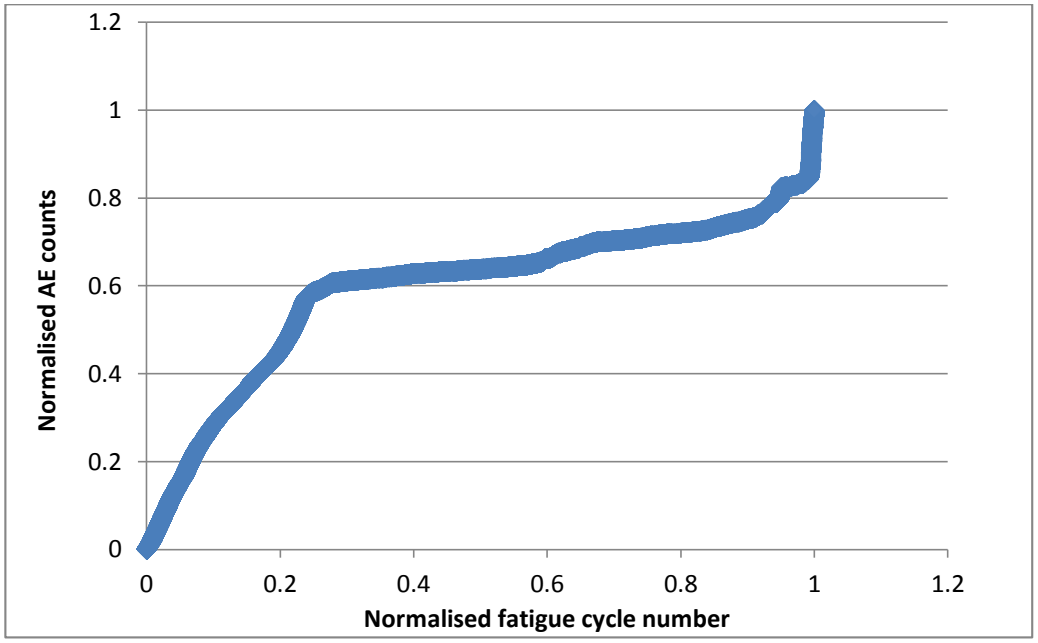

Normalised cumulative counts versus normalized fatigue life cycle for X65-2

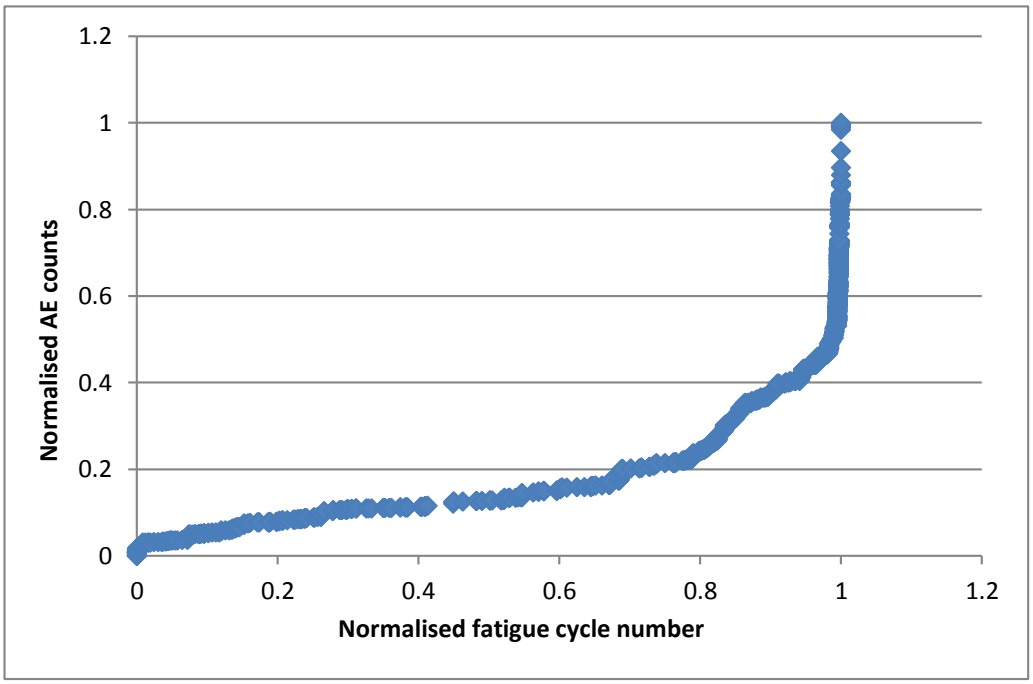

Normalised cumulative counts versus normalized fatigue life cycle for X65-3

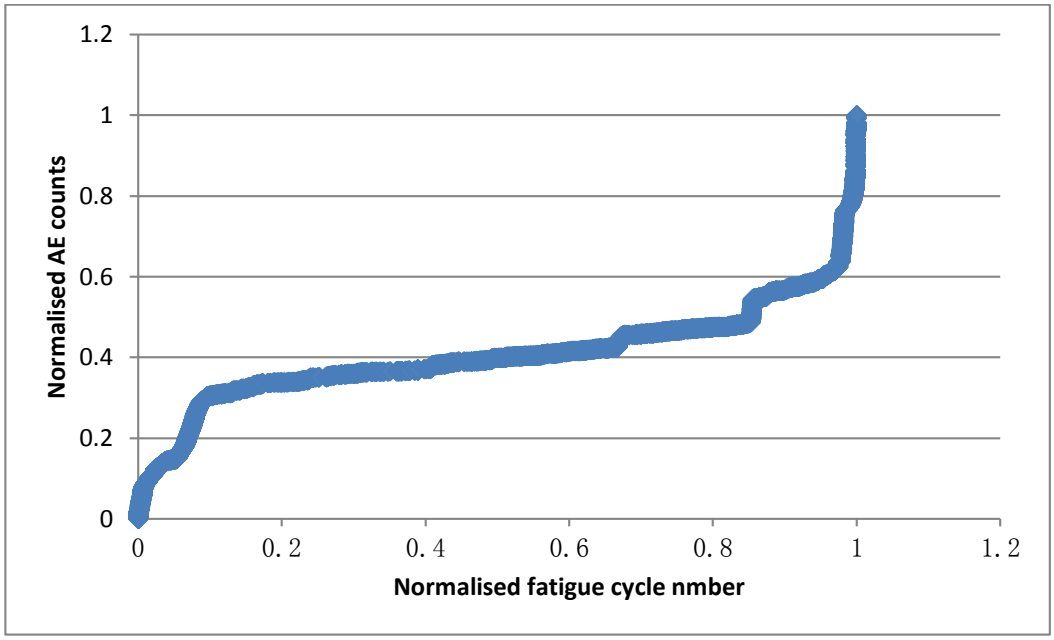

Normalised cumulative counts versus normalized fatigue life cycle for S690

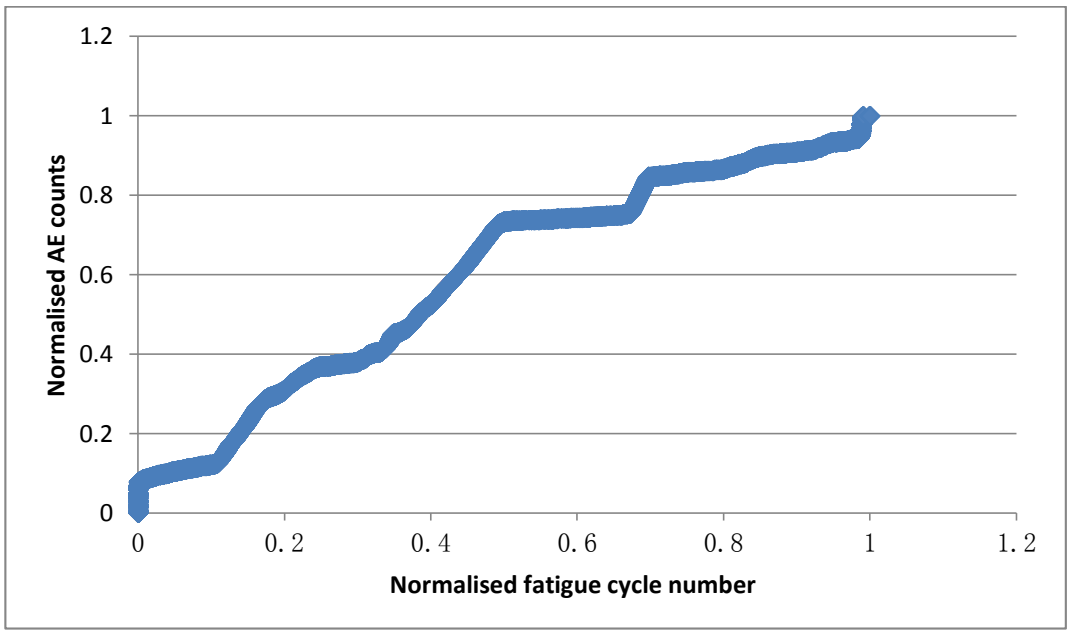

Normalised cumulative counts versus normalized fatigue life cycle for FCA

Figure 53: Normalised cumulative AE counts versus normalised fatigue life cycle for all HSLA steels tested.

In order to assess the behaviour of the AE response with crack growth, cumulative AE energy with increasing crack length has been plotted for the HSLA steels tested. It is obvious that AE cumulative energy is a useful parameter for analysising crack growth in HSLA steels although the characteristics vary from case to case. The results for each HSLA steel grade considered are shown in the plots of Figure 54.

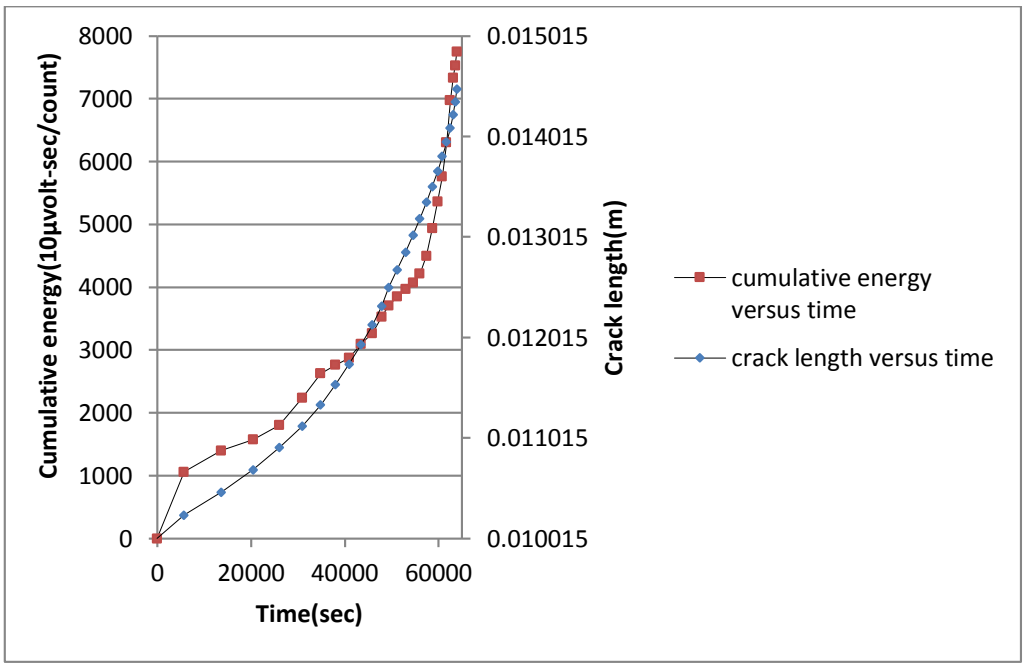

Cumulative energy and crack length with time for a X65-1 specimen

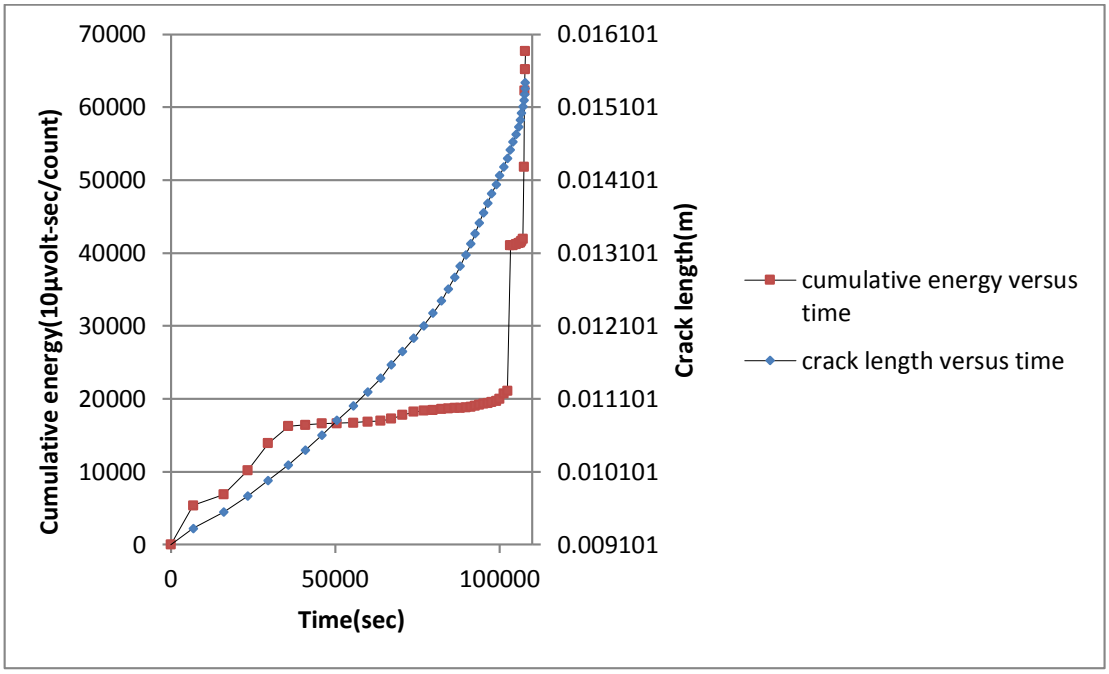

Cumulative energy and crack length with time for X65-2

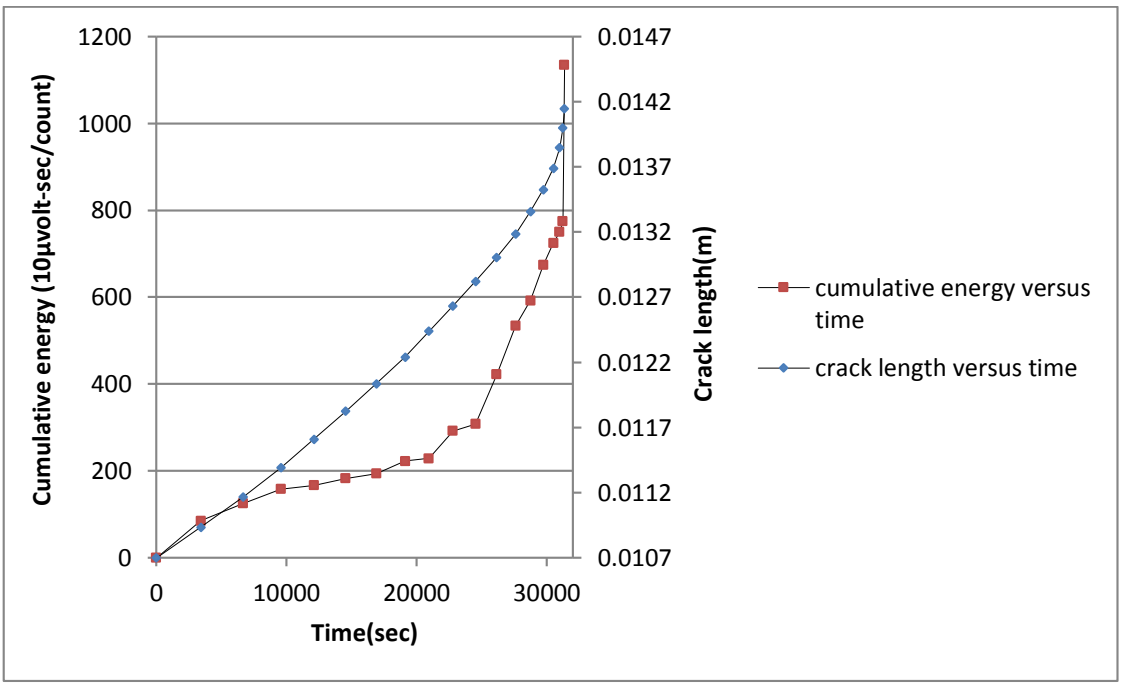

Cumulative energy and crack length with time for X65-3

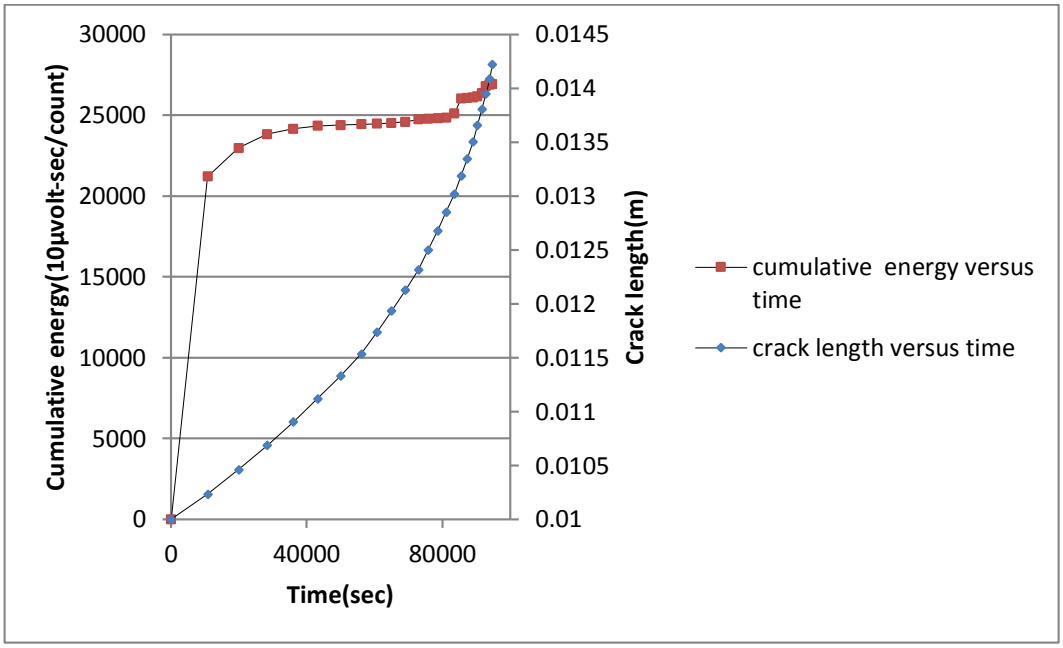

Cumulative energy and crack length with time for S690-1

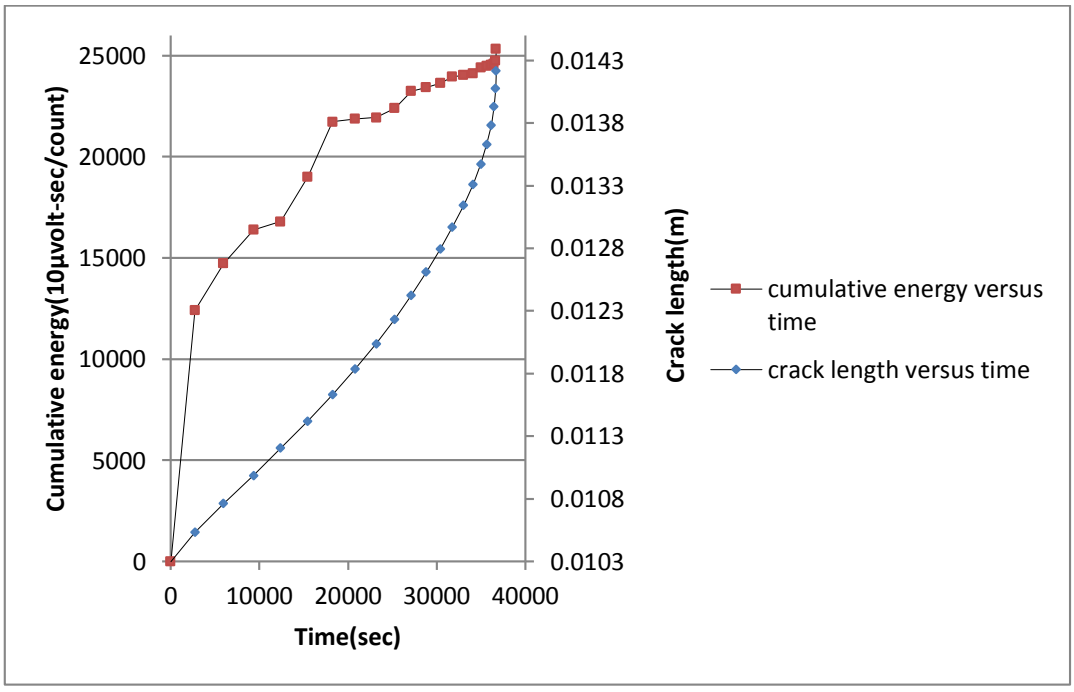

Cumulative energy and crack length with time for FCA

Figure 54: Plots of cumulative AE energy versus crack growth over time for all HSLA steels grades tested.

Another useful tool considered for the assessment of the crack growth rate is based on the calculation of the rate of the AE energy detected during cyclic loading. It has been found that the AE energy rate can be used to evaluate the crack growth rate as shown in the plots presented in Figure 55.

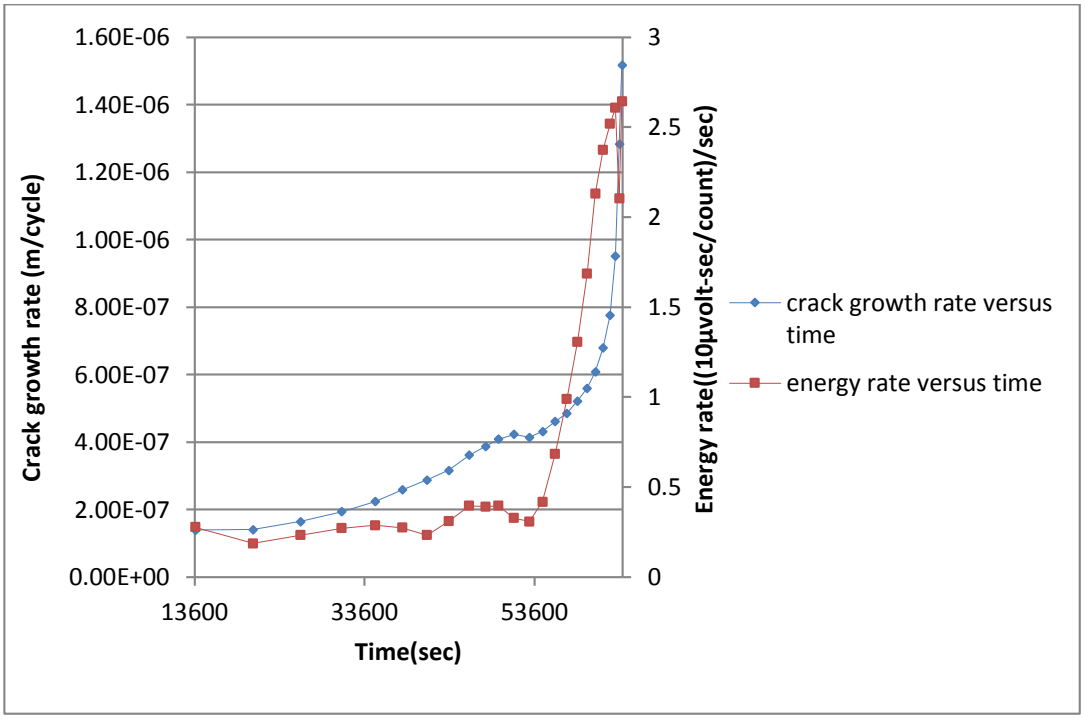

Comparison of crack growth rate and energy rate for X65-1

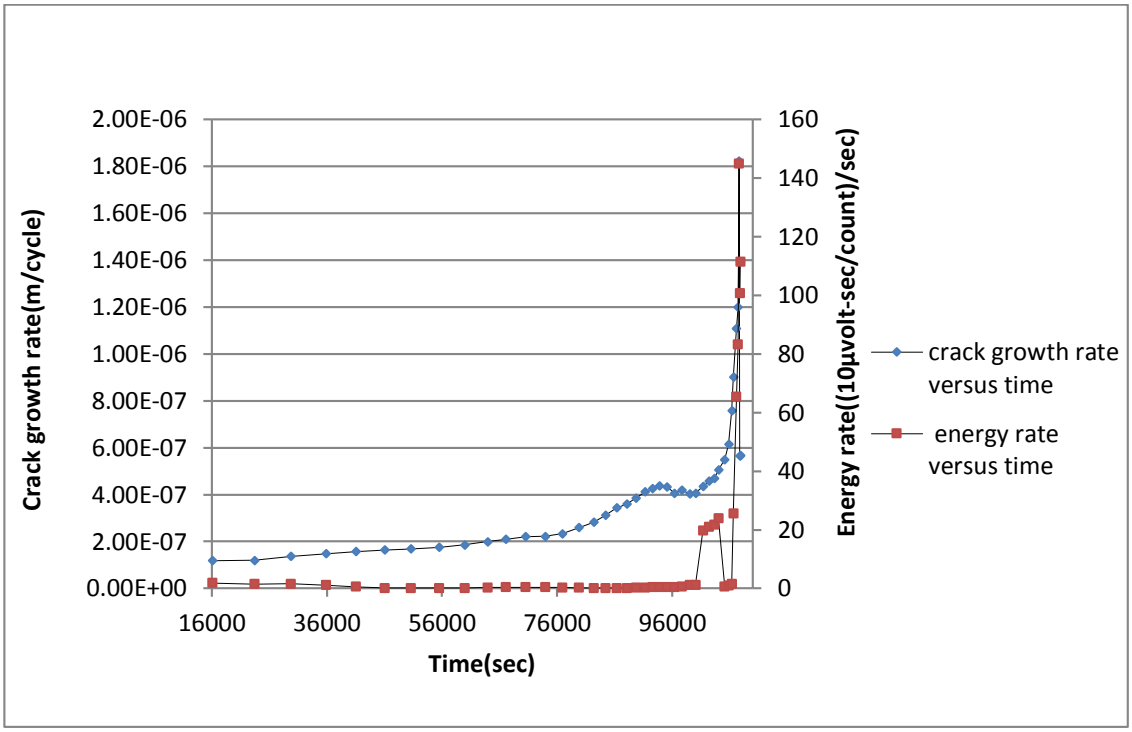

Comparison of crack growth rate and energy rate for X65-2

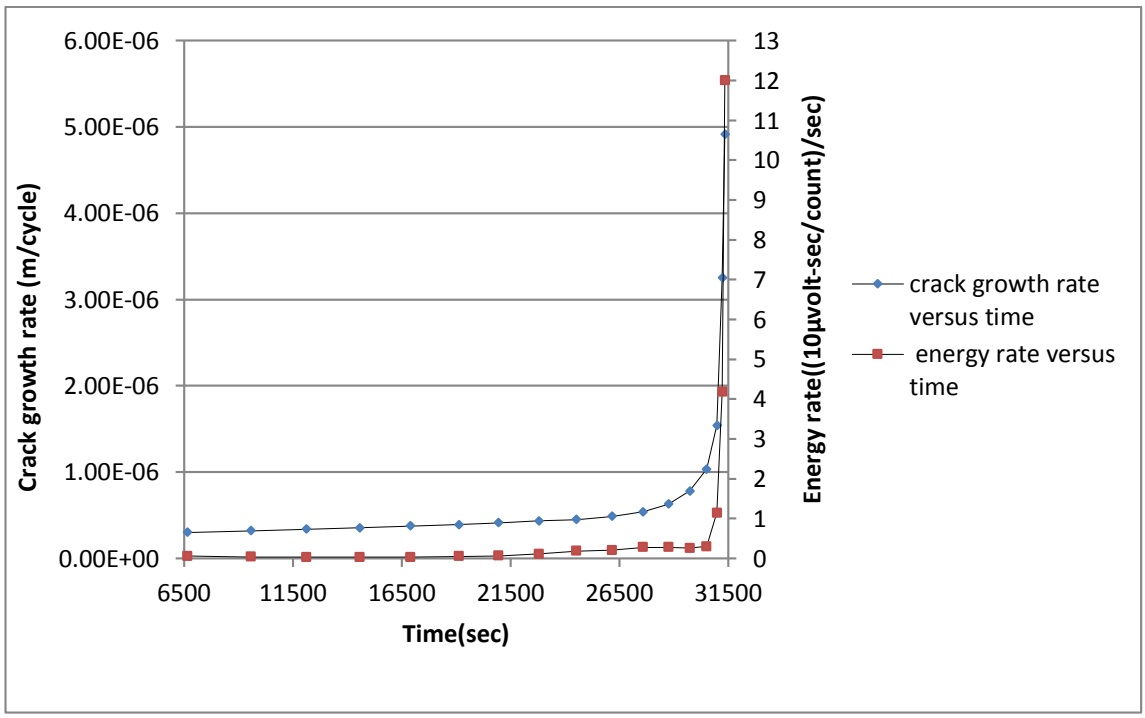

Comparison of crack growth rate and energy rate for X65-3

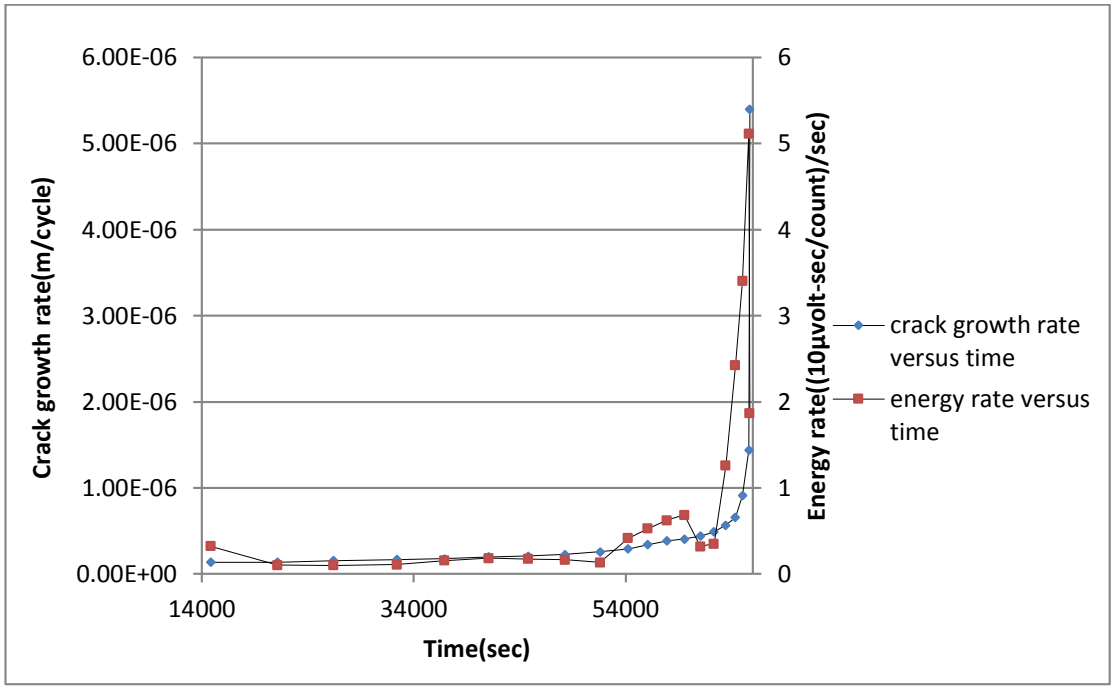

Comparison of crack growth rate and energy rate for S690-1

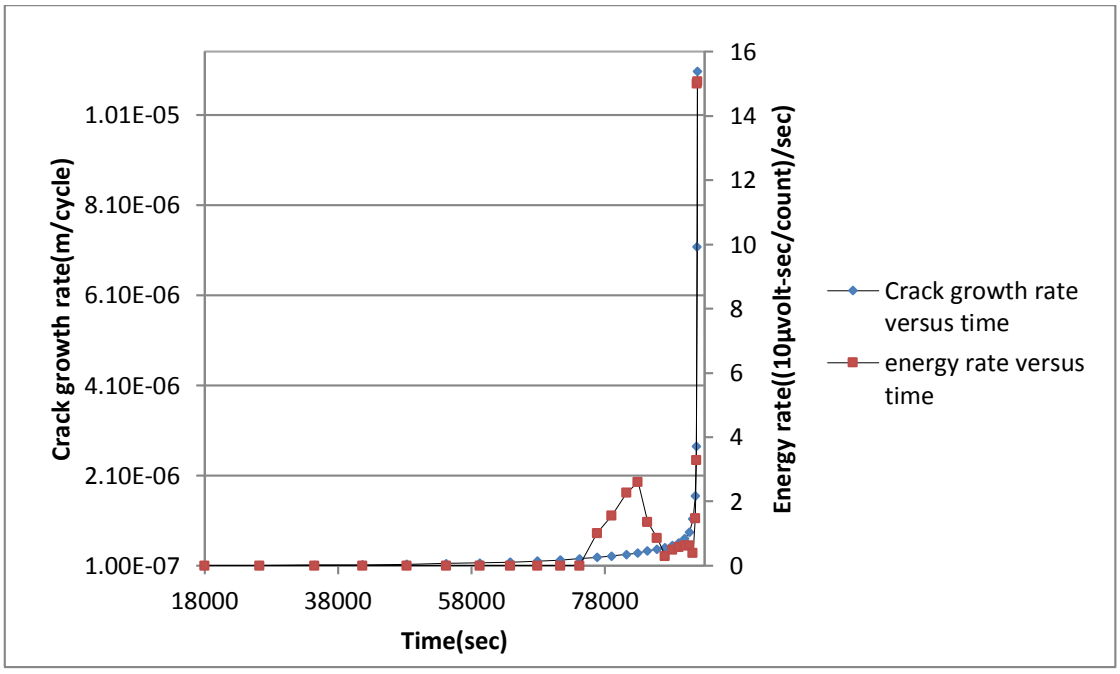

Comparison of crack growth rate and energy rate for FCA

Figure 55: AE energy release rate versus crack growth rate for all HSLA steels grades tested.

From the results presented herewith it is clear that the AE technique can be employed to detect

and monitor crack growth in HSLA steel grades. Moreover, using AE energy rate it is possible to assess the crack growth rate. AE is also capable of detecting instability in crack growth. Furthermore cumulative energy can be used to reveal whether the sample is nearing failure point or not. Thus it is safe to conclude that AE could potentially be used and standardised as a structural health monitoring technique for in-service vessels.

8 Conclusions and future work

AH36 and DH36 are conventional naval steel grades that have been used in the construction of ships for several decades. However, recent changes in regulations imposed by classification societies have specified the requirement of higher thickness plates resulting in heavier vessels and thus increased fuel consumption, lower efficiency and larger engines with higher horsepower. Such engines are more expensive to procure, more costly to run and maintain resulting in higher Capital Expenditure (CAPEXA) and Operational Expenditure (OPEX) for ship operators.

Thus, the maritime industry has been seriously considering the use of alternative steel grades with suitable mechanical properties that offer superior strength and have higher resistance to both crack initiation and propagation. HSLAs have been for a long time considered as a potential alternative to conventional maritime steel grades since they have been used extensively in the offshore oil and gas industry.

In this study we have considered five different HSLA steel grades, including three X65 variants, two different S690 batches and FCA grades. A wide range of mechanical tests including metallography, hardness testing, Charpy, tensile testing, fracture toughness and fatigue crack growth have been carried out. The results of these tests have been compared to those provided by AIMEN for AH36 and DH36. It has been revealed that HSLA steel grades exhibit superior crack initiation and propagation resistance than conventional steel grades. Moreover, they exhibit better or comparable tensile properties and thus they qualify for ship building applications albeit not universal in the case of S690 due to the lower maximum strain tolerance of this particular steel grade. Their energy absorption capability during impact is also acceptable

by classification societies as stipulated in the relevant regulations for conventional naval steel grades.

Acoustic Emission has also been considered in this study in order to evaluate the capability of this technique in detecting and monitoring crack growth in HSLA steels. It has been found that indeed AE can be used to detect crack growth. It can also potentially be used to assess the rate at which a crack grows using AE energy release rate.

Although the mechanical properties exhibited by HSLA steel grades considered in this study are superior to those of conventional naval steel grades it is very important to assess the corrosion resistance of these grades before they can be considered for use in the shipbuilding industry. Suitable coupons should be used for immersion tests in salt water in order to assess corrosion rates and ensure that these fall within acceptable limits and at least comparable to those of conventional steel grades. This work could be carried out as a continuation of the findings arising from this study. Thus corrosion rate results could supplement greatly the results of mechanical tests and AE reported herewith.

Overall it is considered that this study will be useful to the ship building industry and operator as a reference in the short to medium term future.

References

1. GDV. *Section 2.3.3: Mechanical stresses in maritime transport, Chapter 2: Causes of damage/loss during transport,Container Handbook*. [online] 2014 [cited 2014 09/06]; Available from: http://www.containerhandbuch.de/chb_e/stra/index.html?/chb_e/stra/stra_02_03_03.html.
2. Akpan, U.O., et al., *Risk assessment of aging ship hull structures in the presence of corrosion and fatigue.* Marine Structures, 2002. **15**(3): p. 211-231.
3. Kvidahl, L., *An improved high yield strength steel for shipbuilding.* 1985.
4. International, A. *High-Strength Low-Alloy Steels*. [online] 2001 [cited 2014 06/09]; Available from: http://www.asminternational.org/documents/10192/3466171/06117_Chapter%203B.pdf/a764507a-3499-4d23-b348-5536d31c0ba2.
5. Plate, S., *Sheet, or Coil, Age-Hardening Alloy, Structural, High Yield Strength (HSLA-80 and HSLA-100).* MIL-S-24645A (SH), 1990.
6. Chalmers, D.W., *The properties and uses of marine structural materials.* Marine Structures, 1988. **1**(1): p. 47-70.
7. Sarkar, A., *A development study of Microalloyed steel (HSLA) through experimental exploration*, 2012, National Institute of Technology Rourkela.
8. Czyryca, E., *Advances in high strength steel technology for naval hull construction.* Key Engineering Materials, 1993. **84**: p. 491-520.
9. Morrison, W. *Overview of microalloying in steel*. in *The Proceedings of the Vanitec Symposium, Guilin, China*. 2000.

10. Konda, N., et al. *Development of Structural Steel With High Resistance to Fatigue Crack Initiation and Growth: Part 4*. 2011. ASME.

11. Katsumoto, H., et al. *Development of Structural Steel With High Resistance to Fatigue Crack Initiation and Growth: Part 3*. 2005. ASME.

12. Anastasopoulos, A., et al., *Acoustic emission monitoring for detecting structural defects in vessels and offshore structures.* Ships and Offshore Structures, 2009. **4**(4): p. 363-372.

13. Heij, C., G.E. Bijwaard, and S. Knapp, *Ship inspection strategies: effects on maritime safety and environmental protection.* Transportation research part D: transport and environment, 2011. **16**(1): p. 42-48.

14. Knudsen, O.F. and B. Hassler, *IMO legislation and its implementation: Accident risk, vessel deficiencies and national administrative practices.* Marine Policy, 2011. **35**(2): p. 201-207.

15. Eliopoulou, E., et al., *Analysis of tanker casualties after the Oil Pollution Act (USA, 1990).* Proceedings of the Institution of Mechanical Engineers, Part M: Journal of Engineering for the Maritime Environment, 2012. **226**(4): p. 301-312.

16. *Regulation (EC) No. 391/2009 of the European Parliament and of the Council on common rules and standards for ship inspection and survey organisations*, 2009.

17. *European Commission Communication,Strategic goals and recommendations for the EU's maritime transport 2018*, 21 Jan 2009

18. ASTM, *Standard Specification for Structural Steel for Ships*, 2008, ASTM International: West Conshohocken, PA.

19. IGI, S., Y. INOHARA, and T. HIRAI, *High Performance Steel Plates for Shipbuilding—Life Cycle Cost Reduction Technology of JFE Steel—.* JFE technical report, 2005(5): p.

16-23.

20. Bandyopadhyay, P., et al., *Structure and Properties of a Low-Carbon, Microalloyed, Ultra-High-Strength Steel.* Metallurgical and Materials Transactions A, 2011. **42**(4): p. 1051-1061.

21. Specification, A., *5L, Specification for Line Pipe.* Edition March, 2004.

22. El-Danaf, E., et al., *Mechanical, microstructure and texture characterization of API X65 steel.* Materials & Design, 2013. **47**: p. 529-538.

23. Standardization(CEN), E.C.f., *EN 10025: Hot rolled products of structural steels* in *Part 6: Technical delivery conditions for flat products of high yield strength structural steels in the quenched and tempered condition*2009, CEN: Brussel

24. EN, C., *10025: Hot rolled products of structural steels.* Brussels: European Committee for Standardization, 2004.

25. de Jesus, A.M.P., et al., *A comparison of the fatigue behavior between S355 and S690 steel grades.* Journal of Constructional Steel Research, 2012. **79**(0): p. 140-150.

26. Bhadeshia, H. and R. Honeycombe, *Steels - Microstructure and Properties (3rd Edition)*. 2011, Elsevier. p. 17-38.

27. Keytometals. *Control of High Strength Low Alloy (HSLA) Steel Properties*. [online] 2006 [cited 2013 20/06]; Available from: http://www.keytometals.com/page.aspx?ID=CheckArticle&site=kts&NM=182.

28. Armstrong, R.W., *The influence of polycrystal grain size on several mechanical properties of materials.* Metallurgical and Materials Transactions, 1970. **1**(5): p. 1169-1176.

29. Buschow, K.H.J., et al., *Encyclopedia of Materials - Science and Technology, Volumes 1-11*. 2001, Elsevier. p. 8870-8881.

30. ESA. *Hardening Metals*. [online] Unknown [cited 2014 23/06]; Available from: http://www.spaceflight.esa.int/impress/text/education/Mechanical%20Properties/Dislocations_02.html.

31. Rösler, J., H. Harders, and M. Bäker, *Mechanical behaviour of engineering materials: metals, ceramics, polymers, and composites*. Vol. 145. 2007: Springer.

32. Hearn, E.J., *Mechanics of Materials, Volume 1 - An Introduction to the Mechanics of Elastic and Plastic Deformation of Solids and Structural Materials (3rd Edition)*, 1997, Elsevier. p. 4-7.

33. Tarr, M. *Mechanical properties of metals*. [online] Unknown [cited 2014 11/06]; Available from: http://www.ami.ac.uk/courses/topics/0123_mpm/.

34. Nptel. *Lecture 11 : Mechanical properties*. [online] Unknown [cited 2014 08/06]; Available from: http://www.nptel.iitm.ac.in/courses/Webcourse-contents/IIT-ROORKEE/strength%20of%20materials/lects%20&%20picts/image/lect11/lecture11.htm.

35. Callister, W.D. and D.G. Rethwisch, *Materials science and engineering: an introduction*. Vol. 7. 2007: Wiley New York.

36. Keytometals. *Fracture Mechanics*. [online] 2001 [cited 2014 05/07]; Available from: http://www.keytometals.com/page.aspx?ID=CheckArticle&site=kts&NM=45.

37. Mohd, H., S. Shaiful Rizam, and K. Azmi, *Failure analysis on a ruptured petrochemical pipe*. 2010.

38. Metallurgicalconsulting. *Metallurgical*. [online] 2011 [cited 2014 09/06]; Available from: http://www.metallurgicalconsulting.net/metallurgical.html.

39. UMIST. *Failure of Materials*. [online] Unknown [cited 2014 05/07]; Available from: http://pwatlas.mt.umist.ac.uk/internetmicroscope/micrographs/failure.html.

40. Broek, D., *Elementary engineering fracture mechanics*. 1986: Springer.

41. Wikipedia. *SS Schenectady*. [online] 2014 [cited 2014 17/06]; Available from: http://en.wikipedia.org/wiki/SS_Schenectady.

42. Gannon, R., *What Really Sank the Titanic.* Popular Science, 1995. **246**(2,February 1995): p. 49-55.

43. Meikle, J., Steel-munching bacteria are devouring the Titanic, say scientists, The Guardian, Monday, 6 December 2010, *Steel-munching bacteria are devouring the Titanic, say scientists*, in *The Guardian*2010.

44. Kobayashi, H. and H. Onoue, *Brittle Fracture of Liberty Ships.* Failure Knowledge Database, 1943. **100**.

45. Center, N.R. *Fracture Toughness*. [online] Unknown [cited 2014 19/06]; Available from: http://www.ndt-ed.org/EducationResources/CommunityCollege/Materials/Mechanical/FractureToughness.htm.

46. Zhong, Y., et al., *Effect of toughness on low cycle fatigue behavior of pipeline steels.* Materials Letters, 2005. **59**(14): p. 1780-1784.

47. Committee, S.S. *NEW CARISSA - Complete Hull Failure in a Stranded Bulk Carrier*. [online] Unknown [cited 2014 01/07]; Available from: http://www.shipstructure.org/newcar.shtml.

48. Cui, W., *A state-of-the-art review on fatigue life prediction methods for metal structures.* Journal of marine science and technology, 2002. **7**(1): p. 43-56.

49. Vargas-Arista, B., et al., *Normalizing effect on fatigue crack propagation at the heat-affected zone of AISI 4140 steel shielded metal arc weldings.* Materials Research, 2013. **16**(4): p. 722-778.

50. Kujawski, D. and F. Ellyin, *A unified approach to mean stress effect on fatigue threshold conditions.* International Journal of Fatigue, 1995. **17**(2): p. 101-106.

51. Skorupa, M., *LOAD INTERACTION EFFECTS DURING FATIGUE CRACK GROWTH UNDER VARIABLE AMPLITUDE LOADING—A LITERATURE REVIEW. PART I: EMPIRICAL TRENDS.* Fatigue & Fracture of Engineering Materials & Structures, 1998. **21**(8): p. 987-1006.

52. Mscsoftware. *Total Life (S-N) Analysis*. [online] Unknown [cited 2014 01/07]; Available from: http://www.mscsoftware.com/training_videos/patran/Reverb_help/index.html#page/Fatigue%2520Users%2520Guide/fat_theory.15.3.html#ww45787.

53. Murtaza, G. and R. Akid, *Empirical corrosion fatigue life prediction models of a high strength steel.* Engineering Fracture Mechanics, 2000. **67**(5): p. 461-474.

54. Acuña-González, N., et al., *Early Corrosion Fatigue Damage on Stainless Steels Exposed to Tropical Seawater: A Contribution from Sensitive Electrochemical Techniques.* 2012.

55. Miller and O'donnell, *The fatigue limit and its elimination.* Fatigue & Fracture of Engineering Materials & Structures, 1999. **22**(7): p. 545-557.

56. Boardman, B., *Fatigue resistance of steels.* ASM International, Metals Handbook. Tenth Edition, 1990. **1**: p. 673-688.

57. Labossiere, P.E., D. Flores, and C. Vant, *Fracture - ME354a Lecture Notes*, 2007, University of Washington: Washington.

58. Cheng, Y.-W., *The fatigue crack growth of a ship steel in seawater under spectrum loading.* International journal of fatigue, 1985. **7**(2): p. 95-100.

59. Sinclair, G. and R. Pieri, *On obtaining fatigue crack growth parameters from the*

literature. International journal of fatigue, 1990. **12**(1): p. 57-62.

60. Beden, S.M., S. Abdullah, and A.K. Ariffin, *Review of Fatigue Crack Propagation Models for Metallic Component.* EuroJournal, 2009. **28**: p. 364-397.

61. Anderson, T.L., *Fracture mechanics: Fundamentals and Applications*. 1995, Texas: CRC Press.

62. King, R. and G. Britain, *A review of fatigue crack growth rates in air and seawater*. 1998: Health and Safety Executive.

63. Pereira, H.F., et al., *Influence of loading sequence and stress ratio on Fatigue damage accumulation of a structural component.* Ciência & Tecnologia dos Materiais, 2008. **20**(1-2): p. 60-67.

64. El-Shabasy, A.B. and J.J. Lewandowski, *Effects of load ratio,< i> R</i>, and test temperature on fatigue crack growth of fully pearlitic eutectoid steel (fatigue crack growth of pearlitic steel).* International journal of fatigue, 2004. **26**(3): p. 305-309.

65. Richards, C. and T. Lindley, *The influence of stress intensity and microstructure on fatigue crack propagation in ferritic materials.* Engineering Fracture Mechanics, 1972. **4**(4): p. 951-978.

66. Lindley, T., C. Richards, and R. Ritchie, *The mechanics and mechanisms of fatigue crack growth in metals.* The mechanics and physics of fracture, 1975: p. 238-252.

67. Lindley, T., I. Palmer, and C. Richards, *Acoustic emission monitoring of fatigue crack growth.* Materials Science and Engineering, 1978. **32**(1): p. 1-15.

68. Corporation, P.A. *Acoustic Emission Technology*. [online] 2010 [cited 2014 25/06]; Available from: http://www.pacndt.com/index.aspx?go=technologies&focus=acoustic%20emission.htm.

69. Gutkin, R., et al., *On acoustic emission for failure investigation in CFRP: Pattern recognition and peak frequency analyses.* Mechanical Systems and Signal Processing, 2011. **25**(4): p. 1393-1407.

70. Brussel, V.U. *Acoustic Emission Testing*. [online] Unknown [cited 2014 26/06]; Available from: http://mech.vub.ac.be/teaching/info/Damage_testing_prevention_and_detection_in_aeronautics/PDF/acoustic-emission.pdf.

71. Carlos, M.F., *Acoustic emission: heeding the warning sounds from materials.* ASTM standardization news, 2003. **31**(10).

72. Pollock, A., *Acoustic emission inspection.* ASM Handbook., 1989. **17**: p. 278-294.

73. Shiotani, T., *Parametric AE Analysis*, in *Acoustic Emission Testing*, C.U.G.a.M. Ohtsu, Editor. 2008, Springer: Berlin.

74. Physical-Acoustics-Corporation, *AEWin Manual*. 2004, USA: A MISTRAS Holding Company.

75. Muravin. *Open Acoustic Emission Initiative*. [online] Unknown [cited 2014 18 /06]; Available from: http://www.muravin.com/ae/open_acoustic_emission_initiative.html.

76. GmbH, V.S. *AE Testing Fundamentals,Equipment, Applications*. [online] 2002 [cited 2014 17/06]; Available from: http://www.ndt.net/article/v07n09/05/05.htm.

77. Scruby, C., *An introduction to acoustic emission.* Journal of Physics E: Scientific Instruments, 1987. **20**(8): p. 946.

78. Weaver, R. and Y.-H. Pao, *Axisymmetric elastic waves excited by a point source in a plate.* Journal of Applied Mechanics, 1982. **49**: p. 821.

79. Djordjevic, B.B. *Remote Non-Contact Ultrasonic Testing of Composite Materials*. in *Proceedings of the 15th World Conference on Non-destructive Techniques, Rome, www.*

ndt. net. 2000.

80. Huang, M., et al., *Using acoustic emission in fatigue and fracture materials research.* JOM, 1998. **50**(11): p. 1-14.

81. NDT, E. *Kaiser effect*. 2002 [cited 2013 01/05]; Available from: http://www.ndt.net/ndtaz/content.php?id=476.

82. Lavrov, A., *The Kaiser effect in rocks: principles and stress estimation techniques.* International Journal of Rock Mechanics and Mining Sciences, 2003. **40**(2): p. 151-171.

83. Yu, J., et al., *Prediction of fatigue crack growth in steel bridge components using acoustic emission.* Journal of Constructional Steel Research, 2011. **67**(8): p. 1254-1260.

84. Berkovits, A. and D. Fang, *Study of fatigue crack characteristics by acoustic emission.* Engineering Fracture Mechanics, 1995. **51**(3): p. 401-416.

85. Khan, S.A., et al., *Analysis of Acoustic Emission Signals during Tensile Deformation of Fe-Si Steels with Various Silicon Contents.* Metallurgical and Materials Transactions A, 2013: p. 1-12.

86. Han, Z., H. Luo, and H. Wang, *Effects of strain rate and notch on acoustic emission during the tensile deformation of a discontinuous yielding material.* Materials Science and Engineering: A, 2011. **528**(13): p. 4372-4380.

87. Grosse, C.U., et al., *Signal conditioning in acoustic emission analysis using wavelets.* NDT. net, 2002. **7**(9): p. 1-9.

88. Colombo, I.S., I. Main, and M. Forde, *Assessing damage of reinforced concrete beam using "b-value" analysis of acoustic emission signals.* Journal of materials in civil engineering, 2003. **15**(3): p. 280-286.

89. Cone, D.M., *Acoustic emission characterization of the microplastic mechanisms of ductile fracture in Al 6061*. 2006.

90. Aggelis, D.G., *Classification of cracking mode in concrete by acoustic emission parameters.* Mechanics Research Communications, 2011. **38**(3): p. 153-157.

91. Chaswal, V., et al., *Fatigue crack growth mechanism in aged 9Cr–1Mo steel: threshold and Paris regimes.* Materials Science and Engineering: A, 2005. **395**(1): p. 251-264.

92. Chang, H., et al., *Acoustic emission study of corrosion fatigue crack propagation mechanism for LY12CZ and 7075-T6 aluminum alloys.* Journal of materials science, 2005. **40**(21): p. 5669-5674.

93. Serrano, E. and M. Fabio, *Application of the wavelet transform to acoustic emission signals processing.* Signal Processing, IEEE Transactions on, 1996. **44**(5): p. 1270-1275.

94. Khamedi, R., A. Fallahi, and A. Refahi Oskouei, *Effect of martensite phase volume fraction on acoustic emission signals using wavelet packet analysis during tensile loading of dual phase steels.* Materials & Design, 2010. **31**(6): p. 2752-2759.

95. Qi, G. and A.A. Barhorst, *On predicting the fracture behavior of CFR and GFR composites using wavelet-based AE techniques.* Engineering fracture mechanics, 1997. **58**(4): p. 363-385.

96. Horiuchi, T.O.T.K.R., *Acoustic emission during fatigue crack propagation in structural materials.* International Acoustic Emision Symposium, 1980. **5**: p. 137-145.

97. Kohn, D., P. Ducheyne, and J. Awerbuch, *Acoustic emission during fatigue of Ti-6Al-4V: Incipient fatigue crack detection limits and generalized data analysis methodology.* Journal of Materials Science, 1992. **27**(12): p. 3133-3142.

98. Sinclair, A., D. Connors, and C. Formby, *Acoustic emission analysis during fatigue crack growth in steel.* Materials Science and Engineering, 1977. **28**(2): p. 263-273.

99. Bassim, M., *Detection of fatigue crack propagation with acoustic emission.* NDT & E International, 1992. **25**(6): p. 287-289.

100. Oh, K.H., et al., *Acoustic emission behavior during fatigue crack propagation in 304 stainless steel.* Key Engineering Materials, 2004. **261**: p. 1325-1330.

101. Chen, H.-L.R. and J.-H. Choi, *Acoustic emission study of fatigue cracks in materials used for AVLB.* Journal of Nondestructive Evaluation, 2004. **23**(4): p. 133-151.

102. Palmer, I., *Acoustic emission measurements on reactor pressure vessel steel.* Materials Science and Engineering, 1973. **11**(4): p. 227-236.

103. Hamel, F., J.P. Bailon, and M.N. Bassim, *Acoustic emission mechanisms during high-cycle fatigue.* Engineering Fracture Mechanics, 1981. **14**(4): p. 853-860.

104. Schijve, J., *The stress ratio effect on fatigue crack growth in 2024-T 3 Alclad and the relation to crack closure.* 1979.

105. Kumar, R. and S. Garg, *Influence of stress ratio and material properties on effective stress range ratio and crack growth.* Engineering Fracture Mechanics, 1989. **32**(2): p. 195-202.

106. Maddox, S.J., *An investigation of the influence of applied stress ratio on fatigue crack propagation in structural steels*. 1978: Welding Institute.

107. Yılmazer, P., A. Amini, and M. Papaelias, *The structural health condition monitoring of rail steel using acoustic emission techniques.* 2012.

108. Kostryzhev, A., C. Davis, and C. Roberts, *Detection of crack growth in rail steel using acoustic emission.* Ironmaking & Steelmaking, 2013. **40**(2): p. 98-102.

109. Register, L., *Rules and Regulations for the Classification of Ships*, 2006, Part.